DEVELOPMENT OF POTENT AND SELECTIVE INHIBITORS OF *MYCOBACTERIUM TUBERCULOSIS*, *PLASMODIUM FALCIPARUM* AND *STAPHYLOCOCCUS AUREUS* DIHYDROFOLATE REDUCTASE

A Dissertation

by

HUNMIN JUNG

Submitted to the Office of Graduate and Professional Studies of
Texas A&M University
in partial fulfillment of the requirements for the degree of

DOCTOR OF PHILOSOPHY

Chair of Committee,	James C. Sacchettini
Committee Members,	Kevin Burgess
	Marcetta Y. Darensbourg
	J. Martin Scholtz
Head of Department,	Francois Gabbai

December 2014

Major Subject: Chemistry

ABSTRACT

The goal of this study was to develop drugs that exclusively affect pathogenic dihydrofolate reductase (DHFR) without causing harm to the human counterpart. To achieve that goal, a well-known dihydrofolate reductase (DHFR) inhibitors, trimethoprim (TMP), methotrexate (MTX) and trimetrexate (TMQ), were modified, tested, and crystallized on *Mycobacterium tuberculosis* (*Mtb)* dihydrofolate reductase (DHFR), wild type and quadruple mutant *Plasmodium falciparum* (*Pf)* DHFR-thymidylate synthase (TS), *Staphylococcus aureus* DHFR, and human DHFR. We focused on the drug design to utilize the structural differences between the pathogenic DHFRs and the human DHFR; specifically, we focused on a pocket near the substrate binding site where Asp27 and Gln28 of *Mtb* DHFR, and Asp54 and Met55 of *Pf* DHFR-TS are located. The same site is closely packed in human DHFR. From the initial screening and designing process, C-8 benzyl-2,4-diaminoquinazoline TMQ analogs were found to have outstanding selectivity against *Mtb* and *Pf* DHFR. Co-crystal structures of C-8 benzyl TMQ analogs with *Mtb* and *Pf* DHFR showed that the flexibility of Gln28 in *Mtb* DHFR, and Met55 in *Pf* DHFR contributes to extra space and interaction with C-8 benzyl moiety. This flexibility, which is not available in the human DHFR, enables the TMQ analogs to bind exclusively to the pathogenic DHFRs. Our novel C-8 benzyl-2,4-diaminoquinazoline TMQ analogs exhibited great potency and selectivity toward pathogenic DHFRs. In addition, these C-8 benzyl-2,4-diaminoquinazoline TMQ analogs were potent on *Staphylococcus aureus* DHFR as well and we hypothesize based on our

findings that our C-8 benzyl-2,4-diaminoquinazoline TMQ analogs have potential for selective, broad spectrum antimicrobials against whose DHFR share the common structural feature with *Mtb* or *Pf* DHFR, an acid residue and a flexible residue next to it.

ACKNOWLEDGEMENTS

I first would like to thank my God who is alpha and omega, and the author and perfecter of my faith and research for blessing me exceedingly and abundantly.

I also would like to express my deep gratitude to my advisor, Dr. Sacchettini for his generous and sincere guidance throughout the years. My committee members, Dr. Darensbourg, Dr. Burgess, and Dr. Scholtz have been great help and support to my research, and many thanks should be given to them.

Special thanks should also be given to the former and present Sacchettini lab members and the collaborators. We are such a huge group, and without those open-minded members, it would have been impossible for me to finish up this journey. I would like to thank Joel and Kurt for the compounds and the exciting discussions. Dr. Van Vooris and his lab's assay was a critical part of my research.

To my parents, I was, am and will be an apple of their eyes. Their unconditional and sacrificial love stirred me to move forward.

Lastly, but not at all least, I really want to say big 'thank you' to my lovely wife Gayeun and our two blessings, John and James. As time goes by, I love you all the more and I believe that this love will be growing even bigger.

NOMENCLATURE

ASN	Asparagine
ASP	Aspartate
CYS	Cysteine
DHF	Dihydrofolic Acid (Dihydrofolate)
DHFR	Dihydrofolate Reductase
DHPS	Dihydropteroate Synthase
DM	Double Mutant
EC50	Half Maximal Effective Concentration
IC50	Half Maximal Inhibitory Concentration
ILE	Isoleucine
GLN	Glutamine
GLU	Glutamate
MDR	Multi Drug Resistance
MET	Methionine
MRSA	Methicillin-Resistant Staphylococcus Aureus
MTB	Mycobacterium Tuberculosis
MTX	Methotrexate
NADP	Nicotinamide Adenine Dinucleotide Phosphate
NADPH	Nicotinamide Adenine Dinucleotide Phosphate Reduced
PF	Plasmodium Falciparum

PHE	Phenylalanine
PTX	Pyritrexim
PYR	Pyrimethamine
QM	Quadruple Mutant
SA	Staphylococcu Aureus
SHMT	Serine Hydroxymethyltransferase
SMX	Sulfamethoxazole
TB	Tuberculosis
THF	Tetrahydrofolic acid (Tetrahydrofolate)
THR	Threonine
TMP	Trimethoprim
TMQ	Trimetrexate
TRP	Tryptophan
TS	Thymidylate Synthase
WHO	World Health Organization
WT	Wild Type
XDR	Extensively Drug Resistance

TABLE OF CONTENTS

Page

LIST OF FIGURES

LIST OF TABLES

CHAPTER I

INTRODUCTION

Antimicrobials are becoming less effective throughout most species, if not all, due to the development of various resistance (Boucher, Talbot et al. 2009). This problem is further propagated by multi-drug resistant (MDR) strains developing various resistances, which give rise to extensively drug resistant diseases. This illustrates the need for the development of novel, potent and selective drugs for pathogens such as tuberculosis (TB), and malaria (Velayati, Masjedi et al. 2009, Das, Chakraborty et al. 2013).

Tuberculosis has been a serious health threat to the human race since long before the cause of the disease was even identified (1986, Bloom and Murray 1992). The complex combination of drugs and a long duration of treatment make it harder to eradicate this bug (Ditiu 2011) compared to other pathogenic diseases. Furthermore, the cost of treatment is expensive and this resulted in incomplete compliance with the treatment course, which led to the emergence of mutated TBs (Mitchison 2012, Pina, Clotet et al. 2012). For these reasons it is urgently required to put more effort to find a clue to develop a novel, selective, and fast-acting drug (World Health Organization. Regional Office for Europe., Dara et al. 2012). There are some drug targets that exclusively exist in tuberculosis, such as malate synthase and not found in human. However, many other drug targets exist in human and sometimes those two enzymes

have structural similarity, and dihydrofolate reductase is one of them. This is why we need to search for selective and potent inhibitors.

Malaria is also a serious health threat, and the deadliest form of malaria is caused by *Plasmodium falciparum,* which is a protozoan (Bjorkman and Bhattarai 2005). The malaria problem has also been exacerbated by resistance to practically all available drugs (World Health Organization. 2011). The combination of pyrimethamine (PYR, DHFR inhibitor) and sulfadoxine (SMX, dihydropteroate synthase (DHPS) inhibitor) has long been used as first line treatment for malaria (Wernsdorfer and Payne 1991). However, this combination has led to increased drug resistance, and the quadruple mutant of *Pf* DHFR-TS ((N51I/C59R/ S108N/I164L) is known to be most problematic to treat (Terlouw, Nahlen et al. 2003, Mbugi, Mutayoba et al. 2006). Even though WHO released a new 1st line malaria drug in 2010, artemisinin and its derivatives, and tried to minimize the chance of acquiring resistance by controlling the use of artemisinin family, resistance to these new drugs was already been reported (World Health Organization. Director-General's Office. Communications Office. 2006, White 2010).

In clinical and community-based environment, infections are of great concern especially in the United States, and it is still being further aggravated by the resistant strains in which most of the available drugs have already been compromised. *Staphylococcus aureus* is one of the well-known pathogens that cause a lot of infections in both clinical environment and community-based environment, and the methicillin-resistance Staphylococcus aureus (MRSA) has been a specific concern due to its tenacity

and difficulty for treatment. Since it was found in 1961, MRSA has become resistance to many of the available antibiotics such as methicillin, amoxicillin, and penicillin.

Dihydrofolate reductase (DHFR) is an enzyme that catalyzes the conversion of dihydrofolate (DHF) into tetrahydrofolate (THF) in the thymidylate cycle (Figure 1-1), which comprises serine hydroxymethyltransferase (SHMT), thymidylate synthase (TS), and DHFR (Douglas 1987).

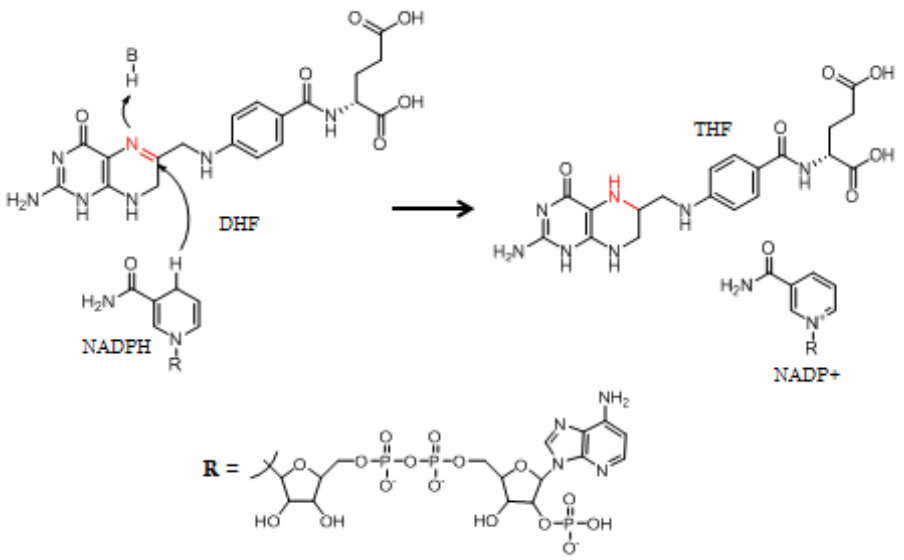

Figure 1-1. DHFR catalyzed conversion of DHF into THF. The reaction shows that a hydride is transferred from NADPH to the C-6 position of DHF to produce THF.

Tetrahydrofolate and dTMP, products of DHFR and TS respectively, are required for DNA and amino acid synthesis, making DHFR an attractive target for drug development in various species for a long time (Hitchings and Smith 1980). DHFR

inhibitors have been used against a number of different diseases from rheumatoid arthritis to psoriasis to cancer (Cody 1985, Zink, Lanig et al. 2004).

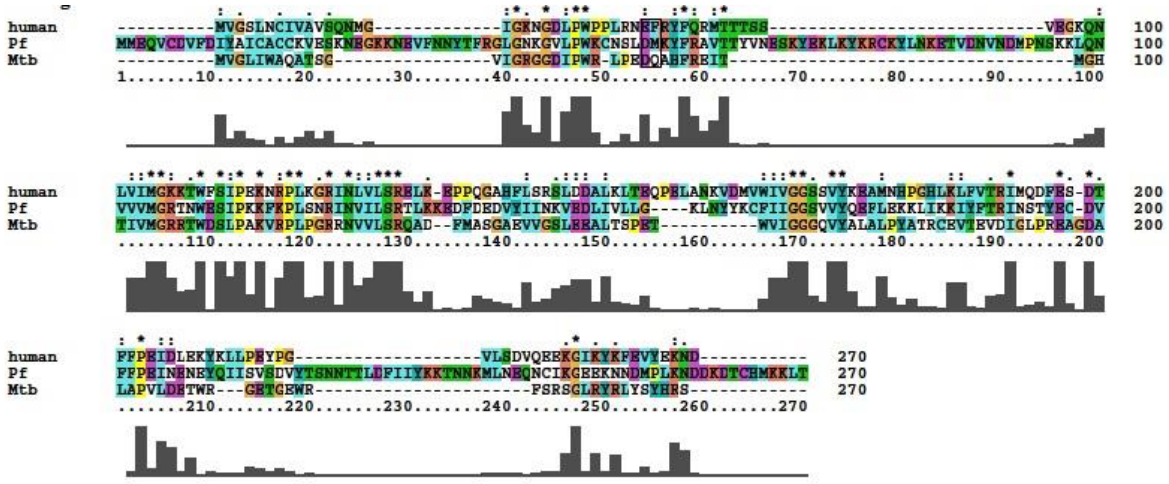

Figure 1-2. Sequence alignments of *M. tuberculosis*, wild type *P. falciparum*, and human DHFRs. Most of the important residues are well conserved such as Asp27, Phe31, or Tyr100 in *Mtb* DHFR.

DHFRs from various species show little sequence identity between them, especially between *Mtb* and human DHFR which is just 29% as we can see in the Figure 1-2, but exhibit surprisingly high similarity in the overall folding (Li, Sirawaraporn et al. 2000, Yuvaniyama, Chitnumsub et al. 2003). As seen in Figure 1-3, the overall structure is characterized by two main clefts, one that fits the cofactor, reduced nicotinamide adenine dinucleotide phosphate (NADPH) and the other for the substrate, dihydrofolate (DHF). *M. tuberculosis* DHFR consists of 159 residues and a monomer under physiological conditions (Li, Sirawaraporn et al. 2000). The overall structure also

contains 8 beta strands and flanking 4 alpha helices. With different inhibitors bound structures exhibited slight difference from this standard structure, i.e. 5 alpha helices instead of 4, but the overall structure is very well conserved throughout all DHFRs in our study. Human DHFR is comprised 186 residues and forms a monomer under physiological conditions. Unlike *Mtb* and human DHFR, *Pf* DHFR forms a complex with thymidylate synthase (TS) as one protein, but the overall folding and the core residues for DHFR active site are similar to *Mtb* DHFR (Yuvaniyama, Chitnumsub et al. 2003).

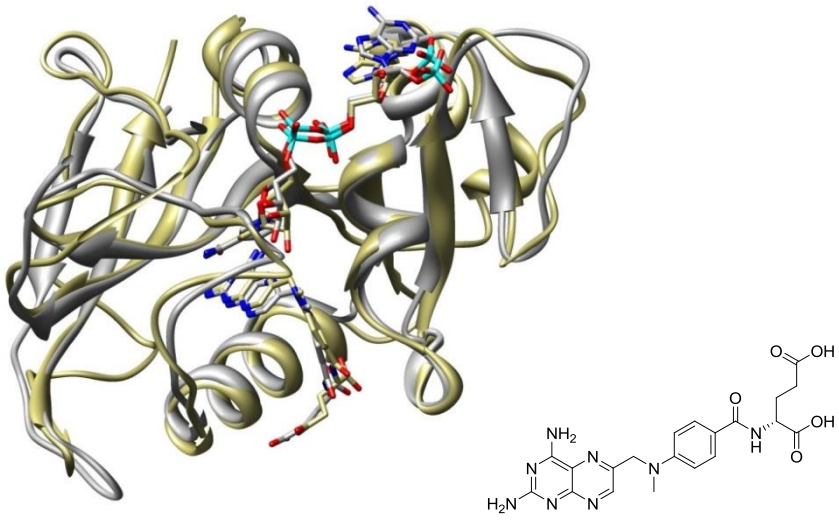

Figure 1-3. Superimposed overall structure of *Mtb* DHFR (gray, 1DF7) and human DHFR (khaki, 1U72) bound with methotrexate (MTX).

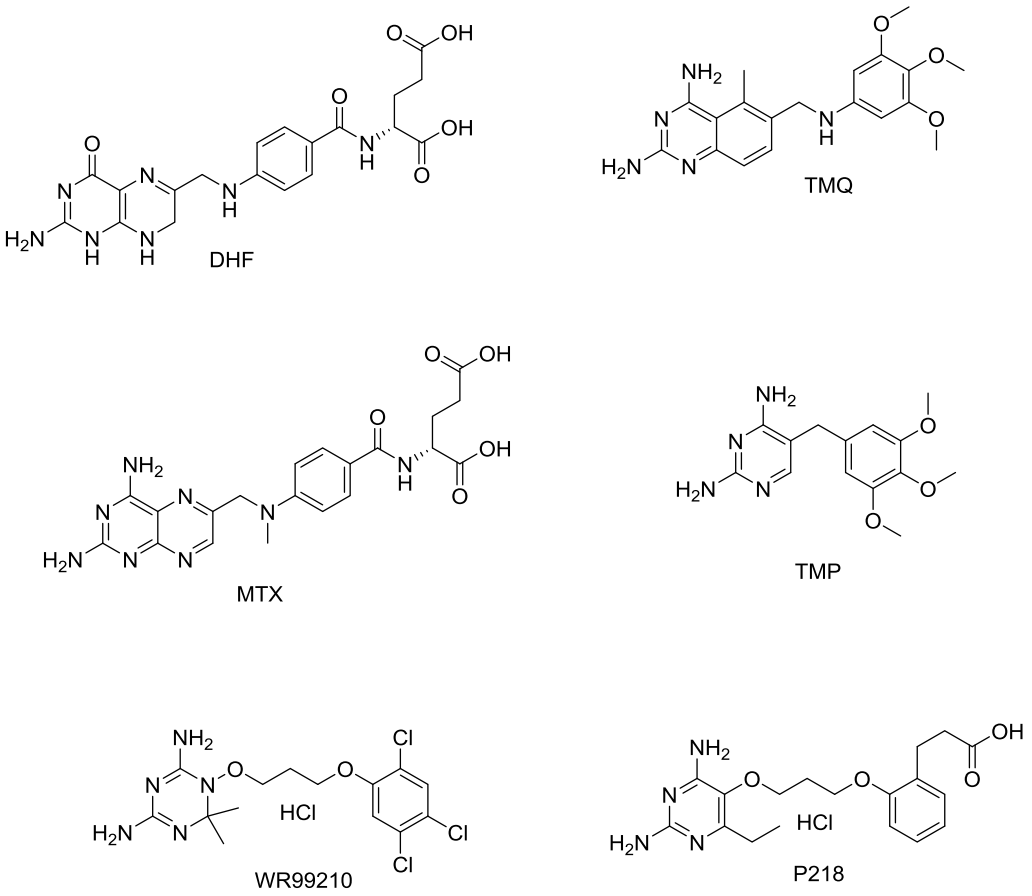

Figure 1-4. Chemical structure of known DHFR inhibitors and DHFR substrate, dihydrofolate (DHF).

Trimethoprim (TMP, Figure 1-4) is a well-known 1st generation DHFR inhibitor that shows great potency against bacteria including *E. coli* in combination with sulfa drugs (Amyes 1982). Trimethoprim and its derivatives are based on 2,4-diaminopyrimidine ring, and TMP has shown great potency and selectivity against many bacteria including *E. coli*. Because TMP is not potent against human DHFR, TMP has long been used as an antibiotic. However, trimethoprim showed only mild activity in *Mycobacterium tuberculosis*, 20 uM of IC_{50} (Unpublished data). Furthermore, it was

reported that TMP was not potent against *M. tuberculosis* without sulfamethoxazole (SMX) while SMX alone was potent enough against *M. tuberculosis* (Suling, Reynolds et al. 1998, Forgacs, Wengenack et al. 2009, Ong, Sievers et al. 2010). This TMP-SMX combination, along with pyrimethamine-SMX combination, caused point mutation in DHFR from many organisms, and in *S. aureus* DHFR, TMP/SMX combination is known to generate resistance through a major point mutation, F98Y. Low potencies have been observed in many of the compounds containing the pyrimidine ring instead of the quinazoline or the pterine ring, yet some of the pyrimidine ring-containing compounds have exhibited on DHFR such as WR99210. There also have been researches on the pyrimidine ring-containing selective inhibitors on *Staphylococcus aureus* DHFR and from other species.

Methotrexate (MTX) is another first generation DHFR inhibitor. It is a structural analog of the substrate of DHFR, dihydrofolate (DHF). It has been 60 years since MTX was first introduced as a DHFR inhibitor, and it is still being actively used as anticancer agent. Leucovorin is usually used along with MTX as a rescue agent. Unlike TMP, MTX and its derivatives are based on 2,4-diaminoquinazoline ring which has one more ring than 2,4-diaminopyrimidine. MTX also has a glutamate moiety with two carboxylic acids, and it is practically impossible to permeate the mycobacterium cell wall by simple diffusion. In human, there are two known transporter for MTX, and another probable transport in low pH has been discovered in 2004 (Wang, Zhao et al. 2004). In our study on mc^27000, which is a vaccine strain of *M. tuberculosis*, MTX displayed no activity up to 100 μM, while trimethoprim exhibited mild activity of 50 μM MIC.

Trimetrexate (TMQ/TMX) is one of the well-known 2nd generation DHFR inhibitors (Hoffman and Welsh 1995). As its name indicates, trimetrexate is a structural combination of two 1st generation DHFR inhibitors, trimethoprim (TMP) and methotrexate (MTX). Trimetrexate has been used to treat a wide variety of diseases including pneumonia and cancer (Ramanathan, Lipsitz et al. 1999, Garcia, Leichman et al. 2003, Senkovich, Bhatia et al. 2005, Short, Gilleece et al. 2009). It is an intriguing candidate for a drug against tuberculosis or malaria because it has a 2,4-diaminoquinazoline ring, which enables the compounds to better interact with DHFR compared to trimethoprim (TMP), but lacks diglutamate moiety, which could interfere with transport across the cell membrane without a specific carrier (Ge, Haska et al. 2007). TMQ has also been evaluated for anticancer agent in combination with leucovorin and 5-fluorouracil, which is a thymidylate synthase inhibitor (Punt, Keizer et al. 2002). Most of the 2nd generation DHFR inhibitors, including TMQ, have the side effect problem because they are potent on human DHFR as well, and some of the DHFR inhibitors are even used for cancer treatment (Matin, Jacobs et al. 2005). To be able to use any given DHFR inhibitor with the 2,4-diaminoquinazoline scaffold as an antimicrobial or antibacterial, selectivity comes into a crucial factor to consider. Unlike the DHFR inhibitors with 2,4-diaminopyrimidine scaffold such as TMP, the 2,4-diaminoquinazoline based compounds interact fairly similarly to both pathogenic DHFR and human DHFR.

Either pyrimidine-based or quinazoline-based DHFR inhibitors, especially for the antibiotic-purpose, selectivity comes into significant factor to consider because DHFR is

also an essential enzyme for human. Usually pyrimidine based DHFR inhibitors are less toxic to human DHFR and a good example is TMP. However, some of the pyrimidine-based DHFR inhibitors, when they have flexible linker as in WR99210, showed great potency on both pathogenic and human DHFRs, and there has been an attempt, on malarial DHFR, to develop a selective inhibitor that exclusively work against a pathogenic DHFR. One of the WR99210 analogs, P218, was published to be a successful compound that is selective against *P. falciparum* DHFR and it is under investigation for the purpose (Yuthavong, Tarnchompoo et al. 2012). Unlike the pyrimidine-based DHFR inhibitors, however, there has not been any report of potent and selective activity exclusively against pathogenic DHFRs.

Structure-based drug design, especially using x-ray crystallography as a main tool, is a well-known concept/methodology to develop a novel drug (Meng, Zhang et al. 2011). Crystal structures could give valuable information to the researchers to design/modify the inhibitors that effectively and exclusively work on the enzyme of interest, and further SAR study with enzymatic assay and/or structure elucidation help to proceed to the next step. Many scientists use a known inhibitor as a starting point and use the structure-based drug design to modify the structure to enhance the desired interactions with the enzyme of their study, and Krieger et al. successfully demonstrated how powerful and efficient this tool could be in the course of drug discovery through the structure-based drug designing study on the inhibitors of *Mycobacterium tuberculosis* malate synthase (Krieger, Freundlich et al. 2012). In our study, the DHFR structures from *M. tuberculosis, P. falciparum*, and *S. aureus* bound with different kind of analogs

of known DHFR inhibitors enabled us to modify the structures further to render the selectivity we desired to the compounds.

Based on the crystal structures available for *Mtb* DHFR and *Pf* DHFR-TS, the active sites, especially the substrate binding site, were closely examined. In the 2000 publication by Li et al. regarding the structural features of *Mtb* DHFR and how it compares to the human DHFR, a significant difference was mentioned (Li, Sirawaraporn et al. 2000, da Cunha, Ramalho et al. 2008). It was in the substrate binding site which is loosely surrounded by hydrophilic residues, while the same site is tightly crowded in human DHFR. One of the crucial differences in residues consisting of the pocket is Gln28 in *Mtb* DHFR, whose counterpart in human DHFR is Phe31. We discovered that flexibility of the residue in the pocket is more important than the hydrophilicity of the pocket. It was also found that the similar pocket is available in *Pf* DHFR substrate binding site. In *Pf* DHFR-TS, Met55 is near that pocket, which is corresponding to Gln28 in *Mtb* DHFR.

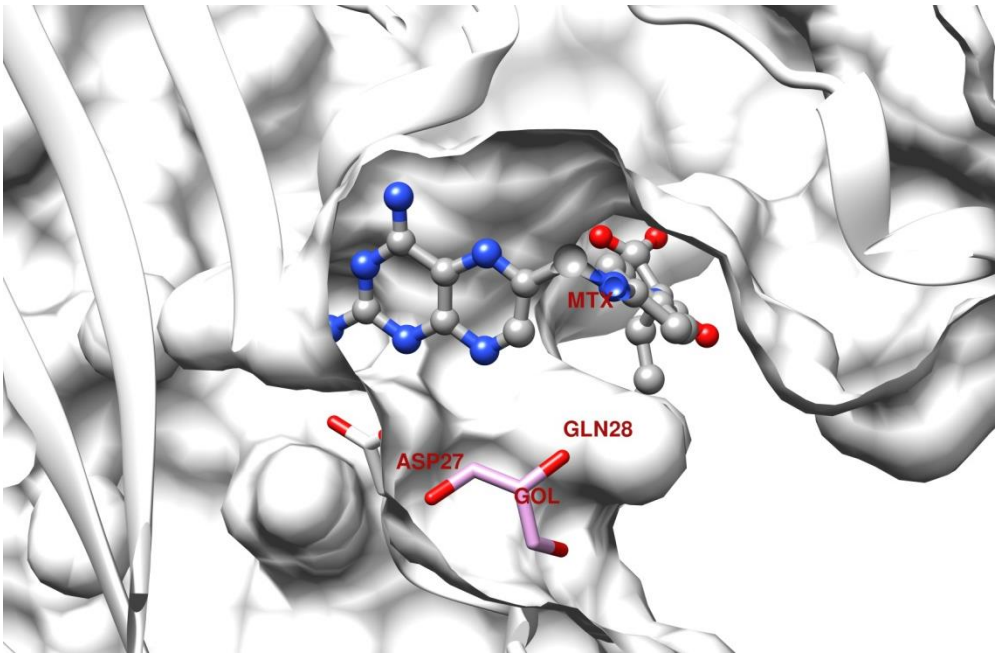

Figure 1-5. Surface view of *Mtb* DHFR:MTX. Asp27 and Gln28 (buried in the surface) are shown, and the glycerol molecule in the glycerol binding pocket. This glycerol binding pocket is the most noticeable difference between *Mtb* DHFR and human counterpart (1DF7). The similar space and a flexible residue (Met55) are available in *Pf* DHFR-TS.

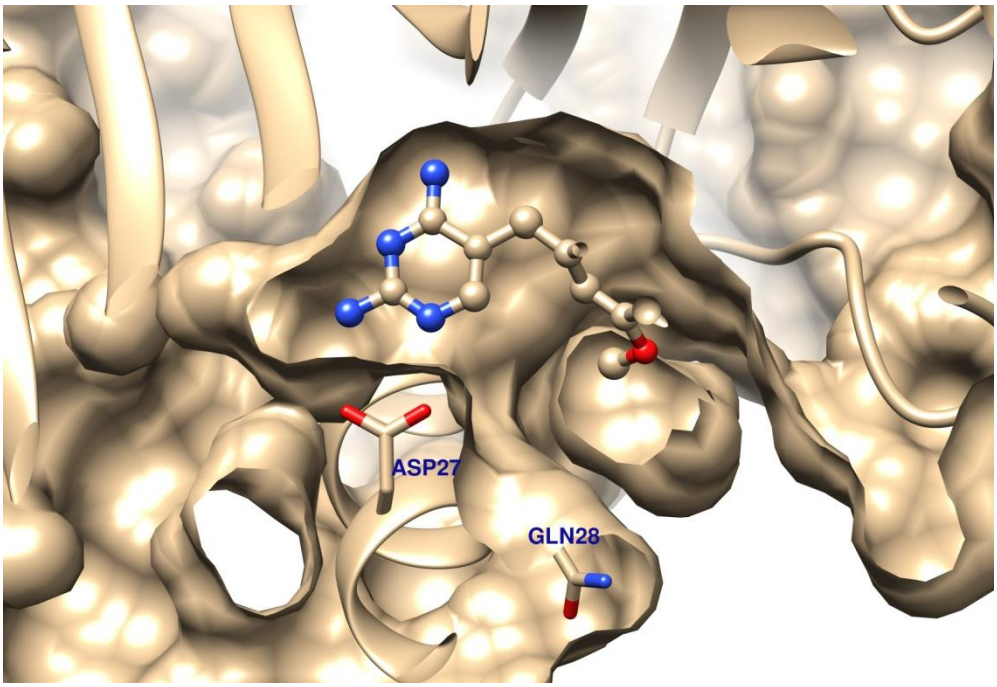

Figure 1-6. Surface view of *Mtb* DHFR:TMP. Though no glycerol was found in the glycerol binding pocket, Gln28 and the space is available in the structure (1DG5).

It was indeed possible to exploit this difference to get selectivity for *Mtb* DHFR and *Pf* DHFR-TS over human DHFR, which is crucial for development of selective drugs. At first, we expected that introducing only hydrophilic groups that can form hydrogen bonding interactions in the pocket may achieve the desired selectivity because it is surrounded by hydrophilic residues such as Trp22 or Gln28 (Figure 1-5, 1-6). But it turned out to be just partially true, and hydrophobic groups including benzyl group was enough to show great selectivity for *Mtb* DHFR and *Pf* DHFR-TS (Figure 1-7).

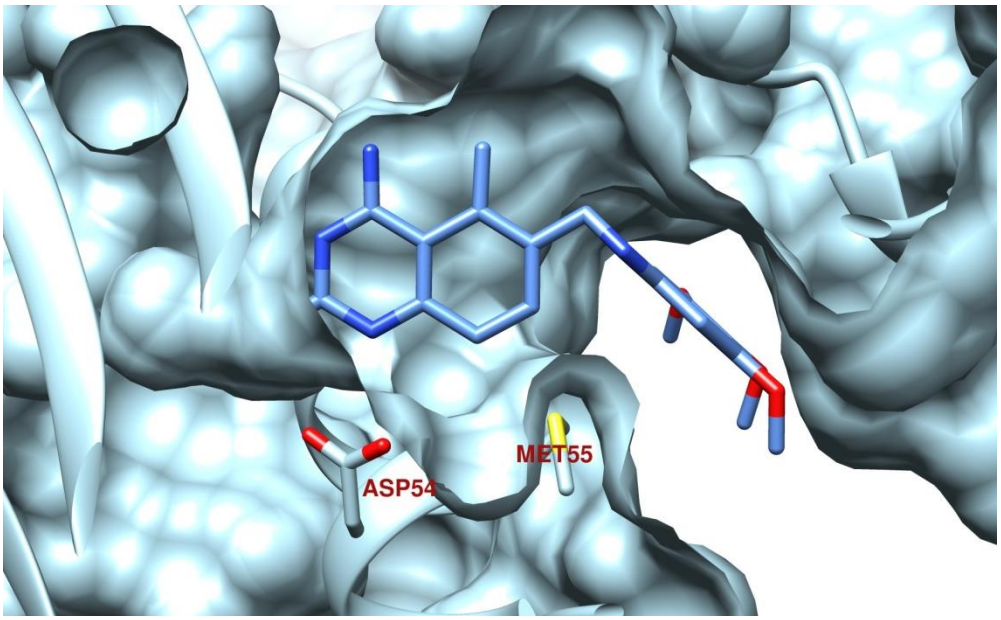

Figure 1-7. Surface view of WT *Pf* DHFR:TMQ. Asp54 and Met55 are shown and Met55 clearly occupies the glycerol binding pocket. This space and the flexible residue are not available in human DHFR.

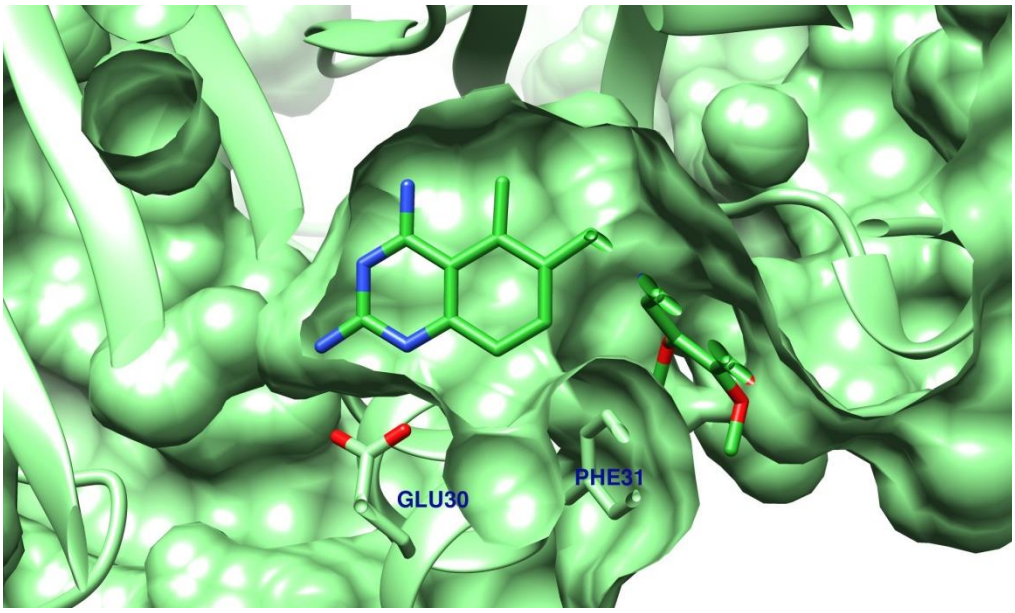

Figure 1-8. Surface view of human DHFR:TMQ. The space corresponding to the glycerol binding pocket in *Mtb* DHFR is occupied by bulky Phe31 and lack of flexibility of Phe31 makes human DHFR distinct from *Mtb* or *Pf* DHFR.

Based on the distinct difference found in *Mtb* DHFR (or *Pf* DHFR-TS) and human counterpart (Figure 1-8), two major modifications on trimetrexate (TMQ) were done, 3,4,5-trimethoxyaniline ring and C-8 position of quinazoline ring, and the selectivity gain, at least from our experiments, came mostly from C-8 quinazoline modification and without C-8 benzyl modification, there was no selectivity gain was observed. This result will be discussed in detail.

Based on the extensive structure-activity relationship (SAR) study on *Mtb* DHFR and human DHFR, we discovered that a residue next to the acid residue, usually Asp or Glu, plays a crucial role for our C-8 benzyl-2,4-diaminoquinazoline TMQ analogs to fit in the substrate binding pocket. The two pathogenic DHFRs we studied, *Mtb* DHFR and

Pf DHFR-TS, have Gln28 (*Mtb*) and Met55 (*Pf*) that are flexible enough with more than two rotational axis, and they were able to allow our C-8 benzyl analogs enough room to fit in. However, in human DHFR the corresponding residue is Phe31 which has a bulky side chain and has just one rotational axis. As a result, human DHFR and its Phe31 did not allow our C-8 benzyl TMQ analogs to sit in the substrate binding pocket. Even though there are many differences between *Mtb* DHFR and *Pf* DHFR-TS, it was quite possible to exploit the common structural feature those two DHFRs share and develop selective inhibitors. Furthermore, this common ground of the structural similarity is not limited to *Mtb* DHFR and *Pf* DHFR-TS. All the pathogenic DHFRs that have the common features that were shown in *Mtb* DHFR or *Pf* DHFR-TS, which are the space similar to the glycerol binding pocket in *Mtb* DHFR and the flexible residue next to the acid residue.

In this perspective, we performed a proof-of-concept validation study of our hypotheses that our C-8 benzyl TMQ could be used as broad spectrum selective antimicrobial/antibiotic using *Staphylococcus aureus* dihydrofolate reductase. This *Sa* DHFR is a very interesting comparison with *Mtb* DHFR, *Pf* DHFR-TS, and human DHFR because it is similar in size with *Mtb* DHFR, has the same acid residue (Asp27), and has Val28 instead of Gln28 compared to *Mtb* DHFR. Valine has much smaller side chain compared to Phenylalanine in human DHFR, but it has just one rotational axis just like Phenylalanine. Therefore, we speculated that it could tell us which factor is more important for our C-8 benzyl TMQ analogs binding, side chain size or rotational freedom. Overall folding of the *Sa* DHFR (wild type and F98Y single mutant) is very

similar to *Mtb* DHFR and the only noticeable difference close the active site came from a helix containing loop region of Ile50-Arg58.

CHAPTER II

SAR STUDY OF TMP AND MTX ANALOGS

II.1. Structure-Activity Relationship (SAR) Study of Trimethoprim (TMP) and its Analogs on *M. tuberculosis* DHFR and Human DHFR, and Methotrexate (MTX) and its Analogs on *Mtb* DHFR, *P. falciparum* DHFR, and Human DHFR

In this chapter, we will be discussing the initial structure-activity relationship (SAR) study of the two well-known DHFR inhibitors, TMP and MTX, and their derivatives. Despite the low sequence homology between *Mtb* DHFR and human DHFR, they share common overall fold and structure. This makes it quite challenging to develop a potent and selective inhibitor against *Mtb* DHFR. However, Li et al. discovered the structural differences between the two DHFRs in 2000 and one of them was a pocket available in *Mtb* DHFR near the substrate binding site and a glycerol molecule from the crystallization condition was found in that pocket in the crystal structure they published (1DF7) and they named the pocket the glycerol binding pocket (Li, Sirawaraporn et al. 2000).

We decided to utilize that glycerol binding pocket and made TMP and MTX our starting point of further SAR study and analogs development. TMP is potent and selective against *E. coli* DHFR, but, unfortunately, this is not the case against tuberculosis. TMP exhibited only mild potency on *Mtb* DHFR with IC_{50} of 19 uM. MTX

also is potent inhibitor for DHFR from various species, and it is potent on human DHFR as well and it has been used as anti-cancer agents. The challenges on these two starting compounds to develop potent and selective inhibitors were exactly opposite. Gaining potency on *Mtb* DHFR was required on TMP derivatization and lowering inhibition on human DHFR was desired on MTX derivatization.

Based on the crystal structures available for *Mtb* DHFR and human DHFR, we modified three well-known DHFR inhibitors, trimethoprim (TMP) and methotrexate (MTX). Trimethoprim (TMP) and methotrexate (MTX) are 1st generation DHFR inhibitors, and trimetrexate (TMQ) is the 2nd generation DHFR inhibitor. Extensive studies have been done on TMP and MTX analogs and we learned important clues to develop selective inhibitors. However, TMP and MTX both have their limitation to be a drug for TB. TMP exhibited low potency and MTX displayed no activity on the whole-cell assay.

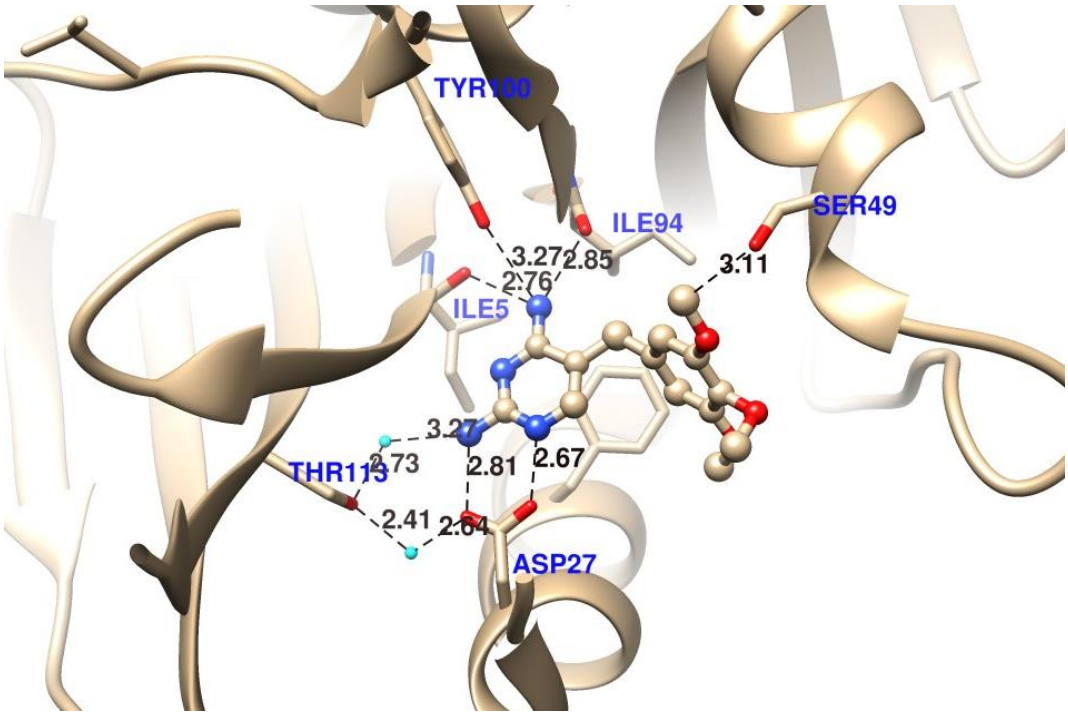

Figure 2-1. The conserved and important hydrogen bond interactions between TMP and *Mtb* DHFR exhibited in the crystal structure, 1DG5. Most of the interactions are with the 2,4-diaminopyrimidine ring, and with the 3,4,5-trimethoxybenzene ring has limited interaction with *Mtb* DHFR. Due to the smaller size of TMP, there is not much interaction on the 3,4,5-trimethoxybenzene ring side with *Mtb* DHFR.

In the trimethoprim (TMP) bound crystal structure of *Mtb* DHFR (1DG5), there are conserved hydrogen bonding interactions between TMP and *Mtb* DHFR residues (Figure 2-1). Asp27 has two hydrogen bonding interactions with 2-amino group and N-1 nitrogen with the distances of 2.81 Å and 2.67 Å, respectively. Asp27 further forms the hydrogen bonding network with Thr113 via a water molecule. The distance between Asp27 and the water molecule is 2.64 Å, and between the water molecule and Thr113 is 2.41 Å. Thr113 has another hydrogen bonding network via a different water molecule

with 2-amino group of TMP, and the distance between Thr113 and this water molecule is 2.73 Å and between the water molecule and the 2-amino group of TMP is 3.27 Å.

For 4-amino group of the 2,4-diaminopyrimidine ring of TMP has three hydrogen bonding interactions with the main chain carbonyl group of Ile5 and with the main chain carbonyl group of Ile94, and with the carbonyl group of Tyr100. The distances are 2.76 Å, 2.85 Å, and 3.27 Å, respectively.

The 3,4,5-trimethoxy ring have less interactions compared to 2,4-diaminopyrimidnie ring, and the closest contact comes with Ser49 and the distance is 3.11 Å. In this structure, the *m*-methoxy group on the benzene ring was approximately 5.5 Å from the glycerol binding pocket near the substrate binding site found in another structure, 1DF7. Even though there are glycerol molecules found in *Mtb* DHFR:TMP structure (1DG5), it is not the glycerol binding site we tried to take advantage of. It was speculated that the addition of a 3- or 4-carbon long aliphatic chain with some functional groups at the end would allow the inhibitor to fit in that pocket. The moiety, which interacts with the residues in the pocket, helped to get better selectivity, but not potency.

Two different categories of functional groups were tried. One group of compounds has a carboxylic acid group as in the substrate, dihydrofolate (DHF). The other group of compounds contains relatively hydrophobic groups including benzene ring. From the initial design, putting propanoic acid or butanoic acid at the *meta*-position of the benzene ring of the trimethoprim seemed an optimal fit into the pocket near the substrate binding site. However, the carboxylic acids in both of the carboxylic acid containing TMP analogs, JCS-1143 and JCS-1147, were found in the different site than the pocket near

the substrate binding site. Instead, the derivatives containing benzene or *p*-methoxy benzene fit in the pocket near the substrate binding site.

Trimethoprim (TMP), 2,4-diamino-5-(3',4',5'-trimethoxybenzyl)pyrimidine, is a well-known DHFR inhibitor. Derivatives of TMP have been synthesized to evaluate the possibility that greater selectivity could be achieved by taking advantage of the pocket near the substrate binding site in *Mtb* DHFR. This pocket is not available in the human DHFR active site. Most of the derivatives have their structural modification on the trimethoxybenzene ring side, although changes on pyrimidine side also appear to contribute significantly to the improved selectivity.

Three methoxy groups do play a role in obtaining better potency on *Mtb* DHFR. JCS-1145, 5-(3-methoxybenzyl)pyrimidine-2,4-diamine, displayed that the degree of potency loss in terms of IC_{50} was about 30%, from 18.8 uM to 26 uM. This JCS-1145 have just one methoxy group and its mother compound, TMP, has three. The IC50 values for the important TMP analogs are listed in Table 2-1.

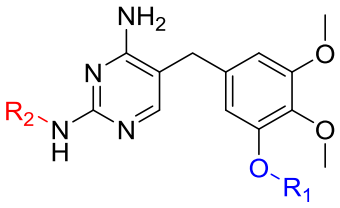

ID Number (JCS-)	Substitution on R_1	Substitution on R_2	IC_{50} on *Mtb* DHFR	IC_{50} on Human DHFR	Selectivity Index (Human/*Mtb*)
Trimethoprim (TMP)	3,4,5-trimethoxybenzene	H	19 uM	230 uM	12.1
1114	4-methoxybenzyl	H	18 uM	36 uM	2
1135	propylbenzyl	H	5.3 uM	1.6 uM	0.3
1143	4-butanoic acid	H	0.9 uM	0.9 uM	1
1147	3-propanoic acid	H	2.4 uM	7.8 uM	3.3
1163	4-carboxybenzyl	H	2.1 uM	13.2 uM	6.3
1168	4-methoxybenzyl	CH_3	26 uM	>1000 uM *	>38.5
1169	4-methoxybenzyl	CH_2CH_3	27 uM	>500 uM *	>18.5

*Higher concentrations could not be tested due to solubility.

Table 2-1. IC_{50} values of the major TMP analogs on *Mtb* and human DHFR. The selectivity values (IC_{50} on human DHFR/IC_{50} on Mtb DHFR) are also shown.

JCS-1163 along with JCS-1168 and -1169 are the TMP analogs that were successfully able to take advantage of the glycerol binding pocket, and they give us an interesting comparison because JCS-1163 has carboxybenzyl group attached on the TMP scaffold, while JCS-1168 and -1169 has methoxybenzyl group attached. This seemingly small difference made a huge difference in terms of selectivity. JCS-1168 has about 12-fold lower potency against *Mtb* DHFR compared to JCS-1163. However, the former has more than 5-fold higher selectivity compared to the latter.

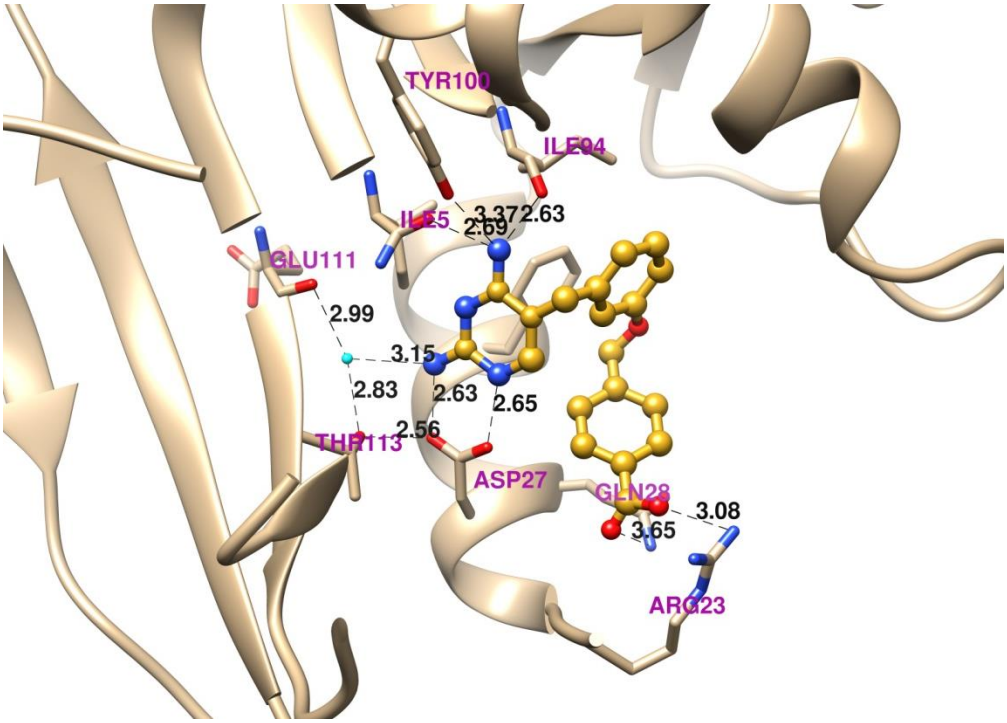

Figure 2-2. The conserved interactions between JCS-1163 and *Mtb* DHFR. 4-amino-Tyr100, 2-amino-Asp27, N1-Asp27, Carboxylic oxygen-Arg23, Carboxylic oxygen-Gln28 are shown. 2,4-diaminopyrimidine of JCS-1163 (gold) ring retains all the major interactions with *Mtb* DHFR. The middle benzene ring is not in a favorable position for interaction with Phe31 in the back. There is no significant interaction on the solvent access side of the DHFR.

In the crystal structure of *Mtb* DHFR:JCS-1163, the 2,4-diaminopyrimidine ring of JCS-1163 (Figure 2-2), similar to in trimethoprim (TMP) bound *Mtb* DHFR structure, has some conserved hydrogen bond interactions with *Mtb* DHFR. However, JCS-1163 displayed some different mode of interactions as well. Asp27 has two hydrogen-bonding interactions with 2-amino group and 1-N nitrogen with the distances of 2.63 Å and 2.65 Å, respectively. Asp27 forms another hydrogen bonding interaction with Thr113 with the distance of 2.56 Å. Thr113 forms hydrogen bonding network with 2-amino group of JCS-1163 via a water molecule, and the distance between the oxygen atom of the hydroxyl group of Thr113 and the water is 2.83 Å, and the distance between the water and 2-amino group is 3.15 Å. This water further forms another hydrogen bonding interaction with the main chain carbonyl group of Glu111 and the distance between the two is 2.99 Å.

For 4-amino group of the 2,4-diaminopyrimidine ring of JCS-1163 has three hydrogen bonding interactions with the main chain carbonyl group of Ile5, with the main chain carbonyl group of Ile94, and with the carbonyl group of Tyr100. The distances are 2.69 Å, 2.63 Å, and 3.37 Å, respectively.

Unlike 2,4-diaminopyrimidine side, 3-(4-benzoate)methoxybenzene ring side does not have much significant interactions with *Mtb* DHFR. The noticeable interactions came with Arg23 and Gln28. The oxygen atoms of the carboxylic acid have hydrogen bonding interactions with Arg23 and Gln28 with the distances of 3.08 Å and 3.65 Å, respectively.

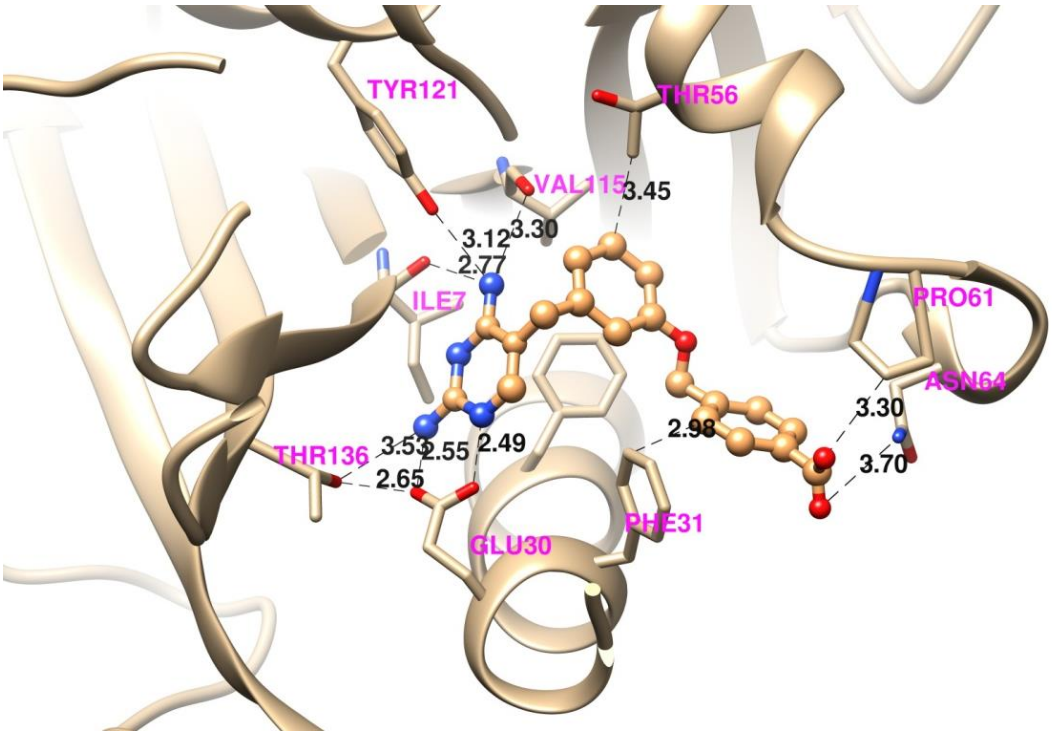

Figure 2-3. The important conserved interactions between JCS-1163 and human DHFR. 2,4-Diaminopyrimidine ring retains the major interactions similar to *Mtb* DHFR:TMP or JCS-1163. However, the 3-(4-benzoate)benzene ring side has much different orientation and mode of interactions compared to *Mtb* DHFR:JCS-1163. The bulky Phe31 keep the substituted benzene ring from coming into the space.

In the crystal structure of human DHFR:JCS-1163, the 2,4-diaminopyrimidine ring of JCS-1163, similar to in trimethoprim (TMP) or JCS-1163 bound *Mtb* DHFR structure, has some conserved hydrogen bond interactions with *Mtb* DHFR (Figure 2-3). However, JCS-1163 displayed some different mode of interactions as well. Glu30, corresponding to Asp27 in *Mtb* DHFR, has two hydrogen-bonding interactions with 2-amino group and 1-N nitrogen of JCS-1163 with the distances of 2.55 Å and 2.49 Å, respectively. Glu30 forms another hydrogen bonding interaction with Thr136,

corresponding to Thr113 in *Mtb* DHFR, with the distance of 2.65 Å. Thr136 forms hydrogen bonding network with 2-amino group of JCS-1163, and the distance between Thr136 and the 2-amino group of JCS-1163 is 3.53 Å.

For 4-amino group of the 2,4-diaminopyrimidine ring of JCS-1163 has three hydrogen bonding interactions with the main chain carbonyl group of Ile7, corresponding to Ile5 in *Mtb* DHFR, with the main chain carbonyl group of Val115 (Ile94 in *Mtb* DHFR), and with the carbonyl group of Tyr121 (Tyr100 in *Mtb* DHFR). The distances are 2.77 Å, 3.30 Å, and 3.12 Å, respectively.

Unlike 2,4-diaminopyrimidine side and unlike *Mtb* DHFR:JCS-1163, 3-(4-benzoate)methoxybenzene ring side does not have much significant interactions with human DHFR, yet more interactions were found than *Mtb* DHFR:JCS-1163. The noticeable interactions came with Pro61 and Asn64. The oxygen atom of the carboxylic acid has hydrogen bonding interaction with the nitrogen atom of Asn64 with the distances of 3.70 Å. The other oxygen of the carboxylic acid is in close proximity with Pro61 and the distance is 3.30 Å. Two other human DHFR residues are in close proximity with JCS-1163. The carbon atom of Thr56 is 3.45 A away from the 5-carbon of the 3-methoxybenzene ring, and the 3-carbon atom of Phe31 is 2.98 A away from 2-carbon atom of the benzoic acid ring. These two residues are not in hydrogen bond interaction with JCS-1163, yet they could be used as leverage for the further SAR study to improve potency or selectivity.

JCS-1163 displayed successfully that substitution on the methoxybenzene ring (4-carboxybenzene in JCS-1163's case) could take advantage of the glycerol binding

pocket, yet it was not enough to gain significant selectivity over human DHFR. This limitation was partially resolved by the alkylation on 2-amino group of the pyrimidine ring.

JCS-1168 (methyl) and JCS-1169 (ethyl) has alkyl group on 2-amino group of the pyrimidine ring and this helped those compounds to gain selectivity despite the loss of some potency on *Mtb* DHFR.

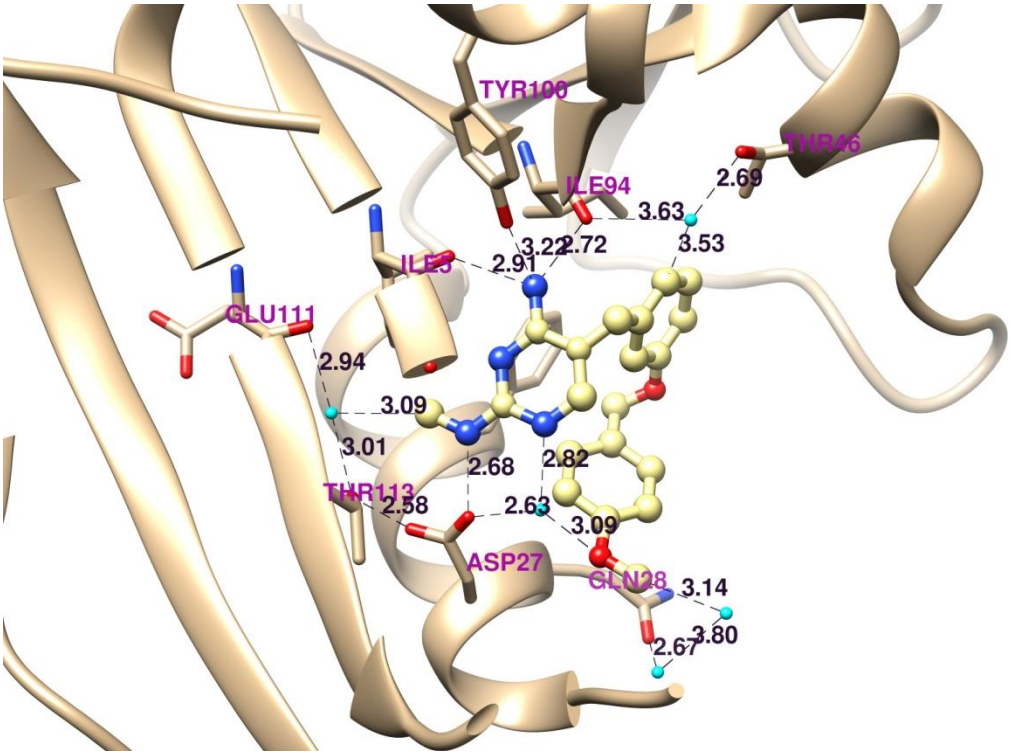

Figure 2-4. The important interactions between *Mtb* DHFR and JCS-1168. Note that interactions with Asp27 are significantly altered by the methyl group on 2-amino group. 4-methoxybenzyl group that is attached to the benzene ring is positioning near the glycerol binding site and Gln28 is pushed down to allow the necessary space to JCS-1168. There is no noticeable interaction near the solvent access site and that could be the reason of lower potency compared to other TMP analogs.

Similar to trimethoprim (TMP) bound *Mtb* DHFR structure, the 2,4-diaminopyrimidine ring of JCS-1168 has some conserved hydrogen bond interactions with *Mtb* DHFR (Figure 2-4). However, due to the methyl group attached to the 2-amino group, JCS-1168 displayed some different mode of interactions as well. Asp27 has just one hydrogen-bonding interaction with 2-amino group with the distance of 2.68 Å. Asp27 forms another hydrogen bonding network with 1-nitrogen atom via water molecule. The distance between Asp27 and the water is 2.63 Å and the distance between the water and 1-N is 2.82 Å. Asp27 further forms the hydrogen bonding network with Thr113 and the distance is 2.58 Å. Thr113 has another hydrogen bonding network via a water molecule with the main chain carbonyl group of Glu111, and the distance between Thr113 and this water molecule is 3.01 Å and between the water molecule and the carbonyl group of Glu111 is 3.15 Å. This water molecule is in close proximity with the 2-amino group of JCS-1168 with the distance of 3.09 Å, and if there is hydrogen bond available atom instead of methyl group, the potency could be enhanced.

For 4-amino group of the 2,4-diaminopyrimidine ring of JCS-1143 has three hydrogen bonding interactions with the main chain carbonyl group of Ile5, with the main chain carbonyl group of Ile94, and with the carbonyl group of Tyr100. The distances are 2.91 Å, 2.71 Å, and 3.22 Å, respectively. It is really interesting and somewhat puzzling even to see that this 4-amino group is well-retained hydrogen bonding interactions with the same groups as TMP or other TMP analogs that does not have methyl (or any group) on 2-amino group. The distances in JCS-1168 are even shorter than in *Mtb* DHFR:TMP. One possible explanation would be the binding of JCS-1168 with the methyl group on

the 2-amino side made some modification of the position of key residues to minimize the effect and loss of potency, and the in-depth follow up research could give us an answer for this observation.

For the 3-(4-methoxybenzoate)benzene ring side, the 5-carbon atom of the benzene ring is in close proximity with Ile94 with the distance of 3.43 Å. 4-carbon atom of the benzene ring is in close proximity with Leu50 with the distance of 3.91 Å. The carbon atom of 3-methoxy group of the benzene ring is in close proximity with Leu57 with the distance of 3.91 Å .Although these carbon atoms are not in hydrogen bonding interactions, they represent a potential venue for enhancing the interactions with DHFR.

JCS-1168 and JCS-1169 have alkyl substituent on 2-amino group of pyrimidine ring. When there is no substituent, 2-amino group along with N-1 nitrogen has hydrogen bonding interaction with Asp27 of *Mtb* DHFR. Based on the crystal structure of *Mtb* DHFR, JCS-1168 has lost significant amount of interactions with *Mtb* DHFR. For the normal pyrimidine or quinazoline rings have two hydrogen bonds with Asp27. However, due to the repulsive interaction of *N*-2 methyl group with water, the whole molecule was pushed away from the optimal position. As a result, JCS-1168's *N*-2 nitrogen has a hydrogen bond with the oxygen of Asp27 with the distance of 2.68 Å. There are three hydrogen bonds available for the nitrogen of *N*-4 amino group, Ile5, Ile94, and Tyr100. In *Mtb* DHFR:JCS-1168 structure, due to its non-optimal position, the distance between *N*-4 amino group and the main chain carboxylic acids of lle5 and Ile94, 2.91 Å and 2.72 Å respectively, is much closer than the hydroxyl group of Tyr100.

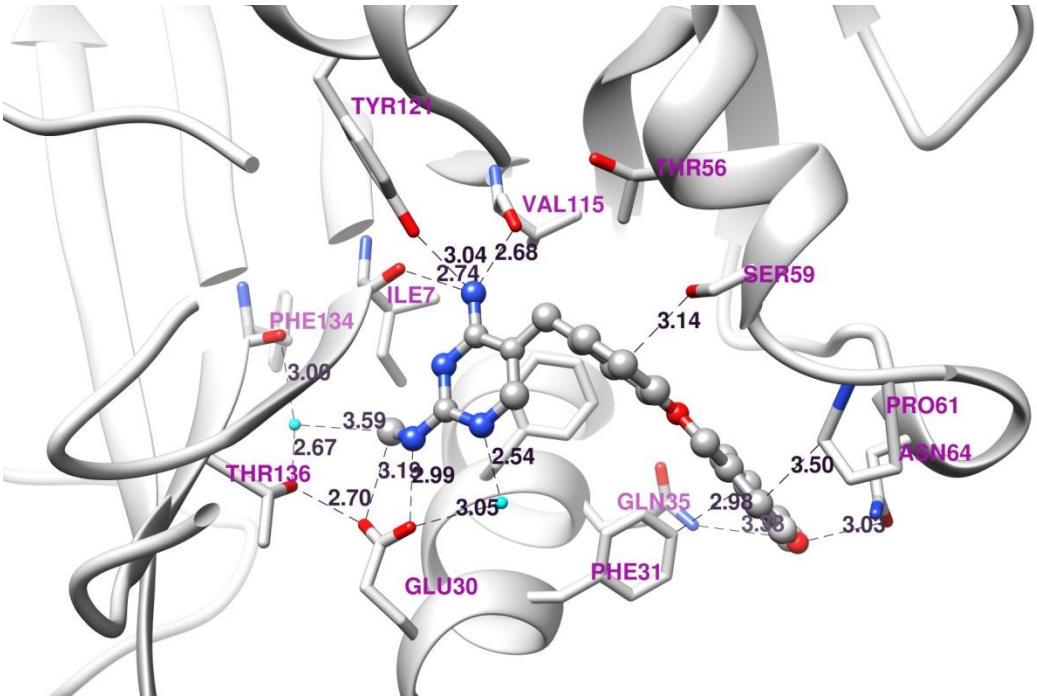

Figure 2-5. The important conserved interactions between JCS-1168 and human DHFR. Compared to *Mtb* DHFR:JCS-1168 structure, the two benzene rings have drastically different positions, while 2,4-diaminopyrimidine ring retains most of the important hydrogen bond interactions with human DHFR.

Similar to TMP or JCS-1168 bound *Mtb* DHFR structure, in the human DHFR, the 2,4-diaminopyrimidine ring of JCS-1168 has some conserved hydrogen bond interactions with human DHFR (Figure 2-5). However, due to the methyl group attached to the 2-amino group, JCS-1168 displayed some different mode of interactions as in *Mtb* DHFR:JCS-1168. Glu30, corresponding to Asp27 in *Mtb* DHFR, has just one hydrogen bonding interaction with 2-amino group with the distance of 2.99 Å. Glu30 also forms another hydrogen bonding network with 1-nitrogen atom via water molecule. The distance between Glu30 and the water is 3.05 Å and the distance between the water and

1-N is 2.54 Å. Glu30 further forms the hydrogen bonding network with Thr136, corresponding to Thr113 in *Mtb* DHFR, and the distance is 2.70 Å. Thr136 has another hydrogen bonding network via a water molecule with the main chain carbonyl group of Phe134, and the distance between Thr136 and this water molecule is 2.67 Å and between the water molecule and the carbonyl group of Phe134 is 3.00 Å. This water molecule is in close proximity with the 2-amino group of JCS-1168 with the distance of 3.59 Å, and if there is hydrogen bond available atom instead of methyl group, the potency could be enhanced.

For 4-amino group of the 2,4-diaminopyrimidine ring of JCS-1143 has three hydrogen bonding interactions with the main chain carbonyl group of Ile7, with the main chain carbonyl group of Val115, and with the carbonyl group of Tyr121. The distances between 4-amino group and those groups are 2.74 Å, 2.68 Å, and 3.04 Å, respectively. As in *Mtb* DHFR:JCS-1168 structure, this human DHFR:JCS-1168 displayed the same retention of the 4-amino group interactions with the key residues and their main chain carbonyl group. Considering that there is methyl group attached to the 2-amino group, this retention, along with *Mtb* DHFR:JCS-1168, is surprising.

For the 3-(4-methoxybenzoate)benzene ring side, the carbon atom of the 4-methoxy group of the terminal benzene ring is in close proximity with the nitrogen atom of Gln35 with the distance of 3.38 Å. The oxygen atom of the same methoxy group has potential hydrogen bond interaction with the oxygen atom of Asn64 and the distance between the two is 3.03 Å. 2-carbon atom of that terminal benzene ring is in close proximity with Pro61 with the distance of 3.50 Å. 5-carbon atom of the same benzene

ring is in close proximity with Phe31 with the distance of 2.98 Å, yet the orientation of the Phe31 is not favorable for any interaction. Although these carbon atoms are not in hydrogen bonding interactions, they represent a potential venue for enhancing the interactions with DHFR.

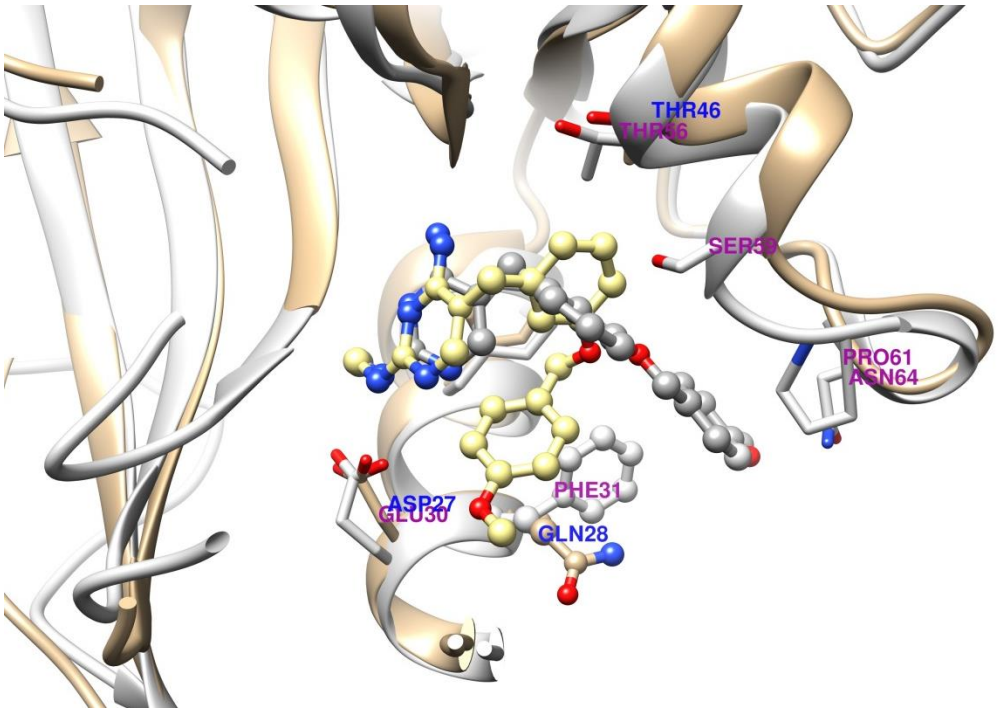

Figure 2-6. Superimposed structure of *Mtb* DHFR:JCS-1168 (khaki) and human DHFR:JCS-1168 (gray). JCS-1168's position is drastically different in each DHFR due to the difference between Phe31 (human) and Gln28 (*Mtb*). All the major residues, which are significantly different than each other, are shown. Human DHFR's loop region containing Pro61 is much closer to the JCS-1168 compared to *Mtb* DHFR.

The first analog that successfully place a functional group near the pocket is JCS-1168, 5-(3-(4-methoxybenzyloxy)benzyl)-N^2-methylpyrimidine-2,4-diamine, which has an *N*-2 methyl group on pyrimidine ring and showed less potency, IC_{50} of 26 uM, compared to trimethoprim (TMP) or its parent compound JCS-1114, 5-(3-(4-methoxybenzyloxy)benzyl)pyrimidine-2,4-diamine, whose IC_{50} on *Mtb* DHFR is 18 uM. However, as seen in Figure 2-6, the selectivity gain over human DHFR (IC_{50} = 1 mM) sufficiently outweighs this small potency loss with IC_{50} on *Mtb* DHFR (IC_{50} = 36 uM). The IC_{50} of TMP on human DHFR is 230 uM while that of JCS-1168 is well over 1 mM, and was limited by solubility. JCS-1168 has a *para*-methoxy group on the benzyl side of the compound and this *p*-methoxy group sits in the pocket near the substrate binding site in *Mtb* DHFR, when the crystal structure was superimposed with the methotrexate (MTX) bound *Mtb* DHFR structure, 1DF7. The 4-methoxybenzene substituent on the benzene ring side of JCS-1168 fits in the pocket near the substrate binding site in *Mtb* DHFR:JCS-1168 structure. Gln28 in the *Mtb* DHFR and its flexibility enable 4-methoxybenzene group to position in the pocket. On the other hands, in the human DHFR:JCS-1168 structure, the residue at the same position is Phe31, and it has drastically less rotational freedom compared to Glutamine. As a result, instead of sitting in the pocket near the substrate binding site, the same 4-methoxybenzene ring stretches toward the surface interacting with Asn64 with the distance of 3.03 Å.

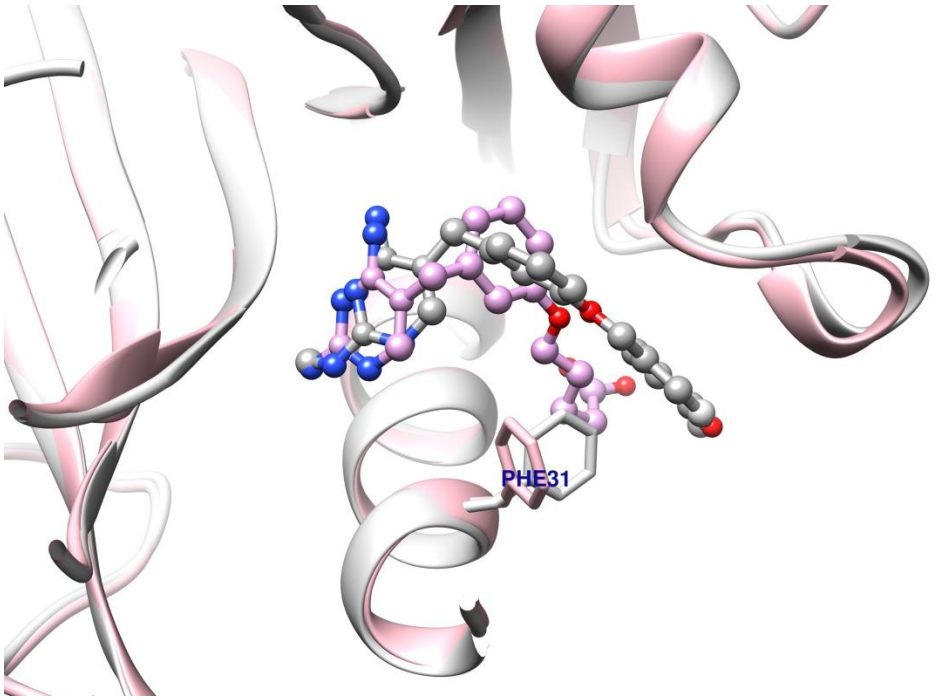

Figure 2-7. Superimposed structure of human DHFR:JCS-1143 (plum) and human DHFR:JCS-1168 (gray). It is clearly seen that JCS-1168 induces position change of Phe31. The bulky benzene ring on both JCS-1168 and human DHFR caused unfavorable positions for both Phe31 and the terminal benzene ring of JCS-1168. On the other hand, relatively flexible glutamic acid moiety of JCS-1143 does not force Phe31 to flip away from its original position.

When comparing human DHFR:JCS-1143 co-crystal structure with human DHFR:JCS-1168 co-crystal structure, in human DHFR:JCS-1168 structure, JCS-1168's benzene ring part stretches toward the loop region so that it could avoid an unfavorable contact with Phe31 (Figure 2-7). Because of this non-optimal position of JCS-1168 in human DHFR, interactions with Phe31/Phe34 are not available and it makes poor hydrogen bonding interaction with Glu30. It is worth mentioning that the only difference between JCS-1114 and JCS-1168 is one methyl group on the *N*-2 position of the

pyrimidine ring. This seemingly small difference has made a huge change in selectivity of the compounds between *Mtb* and human DHFR. Still the selectivity comes mainly from the loss of potency on human DHFR.

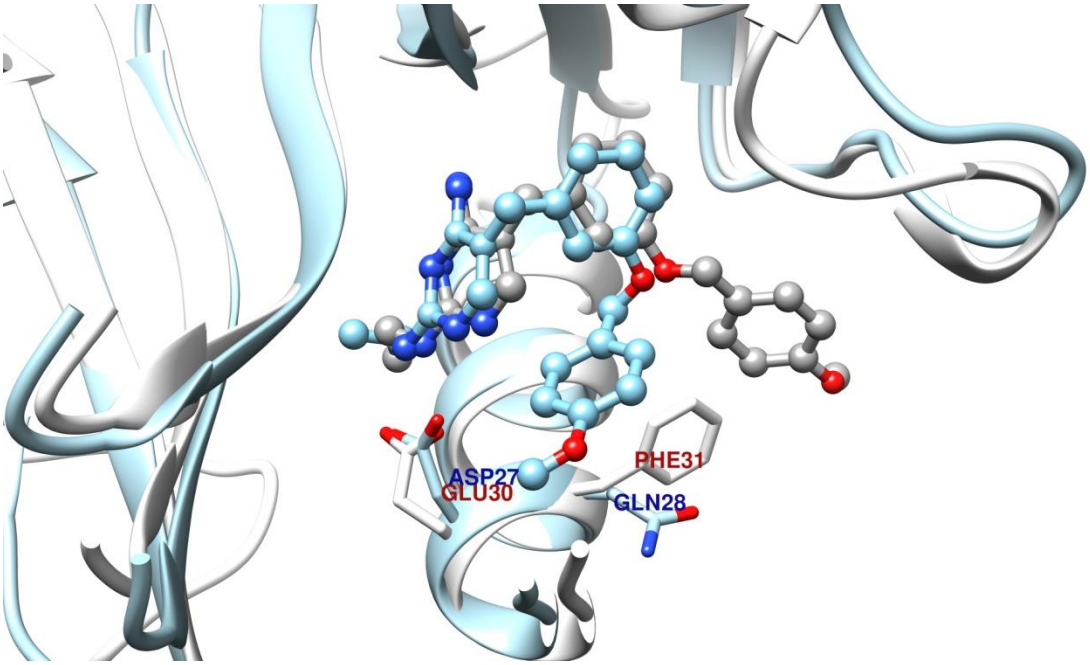

Figure 2-8. Superimposed structure of *Mtb* DHFR:JCS-1169 (blue) and human DHFR:JCS-1169 (gray). As in JCS-1168 bound structures, JCS-1169 has different position in *Mtb* and human DHFR, and bulky Phe31 (human) has kept JCS-1169 from entering the pocket.

The other compound that comes into glycerol binding pocket is JCS-1169, N^2-ethyl-5-(3-(4-methoxybenzyloxy)benzyl)pyrimidine-2,4-diamine (Figure 2-8). This compound has *N*-2 ethyl group on the pyrimidine ring, and shows poorer potency (IC_{50} = 28uM), and less selectivity compared to JCS-1168. One extra carbon and the steric

hindrance caused by it kept the pyrimidine ring from staying its regular position where it facilitates the maximum interaction with Asp27, Ile5, Ile94, and Tyr100. JCS-1168 also showed some degree of loss of position, but the ethyl group in JCS-1169 rather than the methyl group present in JCS-1168 aggravates this.

Superposition of the structures revealed the opportunity that could offer us a glimpse of the possible interactions in human DHFR (Figure 2-8). The same site where the glycerol binding pocket is located in *Mtb* DHFR is crowded by relatively hydrophobic residues like Leu22 or Pro26 in human DHFR. In the case of JCS-1168 or -1169, the bulk *p*-methoxybenzene group on the compound could have some degree of rotational freedom and they ended up positioning totally different than in *Mtb* DHFR avoiding the close contact with Phe31 in human DHFR, yet the position for JCS-1168 or -1169 to interact with DHFR is not the optimal. Also as we could see in human DHFR:JCS-1168 structure, Phe31 and its restricted rotational freedom makes it unfavorable for JCS-1168 and -1169 to bind to human DHFR.

The carboxylic acid moiety containing TMP analogs, such as JCS-1143 or JCS-1147, are more potent on *Mtb* DHFR, compared with the methoxybenzene containing analogs, including JCS-1168. From the crystal structure of *Mtb* DHFR:JCS-1143, it is clear that, due to lack of *N*-2 alkyl substitution, the pyrimidine ring can fit better in the substrate binding site, and better interactions were enabled. As a result, JCS-1143 has about 3 fold better IC_{50}, 0.9 uM, compared to JCS-1168, whose IC_{50} is 26 uM.

The effect of the glutamic acid group on the potency and selectivity has also been investigated. JCS-1143, 4-(3-((2,4-diaminopyrimidin-5-yl)methyl)phenyl)butanoic acid,

which has a carboxylic acid moiety mimicking the substrate, dihydrofolate (DHF), and a well-known DHFR inhibitor, methotrexate. Initially, this carboxylic acid group was thought to reside within the pocket near the substrate binding site. However, this carboxyl acid group stretches far away from the pocket to interact with two arginine residues, Arg32 and Arg60 at distances of 2.67 Å and 2.42 Å, respectively. The same phenomenon was witnessed with JCS-1147, a derivative that was shorter by one carbon, 3-(3-((2,4-diaminopyrimidin-5-yl)methyl)phenyl)propanoic acid

Similar to trimethoprim (TMP) bound *Mtb* DHFR structure, the 2,4-diaminopyrimidine ring of JCS-1143 has well-conserved hydrogen bond interactions with *Mtb* DHFR (Figure 2-9).

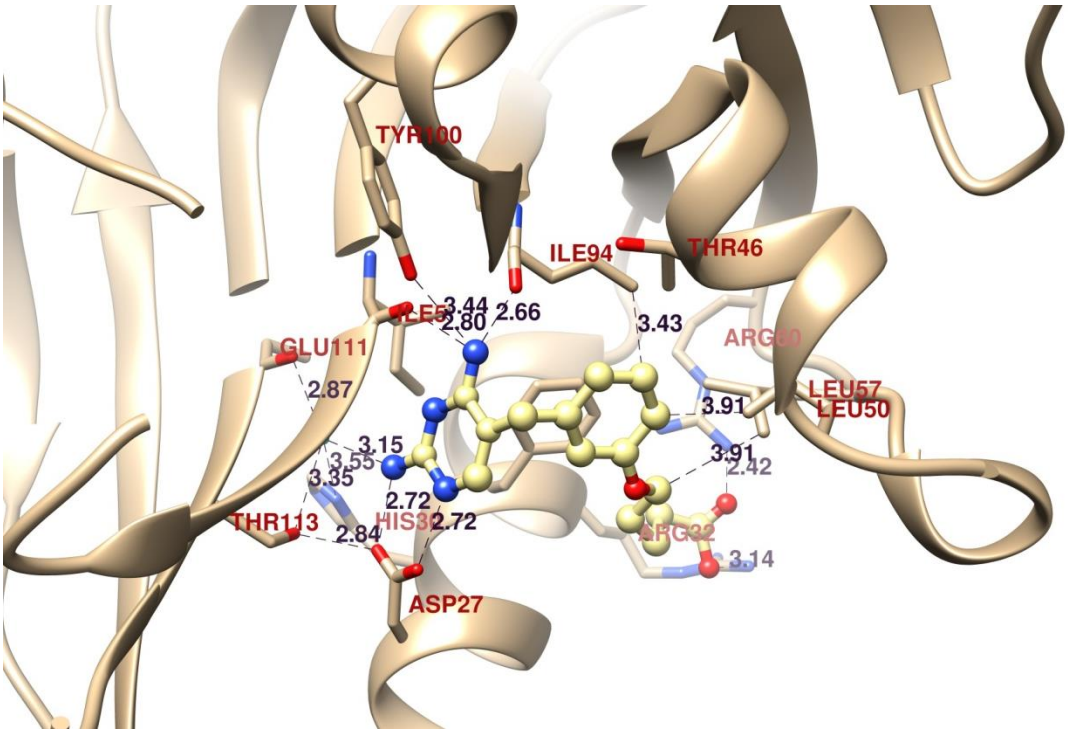

Figure 2-9. The conserved important hydrogen bond interactions between *Mtb* DHFR and JCS-1143. 2,4-diamionpyrimidine ring has pretty similar interactions with *Mtb* DHFR:TMP structure. The 3-pentanoic acid moiety has similar interactions with *Mtb* DHFR:MTX structure. Other than the two arginine residues (50 and 57), not much interactions are available between JCS-1143 and the *Mtb* DHFR.

Asp27 has two hydrogen bonding interactions with 2-amino group and N-1 nitrogen with the distances of 2.72 Å and 2.72 Å, respectively. Asp27 further forms the hydrogen bonding network with Thr113 and the distance is 2.84 Å. Thr113 has another hydrogen bonding network via a water molecule with 2-amino group of the 2,4-diaminopyrimidine ring of JCS-1143, and the distance between Thr113 and this water molecule is 3.35 Å and between the water molecule and the 2-amino group of TMQ is 3.15 Å. This water molecule further forms additional hydrogen bond interactions with

the main chain carbonyl group of Glu111 and the nitrogen of His30 with the distances of 2.87 Å and 3.55 Å, respectively.

For 4-amino group of the 2,4-diaminopyrimidine ring of JCS-1143 has three hydrogen bonding interactions with the main chain carbonyl group of Ile5, with the main chain carbonyl group of Ile94, and with the carbonyl group of Tyr100. The distances are 2.80 Å, 2.66 Å, and 3.44 Å, respectively.

For the 3-(4-butanoate)benzene ring side, the carboxylic acid moiety has two hydrogen bonding interactions with Arg32 and Arg60 with the distances of 3.14 Å and 2.42 Å, respectively. The 5-carbon atom of the benzene ring is in close proximity with Ile94 with the distance of 3.43 Å. 4-carbon atom of the benzene ring is in close proximity with Leu50 with the distance of 3.91 Å. The carbon atom of 3-methoxy group of the benzene ring is in close proximity with Leu57 with the distance of 3.91 Å . Although these carbon atoms are not in hydrogen bonding interactions, they represent a potential venue for enhancing the interactions with DHFR.

When *Mtb* DHFR:JCS-1143 structure is compared with 1DG8, *Mtb* DHFR:NADPH, the RMSD is 1.04 Å over 156 residues with 100% sequence identity. The sequence difference came from the N-terminal extra residues found in our *Mtb* DHFR:JCS-1143 structure. The largest deviations came from Asp48-Val54 loop region where benzene ring side of the compounds are in close contact, and Gly80-Pro89 loop which is away from the active site. When comparing human DHFR:JCS-1143 and human DHFR:folate, the RMSD is 0.60 Å over 184 residues with 100% sequence identity.

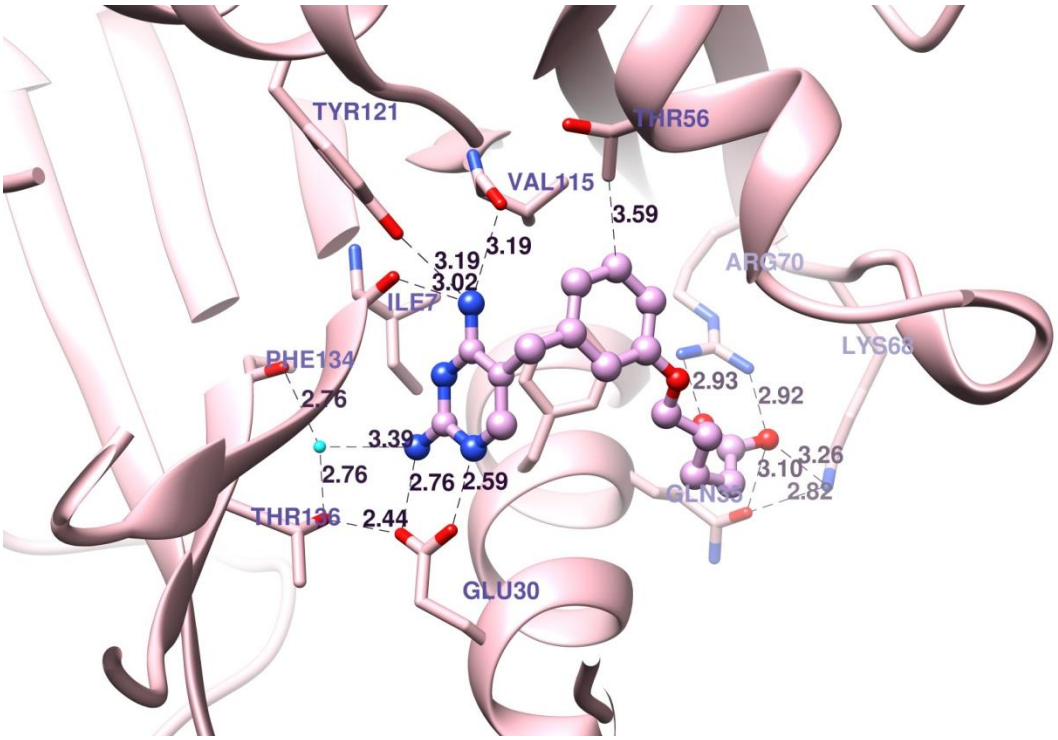

Figure 2-10. The conserved important hydrogen bond interactions between human DHFR and JCS-1143. 2,4-Diamionpyrimidine ring has very similar interactions with *Mtb* DHFR:TMP structure. The 3-pentanoic acid moiety has similar interactions with *Mtb* DHFR:JCS-1143 structure. The carboxylic acid moiety has similar interactions with Mtb DHFR:JCS-1143, but more interactions are available in the human DHFR.

Similar to trimethoprim (TMP) bound *Mtb* DHFR structure, the 2,4-diaminopyrimidine ring of JCS-1143 has well-conserved hydrogen bond interactions with human DHFR as well (Figure 2-10). Glu30, which is corresponding to Asp27 in *Mtb* DHFR, has two hydrogen bonding interactions with 2-amino group and N-1 nitrogen with the distances of 2.76 Å and 2.59 Å, respectively. Glu30 further forms the hydrogen bonding network with Thr136 and the distance is 2.44 Å. Thr136 has another

hydrogen bonding network via a water molecule with 2-amino group of the 2,4-diaminopyrimidine ring of JCS-1143, and the distance between Thr136 and this water molecule is 2.76 Å and the distance between the water molecule and the 2-amino group of TMQ is 3.39 Å. This water molecule further forms additional hydrogen bond interactions with the main chain carbonyl group of Phe134 with the distance of 2.76 Å .

For 4-amino group of the 2,4-diaminopyrimidine ring of JCS-1143 has three hydrogen bonding interactions with the main chain carbonyl group of Ile7, with the main chain carbonyl group of Val115, and with the carbonyl group of Tyr121. The distances of those interactions are 3.02 Å, 3.19 Å, and 3.19 Å, respectively.

For the 3-(4-butanoate)benzene ring side, the carboxylic acid moiety has two hydrogen bonding interactions with the two nitrogen atoms of Arg70 with the distances of 2.93 Å and 2.92 Å, respectively. One of the oxygens of the carboxylic acid further forms additional hydrogen bonding network with Lys68 and the oxygen of Gln35 that looks like a triad. The distance between the carboxylic acid and Lys68 is 3.26 Å, and between the Lys68 and the oxygen of Gln35 is 2.82 Å, and between the oxygen of Gln35 and the carboxylic acid is 3.10 Å. Additionally, the 3-carbon atom of the benzene ring is in close proximity with the carbon atom of Thr56 with the distance of 3.59 Å. Although this carbon atom is not engaged in any kind of hydrogen bonding interaction, this proximity could be taken into account for the further SAR study of the TMP analogs.

The last carboxylic acid containing molecule is JCS-1163, 4-((3-((2,4-diaminopyrimidin-5-yl)methyl)phenoxy)methyl)benzoic acid, whose IC_{50}s against *Mtb* and human DHFRs are 2.1 μM and 13.2 μM, respectively. This benzoic acid moiety

inserts into the pocket near the substrate binding pocket according to the crystal structure of *Mtb* DHFR:JCS-1163. 2-amino group and *N*-1 nitrogen of 2,4-diaminopyrimidine ring have hydrogen bonding interactions with Asp27 with the distances of 2.63 Å and 2.65 Å. 4-Amino group has hydrogen bonding interactions with main chain carbonyls of Ile5 and Ile94 and the distances are 2.69 Å and 2.63 Å, respectively. The carboxylic acid at the benzene ring side of the compound has close contact with Gln28 and the distance is 3.65 Å. JCS-1163 also has a hydrogen bonding interaction with Arg23 with the distance of 3.08 Å.

The different types of compounds have shown strikingly different results in the whole-cell assay as well. All of the carboxylic acid containing compounds, including benzoic acid moiety, exhibited no activity up to 100 uM on $mc^2$7000, although they are more potent in the *in-vitro* enzyme assay. However, all of the compounds containing hydrophobic group showed moderate activity, ranging from 25 uM to 50 uM.

The last two compounds that approach the pocket are JCS-1135, 5-(3-pheneethylbenzyl)pyrimidine-2,4-diamine, and JCS-1163, 4-((3-((2,4-diaminopyrimin-5-yl)methyl)phenoxy)methyl)benzoic acid. The latter has a carboxylic acid group, and will be discussed along with other carboxyl acid containing compounds. From the perspective of drug design, JCS-1135 was a control that could give us a clue for figuring out what kind of group should be attached to benzopyrimidine. It is unexpected that this purely hydrophobic group leans toward the hydrophilic environment of the glycerol binding pocket. This second benzene ring in the compound could be a guide to the entrance of the pocket. Superposition of crystal structure of *Mtb* DHFR with JCS-1135

on the previously known structure of *Mtb* DHFR with methotrexate, 1DF7, revealed that the ethylbenzyl group sits right in the edge of glycerol binding pocket so that any interaction with hydrophilic groups such as Asp27 or main-chain carbonyls could be avoided. It was an important clue for selectivity that all 4 compounds we have that went close or enter the pocket near the substrate binding site contain the benzyl moiety.

It is intriguing to see the results that no TMP analogs, without an aromatic ring on the 3,4,5-trimethoxybenzene ring, was able to reach the glycerol binding pocket of *Mtb* DHFR. For example, JCS-1143 and JCS-1147, which have just aliphatic carboxylic acid on the 3,4,5-trimethoxybenzene ring, exhibited fairly decent potency against *Mtb* DHFR with no selectivity. On the other hand, most of the aromatic ring on 3,4,5-trimethoxybenzene ring containing analogs were able to reach the glycerol binding pocket and displayed selectivity with the degree ranging from mild to more than 30 fold of selectivity. This finding led us to try more aromatic ring containing analogs on TMQ rather than just aliphatic groups later on.

Though creating derivatives of TMP provided compounds with good selectivity over human DHFR, the challenge remained to make compounds with sufficiently high potency against *Mtb* DHFR. The low potency might be due to lack of second aromatic ring of the compounds, i.e. pyrimidine instead of quinazoline, and our subsequent study have shown that this second ring is crucial for interaction with Phe31 of *Mtb* DHFR and for the improved potency.

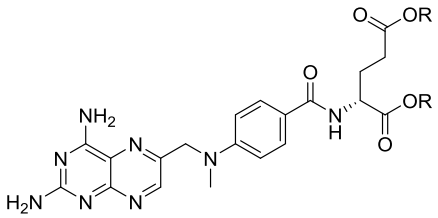

ID (JCS-)	R	IC_{50} on *Mtb* DHFR (nM)	IC_{50} on human DHFR (nM)	Selectivity	MIC on H37Rv (μM)
MTX	H	6	6	1	> 100
1183	$-CH_2CH_3$	30	25	0.8	1.6
1187	$-CH_3$	50	40	0.8	0.4

Table 2-2. IC_{50} and MIC values of MTX and its analogs against *Mtb* DHFR and human DHFR. Selectivity values and MIC values are shown as well.

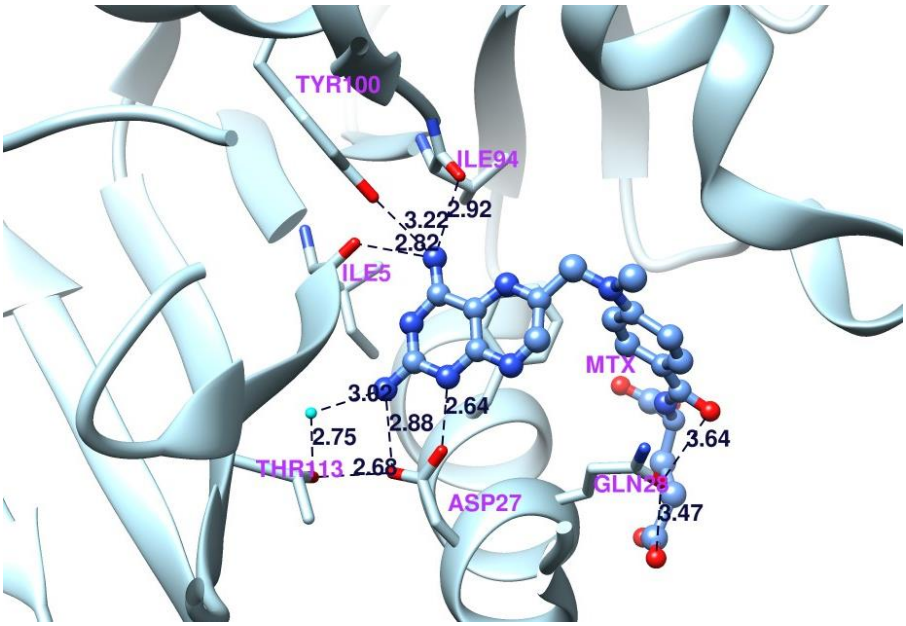

Figure 2-11. The conserved hydrogen bond interactions between MTX and *Mtb* DHFR. Similar to TMP, most of the interactions are on 2,4-diaminoquinazoline ring, and there are additional interactions available with the glutamic acid moiety of MTX not shown in the picture (1DF7).

Methotrexate (MTX) is a well-known 1st generation DHFR inhibitor. The key analogs and their activities are listed in Table 2-2. MTX exhibited excellent potency on *Mtb* DHFR *in-vitro* enzyme assay (IC_{50} = 5 nM), and *Mtb* DHFR crystal structure with MTX bound was solved in 2000 by Li et al.(Li, Sirawaraporn et al. 2000). This *Mtb* DHFR structure bound with MTX displayed the well-conserved hydrogen bonding interactions between *Mtb* DHFR and MTX similar to TMP bound structure (Figure 2-11). Asp27 has two hydrogen bonding interactions with 2-amino group and N-1 nitrogen with the distances of 2.88 Å and 2.64 Å, respectively. Asp27 further forms the hydrogen bonding network with Thr113 and the distance is 2.68 Å. Thr113 has another hydrogen

bonding network via a water molecule with 2-amino group of the quinazoline ring of MTX, and the distance between Thr113 and this water molecule is 2.75 Å and between the water molecule and the 2-amino group of MTX is 3.02 Å.

For 4-amino group of the 2,4-diaminoquinzaoline ring of MTX has three hydrogen bonding interactions with the main chain carbonyl group of Ile5, with the main chain carbonyl group of Ile94, and with the carbonyl group of Tyr100. The distances are 2.82 Å, 2.92 Å, and 3.22 Å, respectively.

The glutamic acid moieties have less interactions compared to 2,4-diaminopyrimidnie ring, and the closest contacts come with Gln28 and the distances are 3.47 Å and 3.64 A. There are additional interactions, available from another glutamic acid moiety, not shown in the picture, and those interactions will be discussed later.

When comparing *Mtb* DHFR:MTX (PDB ID:1DF7) with human DHFR:MTX, the overall protein folding and active site structure is very similar. Both DHFRs have clefts for the substrate (DHF) and the cofactor (NADPH) in the same site, and the overall secondary structures are well overlapped (Figure 2-12).

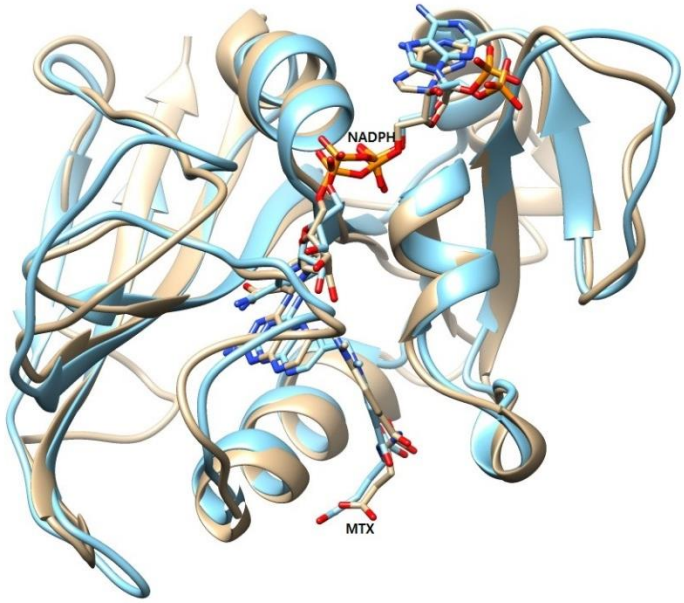

Figure 2-12. Superimposed structure of *Mtb* DHFR:MTX (blue) and human DHFR:MTX. Note that the overall folding, and active sites (substrate and cofactor binding sites) structure are pretty similar. MTX and cofactor (NADPH) are labeled.

The important residues in *Mtb* DHFR that interact with MTX are similar to TMP as well. The distances between 2,4-diaminoquinazoline ring and Asp27 (*Mtb*) are 2.88 Å and 2.64 Å. The corresponding distances in human DHFR are 2.64 Å and 2.60 Å, respectively. In *Mtb* DHFR, Arg60 has a close contact with one of the glutamic acids with the distances of 2.79 Å and 2.66 Å. The corresponding residue in human DHFR is Arg70 (Figure 2-13), and Arg70 has an interaction with carbonyl oxygen with a distance of 2.13 Å. The remaining carboxylate and another carbonyl group right next to the aniline ring have interactions with Asn64 with distances of 3.45 Å and 2.94 Å. Arg32 in

Mtb DHFR has interaction with MTX and the distance is 3.00 Å. The corresponding residue in human DHFR is Gln35, and the distance between MTX and Gln35 is 3.04 Å.

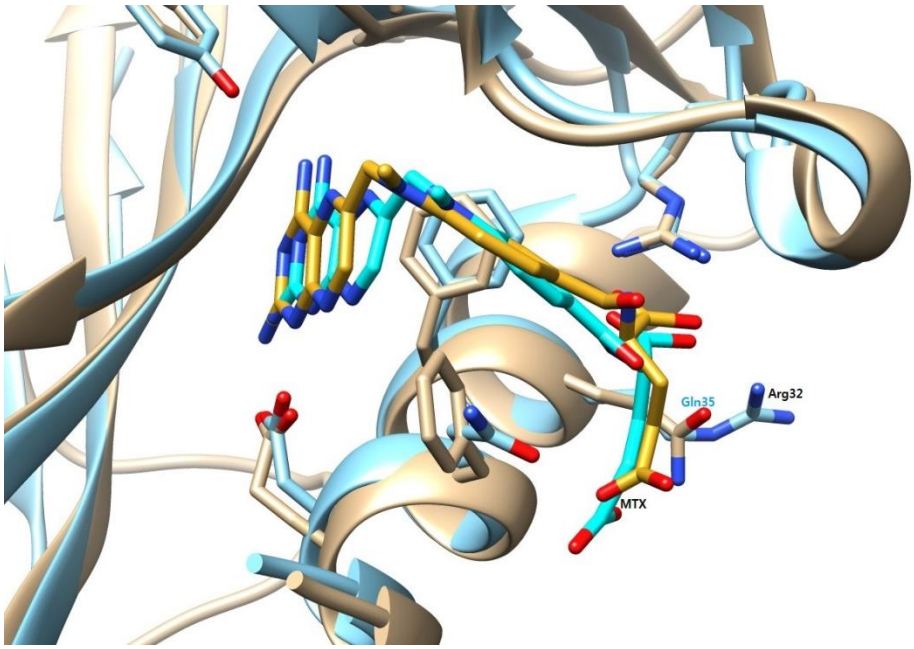

Figure 2-13. Superimposed structure of *Mtb* DHFR:MTX (blue) and human DHFR:MTX in the active site. Di-glutamic acids in MTX have similar interactions in both DHFRs. It is clearly seen that the space near C-8 position of the MTX is very tight in human DHFR due to the presence of a bulky phenylalanine.

In spite of its excellent potency on many DHFRs from different species, MTX did not exhibit great potency on TB whole cell assays, either $mc^2$7000 vaccine strain or H37Rv. This is due to the di-glutamic acid moiety that MTX has and this hydrophilic moiety hinders MTX to pass through TB cell wall without proper transporter. To overcome this challenge, we tried alkylation on MTX's di-glutamic acid moiety. JCS-

1183 (ethyl) and JF-1187 (methyl) showed slightly reduced potency on both Mtb and human DHFR. However, they exhibited great potency on the whole cell assay on H37Rv. These ester-containing MTX derivatives clearly increased the permeability of the MTX through TB cell wall and cell membrane. There should be more in-depth study on whether the esters are hydrolyzed inside the cell before acting on the target or the intact esters are potent enough to exhibit the observed potency on H37Rv.

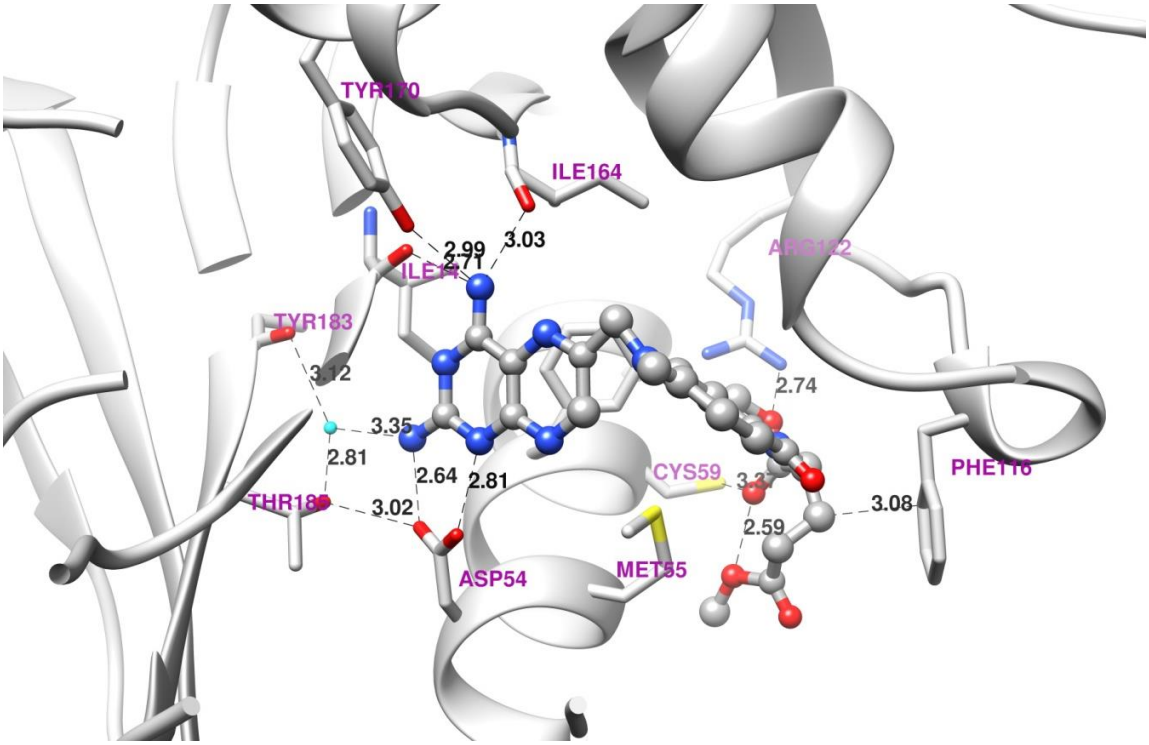

Figure 2-14. The important conserved interactions between WT *Pf* DHFR and JCS-1187. The 2,4-diaminoquinazoline ring retains all the major interactions with Pf DHFR just as in *Mtb* DHFR:MTX structure. There are some differences in interactions in the esterified glutamic acid moiety such as the additional interaction from Arg122 or Cys59.

The crystallization trials to obtain crystal structures of *Mtb* DHFR:JCS-1187 or JCS-1183 were not successful. Instead, we elucidated the crystal structure from WT *Pf* DHFR. There should be some differences between *Mtb* DHFR and *Pf* DHFR, yet this WT *Pf* DHFR:JCS-1187 structure could allow us to understand the ideas regarding the interactions between DHFR and JCS-1187 and other MTX analogs (Figure 2-14).

This WT *Pf* DHFR structure bound with JCS-1187 displayed the well-conserved hydrogen bonding interactions between WT *Pf* DHFR and JCS-1187 similar to MTX bound *Mtb* DHFR structure. Asp54, corresponding to Asp27 in *Mtb* DHFR, has two hydrogen bonding interactions with 2-amino group and N-1 nitrogen with the distances of 2.64 Å and 2.81 Å, respectively. Asp54 further forms the hydrogen bonding network with Thr185 and the distance is 3.02 Å. Thr185 has another hydrogen bonding network via a water molecule with 2-amino group of the quinazoline ring of JCS-1187, and the distance between Thr185 and this water molecule is 2.81 Å and between the water molecule and the 2-amino group of JCS-1187 is 3.35 Å. This water molecule further forms an additional hydrogen bonding interaction with the main chain carbonyl group of Tyr183 with the distance of 3.12 Å.

For 4-amino group of the 2,4-diaminoquinzaoline ring of JCS-1187 has three hydrogen bonding interactions with the main chain carbonyl group of Ile14, corresponding to Ile5 in *Mtb* DHFR, with the main chain carbonyl group of Ile164 (Ile94 in *Mtb* DHFR), and with the carbonyl group of Tyr170 (Tyr100 in *Mtb* DHFR). The distances are 2.71 Å, 3.03 Å, and 2.99 Å, respectively.

The esterified glutamic acid moieties have less interactions compared to 2,4-diaminopyrimidnie ring, and the closest contacts came with Arg122 and Cys56. The methoxy oxygen of one of the methyl ester has a hydrogen bond interaction with the nitrogen of Arg122 with the distance of 2.74 Å. The carbonyl group of the same methyl ester has a hydrogen bonding interaction with the thiol group of Cys56 with the distance of 3.37 Å. This carbonyl group forms further hydrogen bonding interaction with the oxygen atom of the other methyl ester and the distance between the two is 2.59 Å.

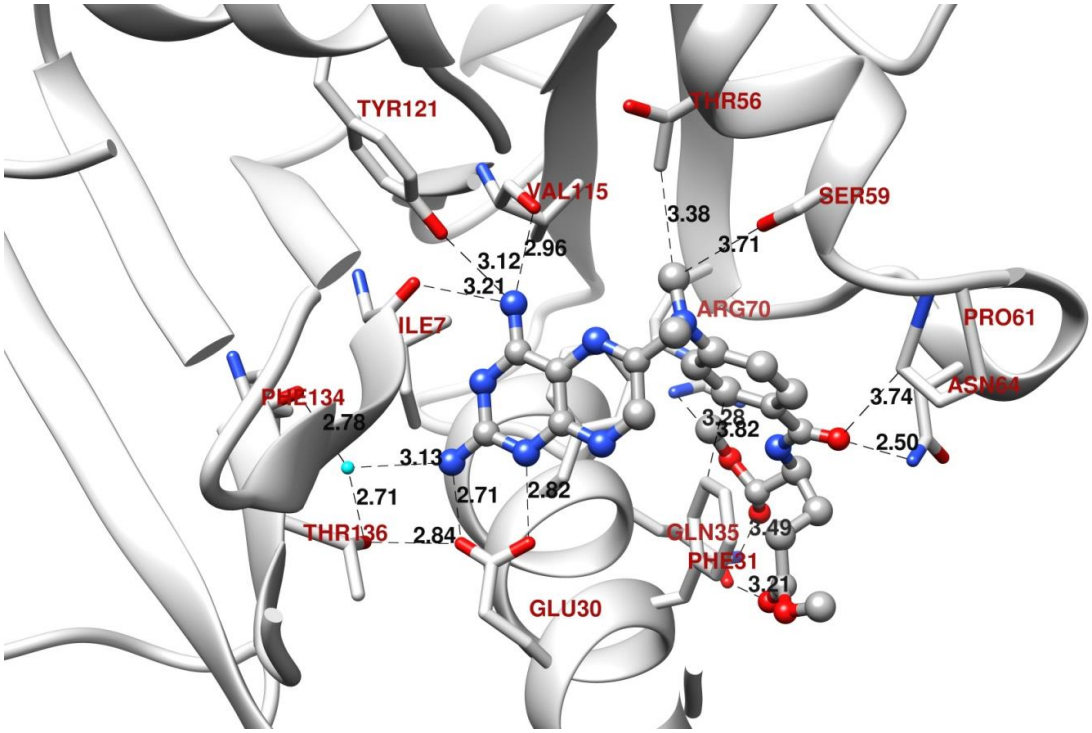

Figure 2-15. The important conserved interactions between human DHFR and JCS-1187. 2,4-Diaminoquinazoline ring retains all the major interactions as in WT *Pf* DHFR:JCS-1187 and other structures. The methyl ester of the glutamic acid has more diverse interactions compared to WT *Pf* DHFR:JCS-1187 with human DHFR including Gln35 or Asn64.

On the other hand, human DHFR structure bound with JCS-1187 displayed the well-conserved hydrogen bonding interactions between human DHFR and JCS-1187 similar to MTX bound *Mtb* DHFR structure or WT *Pf* DHFR:JCS-1187 structure (Figure 2-15). Glu30, corresponding to Asp27 in *Mtb* DHFR, has two hydrogen bonding interactions with 2-amino group and N-1 nitrogen with the distances of 2.71 Å and 2.82 Å, respectively. Glu30 further forms the hydrogen bonding network with Thr136 and the distance is 2.84 Å. Thr136 has another hydrogen bonding network via a water molecule with 2-amino group of the 2,4-diaminoquinazoline ring of JCS-1187, and the distance between Thr136 and this water molecule is 2.71 Å and the distance between the water molecule and the 2-amino group of JCS-1187 is 3.13 Å. This water molecule further forms an additional hydrogen bonding interaction with the main chain carbonyl group of Phe134 with the distance of 2.78 Å.

For 4-amino group of the 2,4-diaminoquinzaoline ring of JCS-1187 has three hydrogen bonding interactions with the main chain carbonyl group of Ile7, corresponding to Ile5 in *Mtb* DHFR, with the main chain carbonyl group of Val115 (Ile94 in *Mtb* DHFR), and with the carbonyl group of Tyr121 (Tyr100 in *Mtb* DHFR). The distances are 3.21 Å, 2.96 Å, and 3.12 Å, respectively.

The methyl ester of the glutamic acid moieties have less interactions compared to 2,4-diaminopyrimidnie ring, yet there are more interactions available compared to WT *Pf* DHFR:JCS-1187. The methoxy oxygen of one of the methyl ester has a hydrogen bond interaction with the nitrogen of Arg70 with the distance of 3.28 Å. The carbonyl groups of both methyl esters have hydrogen bonding interactions with the oxygen and

the nitrogen of Gln35 and the distances are 3.21 Å and 3.49 Å, respectively. The 4-carbonyl group of the aniline ring also has hydrogen bonding interaction with the nitrogen of Asn64 with the distance of 2.50 Å. This carbonyl group is also in close proximity with Pro61 with the distance of 3.74 Å. The carbon atom of the methyl group on the aniline nitrogen is also in close proximity with Thr56 and Ser59 with the distances of 3.38 Å and 3.71 Å, respectively. Though these two interactions are not in hydrogen bonding interactions, they could be used as leverages for the further modification of SAR study.

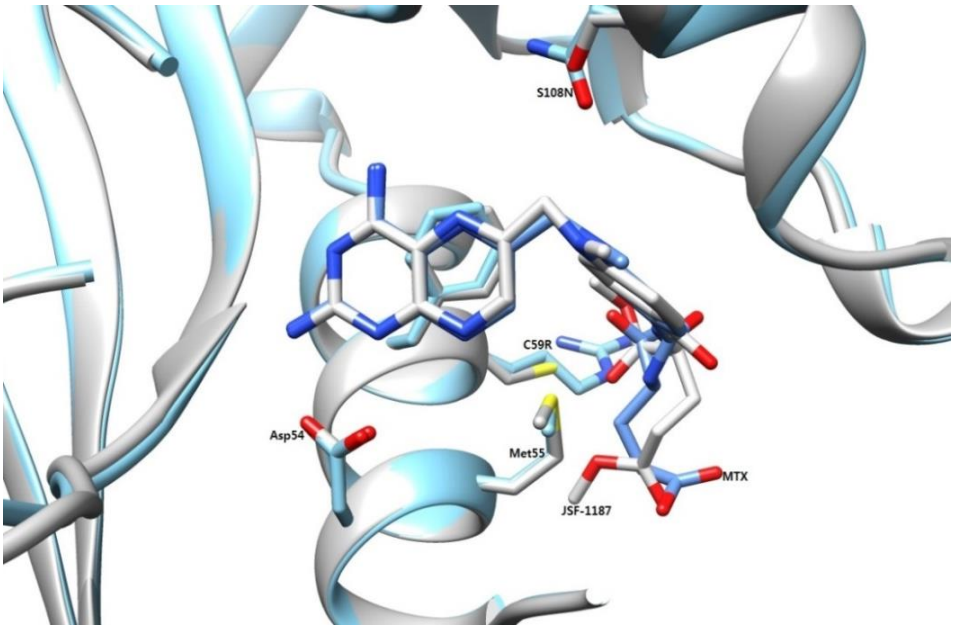

Figure 2-16. Superimposed structure of WT *Pf* DHFR:JCS-1187 (gray) and DM *Pf* DHFR:MTX. C59R and S108N mutations in double mutant (DM) *Pf* DHFR are labeled. Arg59 and Asn108 in DM *Pf* DHFR have closer contact with MTX or its ester analogs.

For some reason, there was difficulty acquiring crystal structure of *Mtb* DHFR:JCS-1187 or *Mtb* DHFR:JCS-1183 structure, so we sought crystal structures in *Pf* DHFR-TS instead, and the trial was successful. Though there is a possibility that the mode of interaction in *Pf* DHFR-TS with MTX analogs could be different in *Mtb* DHFR, these *Pf* DHFR-TS:JCS-1187 structures should be able to let us have a good idea of what interactions are involved in JCS-1187's binding in DHFR and what differences there are compared to MTX.

In the superimposed crystal structures of WT *Pf* DHFR:JCS-1187 and DM *Pf* DHFR:methotrexate (MTX, Figure 2-16), MTX and JCS-1187 have almost identical conformation in the active site. The two mutations in double mutant DHFR do not affect much on the binding, and Arg59 and Asn108 in DM *Pf* DHFR have slightly closer contact with the compounds compared to the wild type DHFR.

In JCS-1187 bound WT *Pf* DHFR-TS structure, the main interactions between DHFR and the compound, and the corresponding distances are as following. 2-amino group:Asp54 (2.57 Å), N-1 nitrogen:Asp54 (2.78 Å), 4-amino group:Tyr170 (2.99 Å), 4-amino group:Ile164 (main chain carbonyl, 3.03 Å), 4-amino group:Ile14 (main chain carbonyl, 2.71 Å), glutamate carbonyl:Cys59 (3.37 Å), and glutamate ester:Arg122 (2.74 Å). Similar interactions were found in human DHFR:JCS-1187 structure, and the interactions and the corresponding distances are as following. 2-amino group:Glu30 (2.71 Å), N-1 nitrogen:Glu30 (2.82 Å), 4-amino group:Tyr121 (3.12 Å), 4-amino group:Ile7 (main chain carbonyl, 3.21 Å), 4-amino group:Val115 (main chain carbonyl,

2.96 Å), benzoic acid carbonyl:Asn64 (2.50 Å), glutamate carbonyl:Gln35 (2.66 Å), and glutamate ester:Arg70 (3.28 Å).

Due to the exceptional potency of JCS-1183 and JCS-1187 on H37Rv strain unlike their parent compound, MTX, a follow-up study is going on and more details such as pharmacokinetics and drug mechanism will be studied. So far a most probable reason for the discrepancy in whole cell assay result is that the ester groups help JCS-1183 and JCS-1187 to pass through TB cell wall by simple diffusion and the ester groups are hydrolyzed in or in the middle of transferring to the active site.

Unfortunately, however, there has not been any selectivity gain from MTX derivatization. It is not surprising when comparing pathogenic and human DHFR with JCS-1187 bound structures. The orientations that JCS-1187 has in both pathogenic and human DHFR are pretty similar and the interactions are almost identical. There were no noticeable difference between Pf DHFR:JCS-1187 and human DHFR:JCS-1187 structure in terms of the interactions of JCS-1187 with DHFR. Therefore, we decided to try another DHFR inhibitor for selective inhibitor development.

CHAPTER III

SAR STUDY OF C-8 NON BENZYL TMQ ANALOGS

III.1. Structure Activity Relationship of TMQ Aniline Analogs and C-8 Non-Benzyl Analogs on *M. tuberculosis* DHFR and Human DHFR

After learning that either boosting TMP's potency against *Mtb* DHFR or decreasing MTX's activity against human DHFR was not achievable, we turned our focus on to a new starting scaffold, trimetrexate (TMQ). TMQ is a well-known 2nd generation DHFR inhibitor and it has been used to treat various diseases including psoriasis, rheumatoid, and even some cancers. As its name indicates, TMQ is a structural hybrid of trimethoprim and methotrexate. It has 2,4-diaminoquinazoline ring instead of 2,4-diaminopyrimidine as in TMP, yet it lacks di-glutamic acid moiety as in MTX which could hinder the diffusion through the pathogen's cell wall or membrane including tuberculosis cell wall.

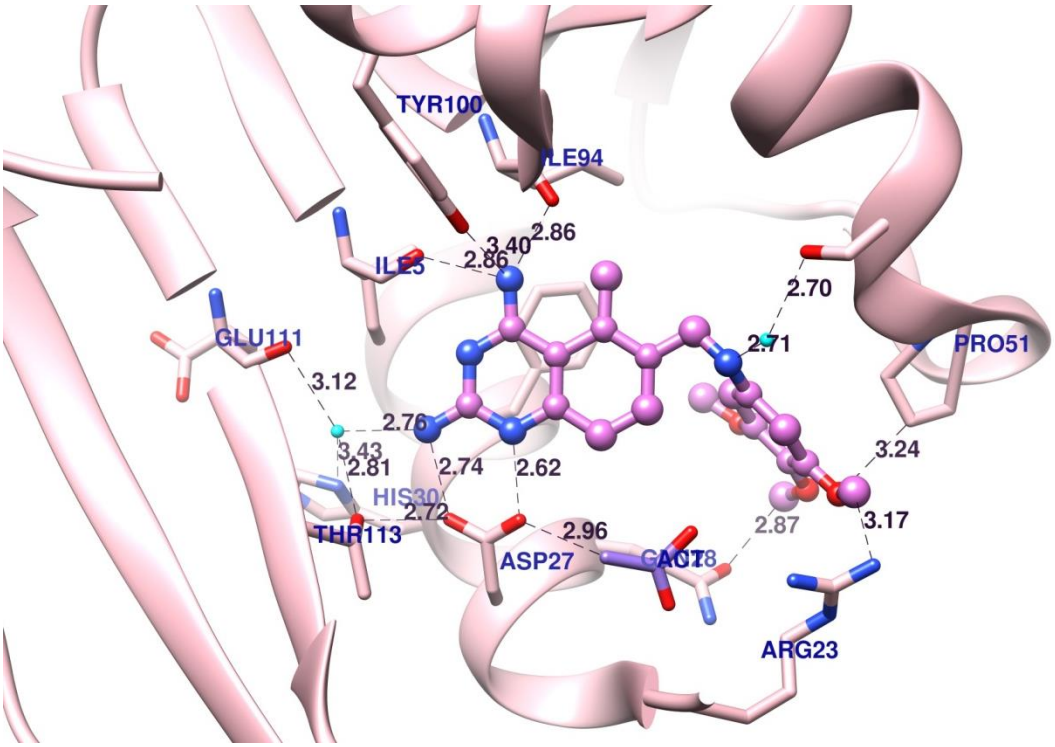

Figure 3-1. *Mtb* DHFR crystal structure bound with TMQ. The well-conserved hydrogen bonding interactions are shown. Instead of glycerol molecule found in the *Mtb* DHFR:TMP structure (1DG5), acetate (ACT) molecule is was found in our TMQ bound structure. Two important water molecules that mediate the hydrogen bonding interaction between TMQ and *Mtb* DHFR are shown in cyan.

Similar to MTX, the 2,4-diaminoquinazoline ring of TMQ has well-conserved hydrogen bond interaction with *Mtb* DHFR (Figure 3-1). This *Mtb* DHFR structure bound with TMQ displayed the well-conserved hydrogen bonding interactions between *Mtb* DHFR and TMQ similar to MTX bound structure. Asp27 has two hydrogen bonding interactions with 2-amino group and N-1 nitrogen with the distances of 2.74 Å and 2.62 Å, respectively. Asp27 has potentially available hydrogen bonding interaction with the acetate molecule in the glycerol binding pocket with the distance of 2.96 Å.

Even though in the structure carbon atom is facing to Asp27, oxygen atoms could be in that direction instead of carbon. Asp27 further forms the hydrogen bonding network with Thr113 and the distance is 2.72 Å. Thr113 has another hydrogen bonding network via a water molecule with 2-amino group of the quinazoline ring of TMQ, and the distance between Thr113 and this water molecule is 2.81 Å and between the water molecule and the 2-amino group of TMQ is 2.76 Å. This water molecule forms another hydrogen bonding interaction with the main chain carbonyl group of Glu111 and the distance is 3.12 Å.

For 4-amino group of the 2,4-diaminoquinzaoline ring of TMQ has three hydrogen bonding interactions with the main chain carbonyl group of Ile5, with the main chain carbonyl group of Ile94, and with the carbonyl group of Tyr100. The distances are 2.86 Å, 2.86 Å, and 3.40 Å, respectively.

For the 3,4,5-trimethoxyaniline ring side, the aniline nitrogen has another hydrogen bonding network with Ser49 via a water molecule. The distance between the aniline nitrogen and the water is 2.71 Å and the distance between the water and the oxygen atom of Ser49 is 2.70 Å. The carbon atom of 3-methoxy group is close proximity with Arg23 and Pro51 with the distance of 3.17 Å and 3.24 Å, respectively. The carbon atom of 4-methoxy group is close proximity with Gln28 oxygen with the distance of 2.87 Å. Although these methoxy groups are not in hydrogen bonding interactions, they represent a potential venue for enhancing the interactions with DHFR.

	Mtb:TMQ (4M2X)	human:TMQ (4MBD)	WT Pf:TMQ (4MAJ)	QM Pf:TMQ (4M96)
Space Group	P1	P1	$P2_12_12_1$	$P2_12_12_1$
Cell Dimension (Å)	36.5, 65.7, 68.9	37.3, 39.6, 71.9	58.1, 156.7, 164.9	57.5, 156.6, 164.9
(°)	93.6, 94.7, 100.9	78.0, 78.5, 67.4	90.0, 90.0, 90.0	90.0, 90.0, 90.0
Resolution (Å)	20.22-1.93 (2.02-1.93)	36.23-2.49 (2.58-2.49)	56.80-2.61 (2.71-2.61)	50.00-3.10 (3.15-3.10)
R_{sym}	0.069 (0.233)	0.045 (0.122)	0.159 (0.562)	0.138 (0.728)
I/σ	7.2 (2.4)	9.7 (2.4)	7.0 (2.4)	7.8 (2.2)
Completeness	94.4 (91.0)	96.1 (94.3)	99.5 (99.1)	94.9 (84.4)
Redundancy	1.96 (1.95)	1.93 (1.94)	7.52 (7.27)	5.60 (3.40)
# or reflections	44374	12392	46270	26569
R_{work}/R_{free}	21.7/26.6	22.4/29.8	25.0/31.7	19.8/26.8
# of Protein atoms	4976	3004	9077	9046
# of Ligand/Ion	300	174	150	97
# of Water	462	27	161	16
B factor – Protein	30.1	62.9	56.8	80.4
Ligand/Ion	30.4	64.4	52.1	74.4
Water	36.1	57.4	45.5	63.8
RMSD – length (A)	0.004	0.006	0.005	0.007
angles (°)	0.713	0.794	0.730	0.854

Table 3-1. Crystallographic data and structure statistics of TMQ bound structures of *Mtb*, *Pf* (WT and QM), and human DHFR.

The crystallographic data and the statistics values from the structure refinement are in table 3-1. Even though they are in different space group with different coefficients, their active site composition and the TMQ binding, especially the 2,4-diaminoquinazoline ring side, are very similar.

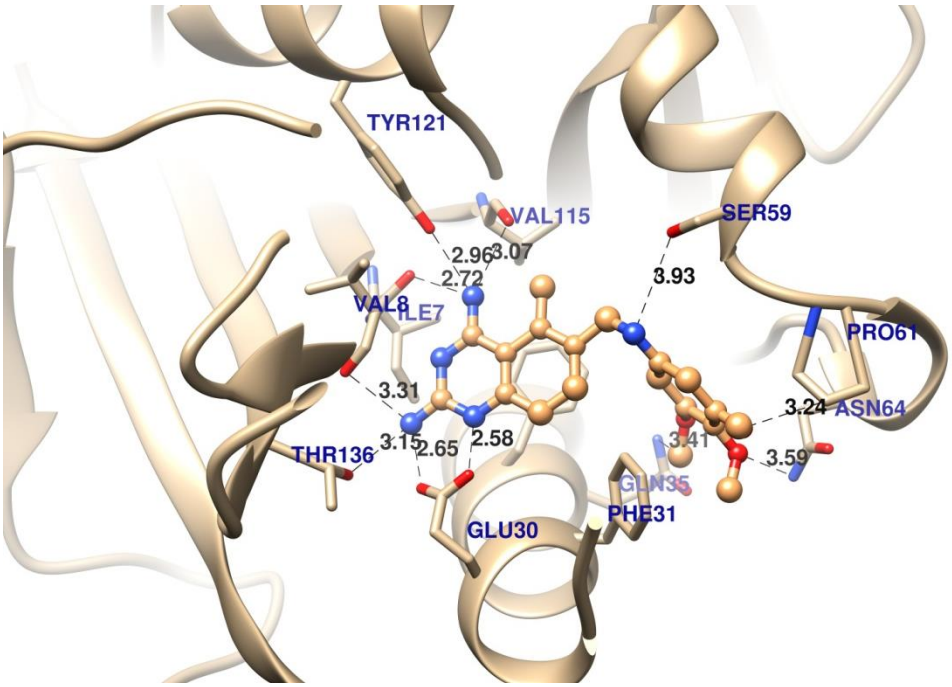

Figure 3-2. Human DHFR structure bound with TMQ. Similar to *Mtb* DHFR:TMQ structure, 2,4-diaminoquinazoline ring has conserved hydrogen bond interaction with DHFR. 3,4,5-trimethoxyaniline ring also has similar interactions with *Mtb* DHFR, and Phe31 partially occupies the space where acetate molecule was found in the *Mtb* DHFR:TMQ structure.

Similar to *Mtb* DHFR:TMQ structure, the 2,4-diaminoquinazoline ring of TMQ has well-conserved hydrogen bond interaction with human DHFR as well (Figure 3-2). This human DHFR structure bound with TMQ displayed the well-conserved hydrogen

bonding interactions between human DHFR and TMQ similar to *Mtb* DHFR:TMQ structure. Glu30, which is corresponding to Asp27 in *Mtb* DHFR, has two hydrogen bonding interactions with 2-amino group and N-1 nitrogen with the distances of 2.65 Å and 2.58 Å, respectively. Glu30 forms the hydrogen bonding network with Thr136 and the distance is 2.70 Å. Thr113 has another hydrogen bonding network with 2-amino group of the quinazoline ring of TMQ, and the distance between Thr113 and the 2-amino group of TMQ is 3.15 Å. 2-amino group of the 2,4-diaminoquinazoline further forms another hydrogen bond interaction with the main chain carbonyl group of Val8 and the distance between the two is 3.31 Å.

For 4-amino group of the 2,4-diaminoquinzaoline ring of TMQ has three hydrogen bonding interactions with the main chain carbonyl group of Ile7, with the main chain carbonyl group of Val115, and with the carbonyl group of Tyr121. The distances are 2.72 Å, 3.07 Å, and 2.96 Å, respectively.

For the trimethoxyaniline ring side, the aniline nitrogen has a weak hydrogen bonding interaction with Ser59, and the distance between the aniline nitrogen and the oxygen atom of Ser49 is 3.93 Å .The carbon atom of 3-methoxy group is close proximity with Pro61 with the distance of 3.24 Å. The oxygen atom of 4-methoxy group is close proximity with the nitrogen atom of Asn64 and the distance between the two atoms are 3.59 Å. The carbon atom of 5-methoxy group is in close contact with the nitrogen atom of Gln35 with the distance of 3.41 Å .Although these methoxy groups are not in hydrogen bonding interactions with human DHFR residues, they represent a potential venue for enhancing the interactions with DHFR. Phe31 occupies the space where an

acetate molecule in our Mtb DHFR:TMQ or a glycerol molecule in Mtb DHFR:MTX (1DF7) structures, and this difference gave us a revenue to take advantage of to develop selective inhibitors against pathogenic DHFRs.

Since TMQ exhibited high potency on both *Mtb* and human DHFR with IC_{50} of 17 nM and 16 nM, respectively, the main focus was naturally lowering the activity against human DHFR rather than enhancing the potency against *Mtb* DHFR. Based on the modelling on *Mtb* and human DHFR crystal structure bound with TMQ, both from quinazoline ring and 3,4,5-trimethoxybenzene ring were feasible to take advantage of the glycerol binding pocket. For the glycerol binding pocket in *Mtb* DHFR is surrounded by some hydrophilic residues such as Trp22 and Gln28, we first thought that there needs to be a hydrophilic group to gain selectivity, but this turned out to be not crucial.

To improve the potency on *Mtb* DHFR, we turned our main focus from trimethoprim (TMP) analogs to trimetrexate (TMQ), whose IC_{50} on *Mtb* DHFR is 17 nM and IC_{50} on human DHFR is 16 nM, and its analogs. The converted K_i of TMQ on *Mtb* DHFR is only 1.8 nM, but the problem is IC_{50} on TMQ is 16 nM and K_i on human DHFR is 1.1 nM as well. Hence the main goal of TMQ modification is to increase the selectivity on *Mtb* DHFR over human DHFR. Two different modifications have been tried on trimetrexate (TMQ) to improve selectivity.

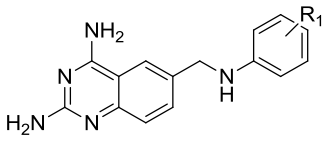

ID Number	Substitution R_1	*Mtb* IC_{50} nM	Human IC_{50} nM	Selectivity Index (SI) Human/*Mtb*
TMQ	3,4,5-trimethoxy w/ C5-methyl	17	16	1
1373	4-methoxy	540	120	0.4
1376	3-methoxy	970	170	0.2
1378	H	1120	62	0.05
1379	2,4-dimethoxy	770	66	0.1
1380	3,4-dimethoxy	590	30	0.05
1381	3,5-dimethoxy	240	240	1
1400	3,5-dimethoxy, C8-bromo	740	130	0.2
1382	3-hydroxyl	1200	400	0.3
1402	2-hydroxyl	2300	550	0.2
1395	benzodioxane	1800	70	0.04
1409	benzo[*d*][1,3]dioxole	200	200	1
1410	4-hydroxyl, C8-bromo	460	170	0.4
1441	2,5-diethoxy	5150	1850	0.4

Table 3-2. IC_{50} values of TMQ aniline analogs. These analogs have no modification on 2,4-diaminoquinazoine ring. No compound exceeded 1 of selectivity which means they are all more potent (some of them are the same) on human DHFR.

The first modification we made was a modification of C-8 position of the 2,4-diaminoquinazoline ring, and the second modification was on the trimethoxy benzene ring. To facilitate the synthesis of the compounds, we tried 2,4-dimethoxybenzene

analogs instead of 2,3,4-trimethylbenzene as in trimetrexate and removed C-5 methyl group from the quinazoline ring. Compared to the parent compound, TMQ, JCS-1381, 6-((3,5-dimethoxyphenylamino)methyl)quinazoline-2,4-diamine, lost about 10 fold activity but retained the selectivity. The IC_{50} values are listed in Table 3-2.

TMQ	Asp27 (O):2-amino (N)	Asp27 (O):N-1	Ile5 (main chain O):4-amino (N)	Ile94 (main chain O):4-amino (N)	Tyr100 (O):4-amino (N)
Mtb DHFR	2.74	2.62	2.86	2.86	3.40
WT *Pf* DHFR	2.93 (Asp54)	2.88 (Asp54)	2.63 (Ile14)	2.99 (Ile164)	2.99 (Tyr170)
QM *Pf* DHFR	2.89	3.13	2.86	3.26 (Leu164)	3.22
Human	2.65 (Glu30)	2.58 (Glu30)	2.72 (Ile7)	3.07 (Val115)	2.96 (Tyr121)

Table 3-3. The conserved hydrogen bond interactions of TMQ in *Mtb, Pf,* and human DHFR, and the corresponding distances. The interacting residues are all specified in parentheses.

As shown in the table 3-3, TMQ and DHFR from difference species have very well conserved hydrogen-bond interactions mainly through 2,4-diaminoquinazoline ring. Human DHFR has tighter interaction (shorter distances) with TMQ compared to the pathogenic DHFRs, and that illustrates how difficult it would be to gain selectivity on this TMQ compound.

A variety of C-8 functionalization have been synthesized and tested. In the initial designing step, we expected hydrophilic moiety from C-8 position would be more effective in approaching the pocket near the substrate binding site. However, this turned out that the flexibility of the bridging carbon chain and the suitable length of the functional group are more crucial factors for rendering selectivity. We will be using the selectivity index (SI) which is simply the ratio of IC_{50}s of *Mtb* and human DHFR hereafter. The greater the value, the larger the selectivity goes.

JCS-1373, which has 4-methoxyaniline ring, lost potency on both *Mtb* (IC_{50} = 540 nM) and human DHFR (IC_{50} = 120 nM) compared to TMQ, which has 3,4,5-trimethoxyaniline ring. JCS-1441, which has 2,5-diethoxyaniline ring, on the other hands, lost even greater potency on both *Mtb* (IC_{50} = 5150 nM) and human (IC_{50} = 1850 nM) DHFR. In the superimposed crystal structures of *Mtb* DHFR:JCS-1373 and *Mtb* DHFR:JCS-1441, a probable reason for this drastic loss of potency could be explained. The interactions on the 2,4-diaminoquinazoline ring side are pretty much the same between the two structures. However, on the aniline ring side interactions, much bulkier 2,5-diethoxy group pushed the DHFR loop region (Ser49-Arg55) away from JCS-1441. Compared to *Mtb* DHFR:JCS-1373, the residue-to-residue deviations in *Mtb* DHFR:JCS-1441 range from 0.89 Å to 1.78 Å.

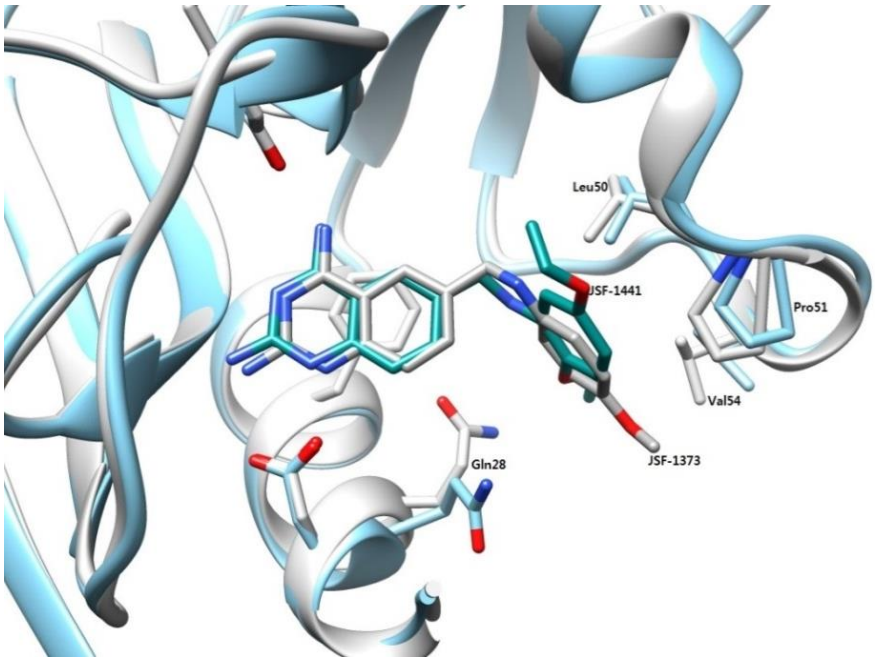

Figure 3-3. Superimposed structure of *Mtb* DHFR:JCS-1373 (gray) and *Mtb* DHFR:JCS-1441. Bulkier 2,5-diethoxy group in JCS-1441 pushed the loop region away from its normal position.

Introducing functionalities on the aniline ring alone ended up hurting the selectivity. No compound has shown improved selectivity and some of the analogs in this category are significantly more potent on human DHFR with 0.04-0.05 folds selectivity. There were just two analogs with the equal potency on both DHFRs. JCS-1409 (Benzo[*d*][1,3]dioxole group) and JCS-1381 (3,5-dimethoxy group) with low potency for both DHFRs (Figure 3-3). JCS-1381 (3,4-dimethoxyaniline group) exhibited 240 nM of IC_{50} on both DHFRs and JCS-1409 (benzodioxoaniline group) exhibited 200 nM of IC_{50} on both DHFRs.

Interestingly enough, other than benzyl substitution, most of the other C-8 substitutions have shown diminished selectivity. For the compounds that gained selectivity, they displayed very low potencies. The analog with highest potency and selectivity in this category is phenethyl substitution (JCS-1439) with 160 nM of IC_{50} on *Mtb* DHFR and 1300 nM of IC_{50} on human DHFR (8 fold selectivity). JCS-1439 is just one carbon longer than its C-8 benzyl counterpart, JCS-1425. Compared to the analogs in TMQ-aniline category, non-benzyl C-8 substitution has increased IC_{50}s more against human DHFR than *Mtb* DHFR and this result led us to successful trial on benzyl C-8 derivatization. This trend is more noticeable with small functional groups such as methyl (JCS-1420) or ally (JCS-1426) group, as the smaller pocket in human DHFR was more severely affected by the bulkier groups. The IC_{50} values are listed in Table 3-4.

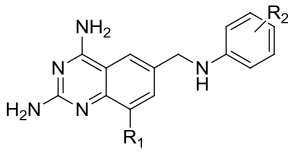

ID Number	Substitution R_1	Substitution R_2	*Mtb* IC_{50} nM	Human IC_{50} nM	Selectivity Index(SI) Human/*Mtb*
1401	Ph	3,5-dimethoxy	5400	1700	0.3
1420	CH3	3,5-dimethoxy	1100	150	0.1
1426	allyl	3,5-dimethoxy	260	260	1
1433	vinyl	3,5-dimethoxy	250	50	0.2
1437	n-prOH	3,5-dimethoxy	240	120	0.5
1438	CHOHEt	3,5-dimethoxy	440	110	0.2
1439	phenethyl	3,5-dimethoxy	160	1300	8
1450	styryl	3,5-dimethoxy	550	2700	4.9
1452	cyclopropyl	3,5-dimethoxy	610	390	0.6
1458	vinylcyclohexyl	3,5-dimethoxy	6200	5500	0.9
1459	ethylcyclohexyl	3,5-dimethoxy	1400	2800	2
1465	ethyl	3,5-dimethoxy	380	180	0.5
1464	2-thiophene	3,5-dimethoxy	5600	11700	2.1
1490	vinylcyclopropyl	3,5-dimethoxy	220	60	0.3
1493	vinyl t-butyl	3,5-dimethoxy	1300	13200	10
1498	ethyl t-butyl	3,5-dimethoxy	1100	5900	5.4
1502	bromo	3,4,5-trimethoxy	3900	470	0.1
1529	ethylcyclopropyl	3,5-dimethoxy	220	250	1.1
1540	styryl	3,4,5-trimethoxy	900	5300	6.0
1541	phenethyl	3,4,5-trimethoxy	380	980	2.6

Table 3-4. IC_{50} values against *Mtb* DHFR and human DHFR of C-8 non-benzyl TMQ analogs. Some of the analogs with bulky group on C-8 position exhibited moderate selectivity with more than 2 fold of selectivity.

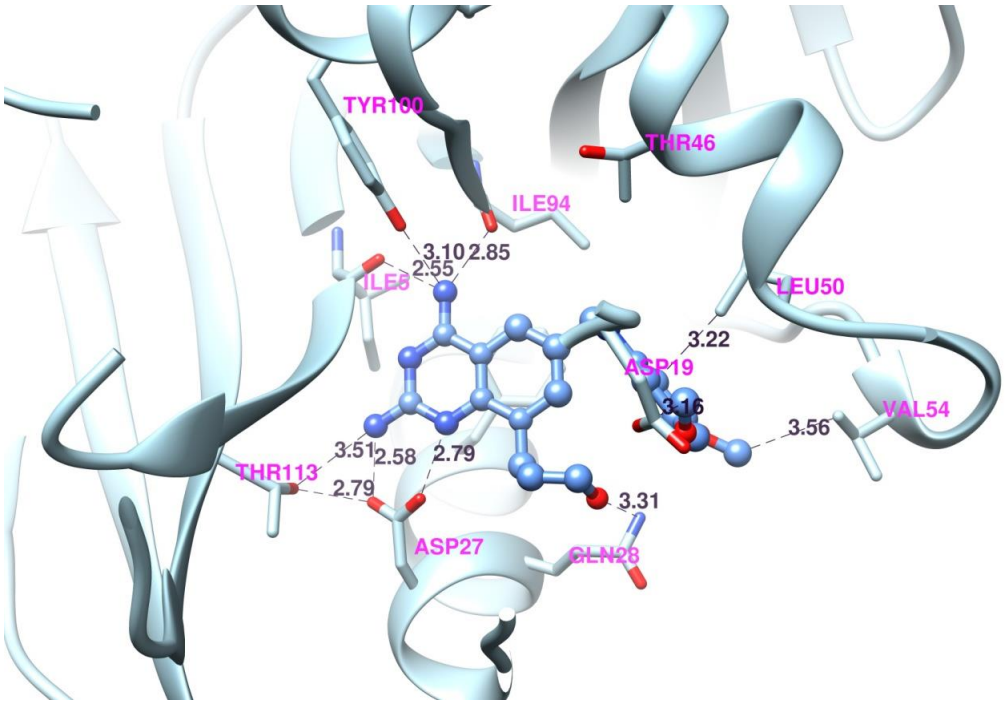

Figure 3-4. The important conserved interactions between *Mtb* DHFR and JCS-1437. 2,4-diaminoquinazoline ring retains most of the important hydrogen bonding interactions just as in TMQ or other TMQ analogs bound *Mtb* DHFR. The 4-butanol group is pushing the 3,5-dimethoxybenzne ring toward the solvent access region.

Similar to *Mtb* DHFR:TMQ structure, the 2,4-diaminoquinazoline ring of JCS-1437 has well-conserved hydrogen bond interaction with *Mtb* DHFR (Figure 3-4). This *Mtb* DHFR structure bound with JCS-1437 displayed the well-conserved hydrogen bonding interactions between *Mtb* DHFR and JCS-1437 similar to *Mtb* DHFR:TMQ structure. Asp27 has two hydrogen bonding interactions with 2-amino group and N-1 nitrogen with the distances of 2.58 Å and 2.79 Å, respectively. Asp27 also forms the hydrogen bonding network with Thr113 and the distance is 2.79 Å. This Thr113 has

another hydrogen bonding network with 2-amino group of the 2,4-diaminoquinazoline ring of TMQ, and the distance between Thr113 and the 2-amino group of TMQ is 3.51 Å.

For 4-amino group of the 2,4-diaminoquinzaoline ring of TMQ has three hydrogen bonding interactions with the main chain carbonyl group of Ile5, with the main chain carbonyl group of Ile94, and with the carbonyl group of Tyr100. The distances are 2.55 Å, 2.85 Å, and 3.10 Å, respectively.

For the 3,5-dimethoxyaniline ring side, the carbon atom of 3-methoxy group is close proximity with Val54 with the distance of 3.56 Å .The 2-position carbon atom of the aniline ring is close proximity with the carbon atom of Leu50 and the distance between the two atoms are 3.22 Å. The carbon atom of 5-methoxy group is in close contact with the oxygen atom of Asp19 with the distance of 3.16 Å .Although these methoxy groups and the carbon atoms are not in hydrogen bonding interactions with *Mtb* DHFR residues, they represent a potential venue for enhancing the interactions with DHFR.

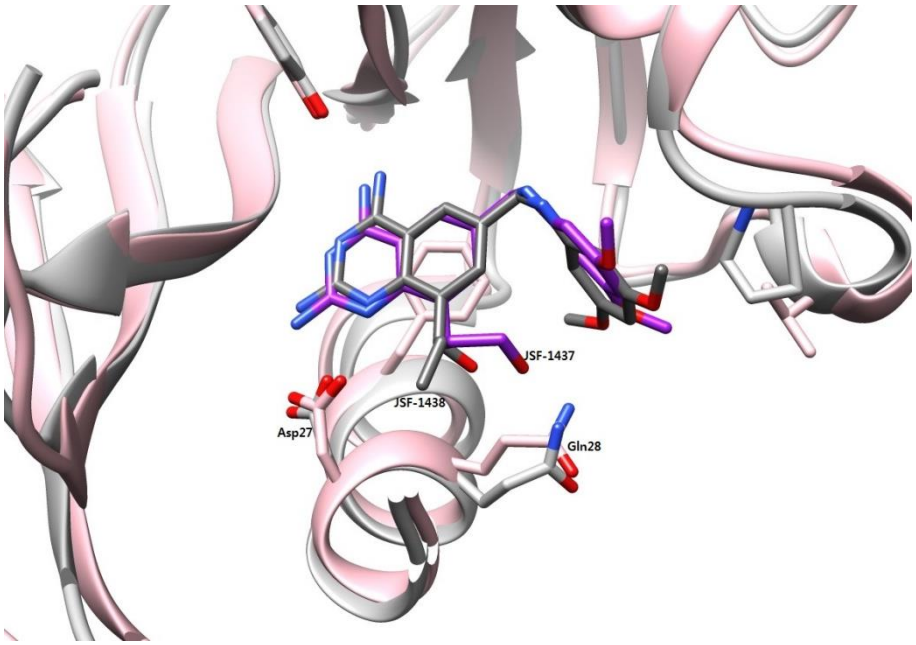

Figure 3-5. Superimposed structure of *Mtb* DHFR:JCS-1437 (plum) and *Mtb* DHFR:JCS-1438. Both of the hydroxyl groups in C-8 propyl (JCS-1437) and isopropyl (JCS-1438) face the same direction. Still JCS-1437 pushed the loop region close the 3,5-dimethoxybenzyl group in the compound is located and gained more space compared to JCS-1438.

JCS-1437 (C-8 propanol) and JCS-1438 (C-8 *iso*-propanol) make an interesting comparison in Figure 3-5. The IC_{50} for JCS-1437 on Mtb DHFR is 240 nM and that of JCS-1438 is 440 nM. In both structures, hydroxyl groups of the two propanol position in a way that they could form hydrogen bonding interaction with Gln28. The distance between the hydroxyl group of JCS-1437 and Gln28 is 3.31 Å, and the distance between the hydroxyl group of JCS-1438 and Gln28 is 3.42 Å. Other than slightly longer distance, due to the extra ethyl group that sits in the opposite direction of the hydroxyl group, JCS-1438 showed about 2 fold lower potency on *Mtb* DHFR.

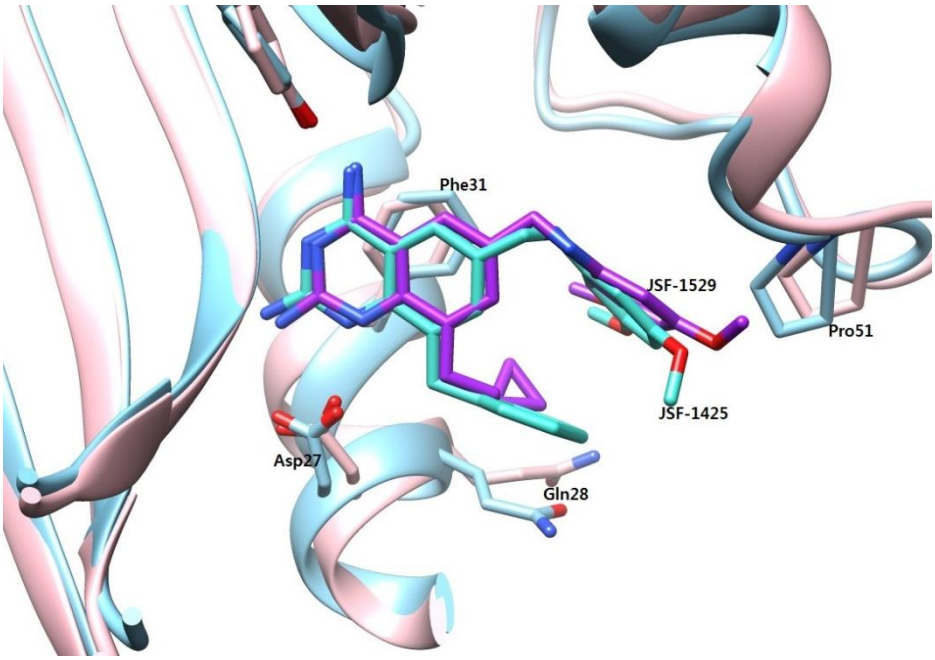

Figure 3-6. Superimposed structure of *Mtb* DHFR:JCS-1425 (blue) and *Mtb* DHFR:JCS-1529. JCS-1529 binding induces significant conformational changes of *Mtb* DHFR, especially for the major residues for inhibitor binding such as Asp27, Gln28 and Phe31.

JCS-1529, 8-(2-cyclopropylethyl)-6-(((3,5-dimethoxyphenyl)amino)methyl)quinazoline-2,4-diamine, offers another interesting comparison on *Mtb* and human DHFR (Figure 3-6). The ethylcyclopropyl group on C-8 position is even longer than C-8 benzyl series, but this group has much smaller functional group (cyclopropane) compared to the benzene ring of C-8 benzyl derivatives. To be able to accommodate the longer substituent, ethylcyclopropyl group, *Mtb* DHFR compromised its optimal interaction with 2,4-diaminoquinazoline ring and its 2-amino group and N-1 nitrogen. The distance between Asp27 and the N-1 nitrogen is 2.74 Å which is pretty similar to the TMQ and *Mtb* DHFR interaction, but the distance between

Asp27 and 2-amino group is 3.64 Å which is far longer than in *Mtb* DHFR:TMQ or Mtb DHFR:JCS-1425 structures. Furthermore the orientation of the JCS-1529 in the substrate binding site is abnormally distorted compared to JCS-1425 or TMQ.

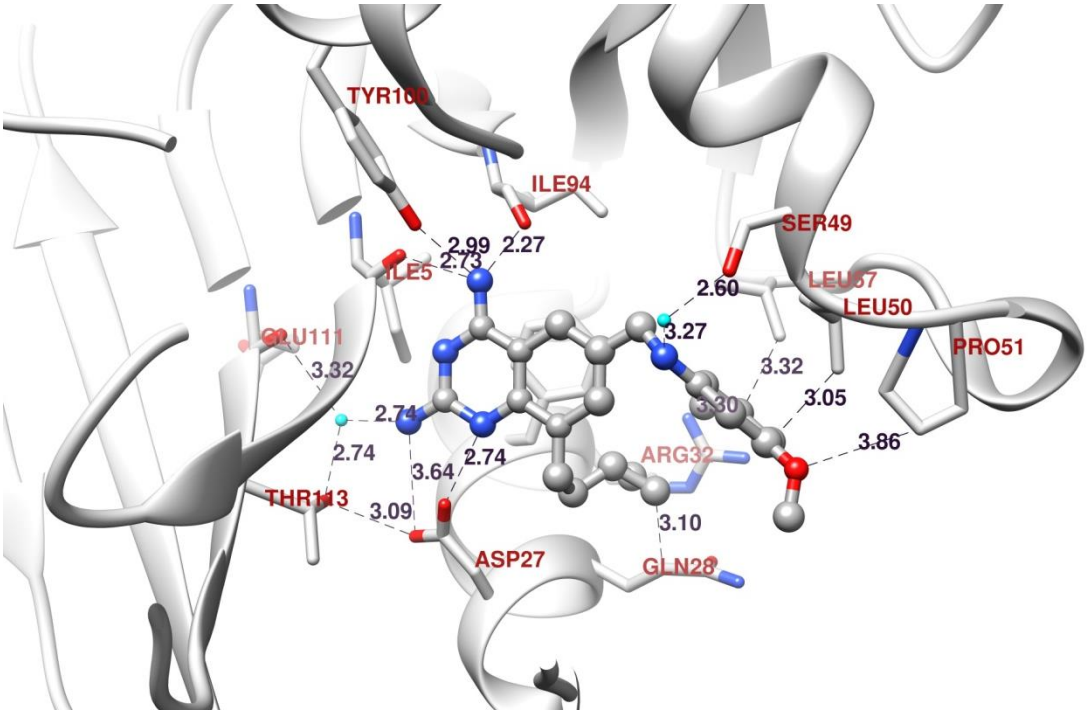

Figure 3-7. *Mtb* DHFR:JCS-1529 structure in the active site of *Mtb* DHFR. Due to C-8-(1-cyclopyropl)propyl group, distortion of the compound from the optimal interaction with Asp27 and Phe31 is clearly shown. Though cyclopropyl group is relatively smaller, the overall length of the C-8 substituent forced this unfavorable position and the overall orientation of the molecule is different than TMQ. Yet, all the major interactions are still retained on 2,4-diaminoquinazoline ring side.

Similar to *Mtb* DHFR:TMQ structure, the 2,4-diaminoquinazoline ring of JCS-1529 has well-conserved hydrogen bond interaction with *Mtb* DHFR (Figure 3-7),

despite the interactions with Asp27 distorted significantly. Still, this *Mtb* DHFR structure bound with JCS-1529 displayed the well-conserved hydrogen bonding interactions between *Mtb* DHFR and JCS-1529 similar to *Mtb* DHFR:TMQ or other TMQ analogs bound structures. Asp27 has two hydrogen bonding interactions with 2-amino group and N-1 nitrogen with the distances of 3.64 Å and 2.74 Å, respectively. Asp27 also forms the hydrogen bonding network with Thr113 and the distance is 3.09 Å. This Thr113 has another hydrogen bonding network with 2-amino group of the 2,4-diaminoquinazoline ring of JCS-1529 via a water molecule, and the distance between Thr113 and this water molecule is 2.74 Å, and the distance between the water molecule and the 2-amino group of JCS-1529 is 2.74 Å. This water molecule further forms another hydrogen bonding interaction with the main chain carbonyl group of Glu111 and the distance between the two is 3.32 Å.

For 4-amino group of the 2,4-diaminoquinzaoline ring of JCS-1529 has three hydrogen bonding interactions with the main chain carbonyl group of Ile5, with the main chain carbonyl group of Ile94, and with the carbonyl group of Tyr100. The distances are 2.73 Å, 2.27 Å, and 2.99 Å, respectively.

For the 3,5-dimethoxyaniline ring side, the carbon atom of 3-methoxy group is close proximity with Arg32 with the distance of 3.30 Å .The oxygen atom of the same methoxy group is in close proximity with Leu57 and the distance is 3.32 Å. The 4-position carbon atom of the aniline ring is close proximity with the carbon atom of Leu50 and the distance between the two atoms are 3.05 Å. The oxygen atom of 5-methoxy group is in close contact with Pro51 with the distance of 3.86 Å .Although

these methoxy groups and the carbon atoms are not in hydrogen bonding interactions with *Mtb* DHFR residues, they represent a potential venue for enhancing the interactions with DHFR. The nitrogen atom of the aniline ring forms a hydrogen bonding network with the oxygen atom of Ser49 via a water molecule. The distance between the aniline nitrogen and this water molecule is 3.27 Å and the distance between the water molecule and the oxygen atom of Ser49 is 2.60 Å.

To be able to accommodate this long C-8 substituent, JCS-1529 had an unfavorable position in the active site compared to other TMQ analogs. The distance between Asp27 and N-1 nitrogen is 2.74 Å. But the distance between Asp27 and 2-amino group is 3.64 Å, due to the forced distortion. Also the angles of the two interactions are not the optimal angles compared to TMQ. Though the cyclopropyl group is relatively small group, due to the long bridge (2-carbon atoms excluding the cyclopropyl carbon), the optimal angle or distance could not be retained. Also this is why we decided to try the benzyl group as the main scaffold of our SAR study to develop selective inhibitors against *Mtb/Pf* DHFR over human counterpart.

CHAPTER IV

SAR STUDY OF C-8 BENZYL TMQ ANALOGS

IV.1. C-8 benzyl TMQ Analogs; Selective, Potent Inhibitors of *M.tuberculosis* DHFR and *P. falciparum* DHFR-TS and their SAR Study on *Mtb* DHFR, Wild Type (WT) and Quadruple Mutant (QM) *Pf* DHFR-TS, and Human DHFR.

In this most important chapter, the detailed outcome of our C-8 benzyl TMQ analogs that displayed exceptional selectivity against both *Mtb* DHFR and *Pf* DHFR-TS (WT and QM) will be discussed. The results we earned from the previous two chapters helped us to develop the potent and selective C-8 benzyl TMQ analogs. Though the detailed structure of C-8 benzyl group in the *M. tuberculosis* and *P. falciparum* DHFR was different than our initial design and needs to be studied further, C-8 benzyl group itself was sufficient to exert great selectivity against pathogenic DHFRs over human counterpart.

As previously stated in the introduction, *Mtb* DHFR and *Pf* DHFR-TS share common structural features that we were able to take advantage of. One is a pocket near the substrate binding site, which was dubbed the glycerol binding pocket in *Mtb* DHFR structure (1DF7), and a flexible residue near the acid residue (Asp27 in *Mtb* DHFR or Asp54 in *Pf* DHFR-TS).

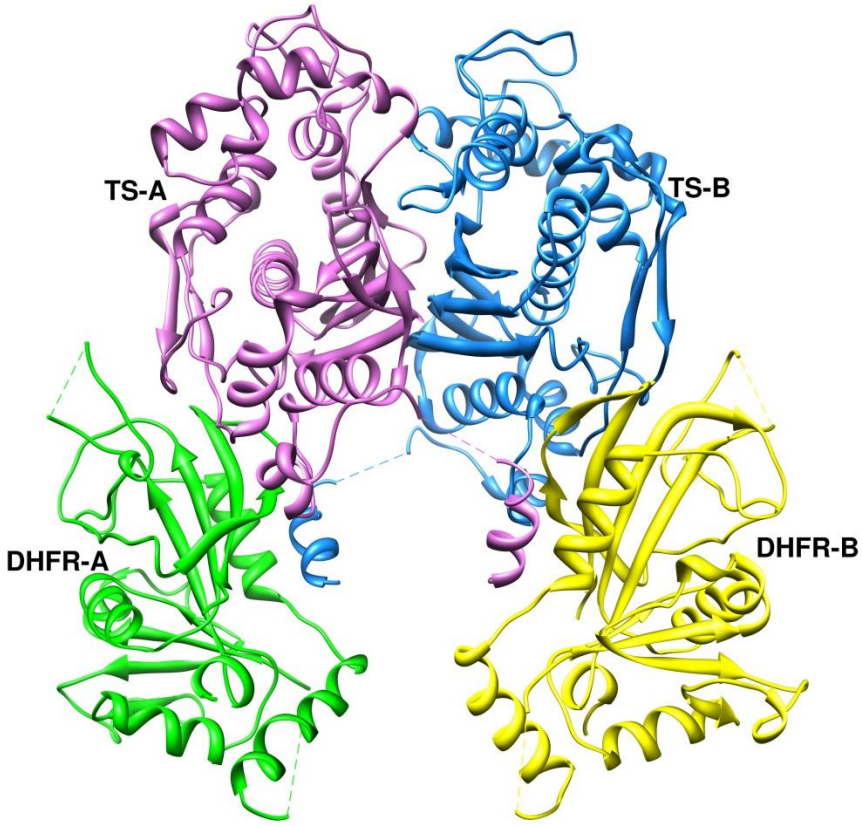

Figure 4-1. Overall structure of *Pf* DHFR-TS. *Pf* DHFR-TS exists as homo dimer (Two DHFR-TS) in physiological condition and TS domains are connected to each other. There are missing densities between DHFR and TS domains (a junction region), and the detailed function of this 'junction region' is not known clearly yet.

For *Pf* DHFR-TS (Figure 4-1), wild-type, double mutant (C59R/S108N), and quadruple mutant (N51I/C59R/S108N/I164L) were cloned, expressed, purified and crystallized. All three *Pf* DHFR-TS contained the pockets near the substrate binding site similar to the glycerol binding pocket, and the mutations other than I164L are distant

from the active site. I164L did not affect much on the active site binding of the inhibitors either.

The similarity between DHFRs made it likely that trimetrexate (TMQ), a DHFR inhibitor used in human diseases, would also have high affinity for the pathogenic DHFR proteins. Our own enzyme assay results confirmed that TMQ strongly inhibited *Mtb* and wild type *Pf* DHFR-TS (IC_{50} of 17 nM and 5 nM, respectively). The structures of *Mtb* DHFR bound with TMQ showed that it binds in the substrate binding cleft with the 2,4-diaminoquinazoline end fitting into the inside of the substrate binding pocket and the trimethoxyaniline ring stretching toward the solvent opening. The *Mtb* DHFR structures bound with TMQ and its analogs show that TMQ and its analogs have conserved hydrogen bonding interactions with the Asp27 through the 2-amino group and the *N*-1 nitrogen of the 2,4-diaminoquinazoline ring, and with the main chain carbonyl groups of Ile94 and Ile5 through the 4-amino group of the 2,4-diaminoquinazoline ring. These interactions form a network of hydrogen bonds that is conserved in the DHFR crystal structures from human and pathogens. The comparison of pathogenic and human DHFR substrate binding sites using the TMQ bound DHFR structures revealed that the RMSD between *Mtb* DHFR and human DHFR is 1.28 Å over 144 Cα carbons, and between *Pf* DHFR and human DHFR the RMSD is 1.09 Å over 164 C_α carbons. The greatest deviation came from the loop region where the trimethoxyaniline ring is located (Leu50-Arg55 in *Mtb* DHFR).

In *Mtb* DHFR, Asp27, corresponding to Glu30 in human DHFR and Asp54 in *Pf* DHFR-TS, plays a role as an acid that donates hydrogen atom to the substrate (DHF) to

produce tetrahydrofolate (THF). Right next to this acid residue of pathogenic DHFRs, there is a flexible residue (Gln28 in *Mtb* DHFR and Met55 in *Pf* DHFR) that could offer flexibility to the substrate binding site. These residues have 2 or more carbon bridging that could confer high degree of rotational freedom along with the smaller size of their side chains. On the other hand, Phe31 is located in the same position in human DHFR, and Phe31 cannot offer the similar flexibility due to the bulkier size of phenyl group and no rotational freedom from the one bridging carbon that the Phe31 has. Our aim was to exploit the increased space afforded by the smaller and more flexible amino acids in the *Mtb* and *P. falciparum* substrate binding sites to add functional groups to the existing TMQ framework, to increase the inhibitor's selectivity and/or potency against the pathogenic DHFRs.

The IC_{50} of TMQ against *Mtb* DHFR is 17 nM, nearly the same as against the human protein (IC_{50} = 16 nM). Potency in the *P. falciparum* wild-type and quadruple mutant (QM) DHFRs was also strong at 5 nM and 6 nM, respectively. The main interactions in the substrate binding pocket are preserved between species, the quinazoline ring itself maintains interactions in both the human and pathogenic DHFRs through the acidic residue (Asp27 in *Mtb* DHFR) and the aromatic residue (Phe31 in *Mtb* DHFR), so we focused our efforts on utilizing the glycerol binding pocket and the additional space available by the help of the flexible residues (Gln28 in *Mtb* DHFR and Met55 in *Pf* DHFR) that are exclusively available in the pathogenic DHFRs by modifying the C-8 position of the 2,4-diaminoquinazoline ring and the trimethoxyaniline ring.

Our initial designs all contain hydrophilic groups such as dihydroxyl group or imidazole to mimic the interaction of glycerol with *Mtb* DHFR residues in the glycerol binding pocket including Trp22 and Arg23 (Figure 4-2). However, the synthesis was challenging and those hydrophilic groups turned out to be not crucial for selectivity thanks to the existence of the flexible residue such as Gln28 in *Mtb* DHFR.

Development of an inhibitor based on the *Mtb* DHFR:TMQ structure was directed at the interactions between the acetate molecule found in the glycerol binding pocket and the nearby residues including Trp22, Arg23, Asp27, and Gln28. Our initial additions to the TMQ rings were compounds that would fit into the substrate binding pocket and strengthen these interactions to the point where our inhibitors were more potent selectively against the pathogenic DHFRs. Carbon linkers of various lengths were added to C-8 of the 2,4-diaminoquinazoline ring to enable binding in both the substrate binding site and the glycerol binding pocket (Figure 4-2). Out of the 16 initial compounds, six compounds exhibited increased selectivity against *Mtb* DHFR over human DHFR, and the benzyl group (JCS-1425) showed the best potency and selectivity. All six compounds contained bulky groups (benzene ring, cyclohexyl, or t-butyl group) and their selectivity gain was mainly due to activity loss in the human DHFR compared to the *Mtb* counterpart. Most of them showed low potency on *Mtb* DHFR (400 – 1500 nM) except for the C-8 benzyl analog (JCS-1425 at 59 nM) and the C-8 phenethyl analog (JCS-1439 at 160 nM).

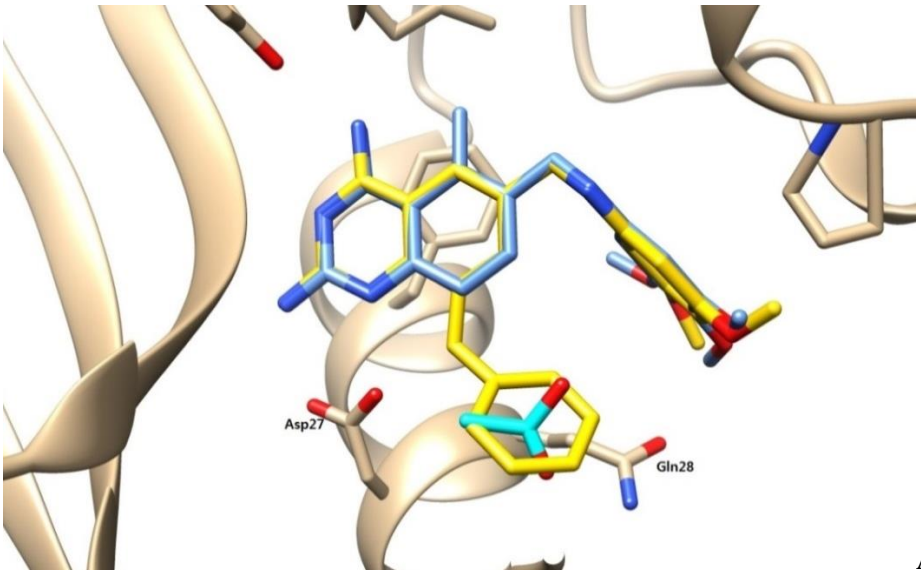

A)

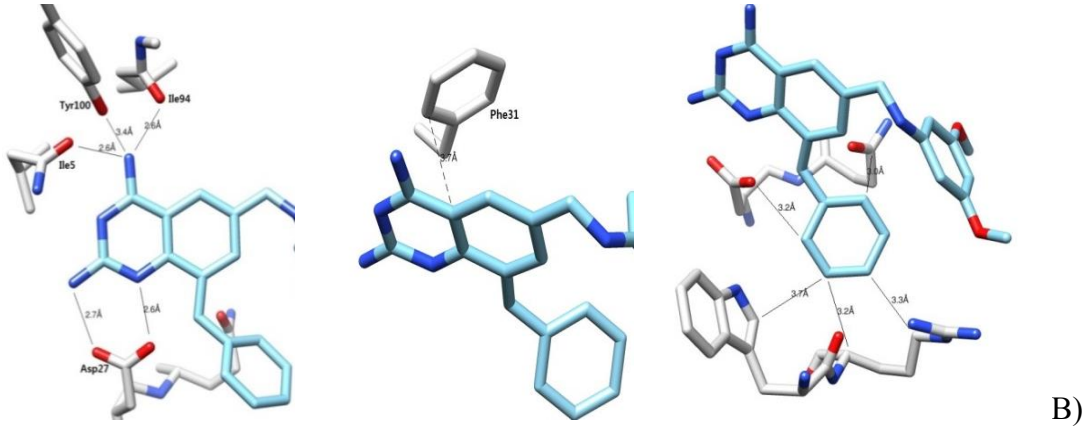

B)

Figure 4-2. Designing the initial C-8 benzyl compounds. Using the *Mtb* DHFR:TMQ showing the TMQ (blue) and acetate (cyan) molecules. B) In the design, the C-8 benzyl compound retained the hydrogen bond interaction with Asp27, Ile5, Ile94, and Try100 (Top, Left) and the *pi*-stacking interaction with Phe31 (Top, Right). C-8 benzyl group sits well in the binding pocket where an acetate molecule was found in *Mtb* DHFR:TMQ structure. The C-8 benzyl group has possible interaction with Trp22, Arg23, Asp27, and Gln28 (Bottom).

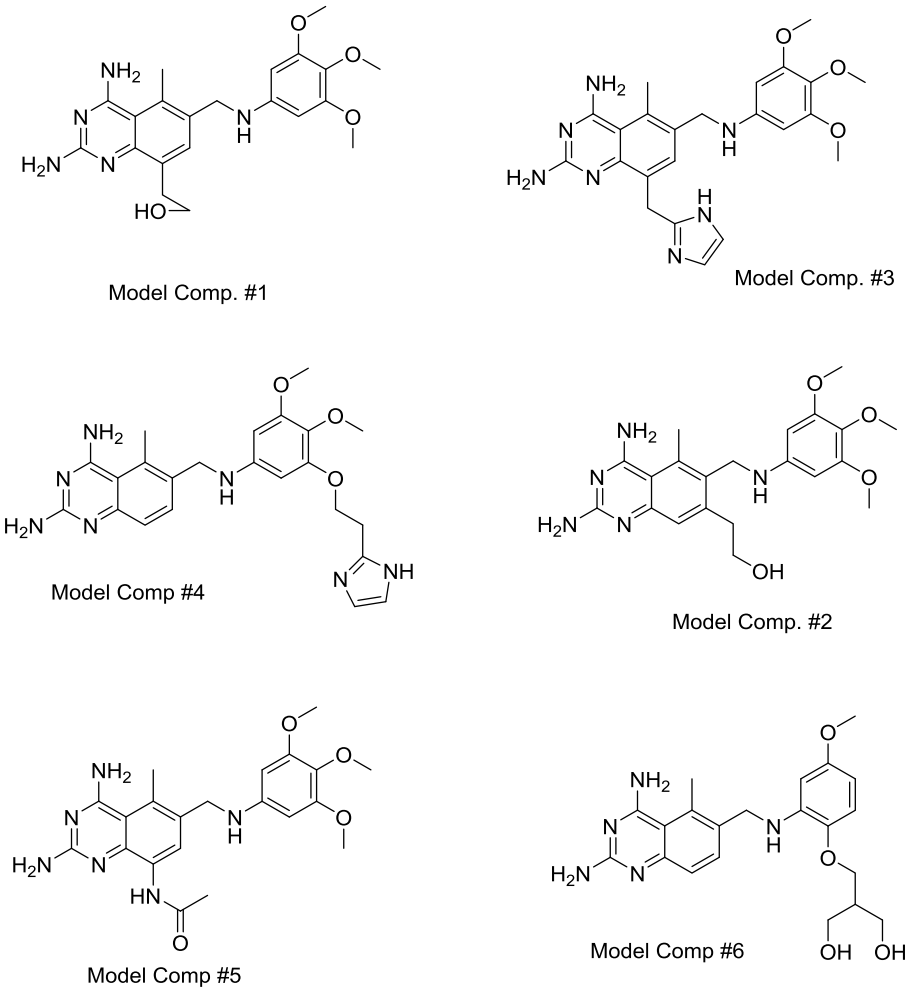

Figure 4-3. Example of the initially designed compounds. We made derivatization attempts from C-7 or C-8 of quinazoline ring and C-2 of trimethoxybenzene ring targeting the glycerol binding pocket found in the *Mtb* DHFR structure, 1DF7. We tried to synthesize and evaluate hydrophilic group containing molecules first, but it turned out that hydrophilic group was not crucial part for gaining selectivity.

Additionally, though the structure of the inhibitors in the initial test did not follow the predicted models, it did provide a new avenue of development of selective inhibitors (Figure 4-3).

DHFR's role in DNA and amino acid synthesis makes it a universally present protein, but there is a low sequence identity between proteins, with *Mtb* and *P. falciparum* sharing only a 20% sequence identity. However, the overall fold of the protein is largely preserved requiring detailed understanding of the differences and similarities between species to create a specific inhibitor. Both the *Mtb* DHFR and *P. falciparum* DHFR-TS have eight central β-strands surrounded by four α-helices. The active site is divided into two main clefts: one cleft fits the cofactor (NADPH) and the other fits the substrate (DHF). *P. falciparum* DHFR differs from the *Mtb* protein in that it forms a complex with thymidylate synthase, but the overall fold and interactions in the active site remain the same.

The similarities between *Mtb* and *P. falciparum* DHFR are only important to inhibitor development if they share features that are different in the human DHFR. The sequence identity between *Mtb* DHFR and the human counterpart is actually higher than between *Mtb* and *P. falciparum*; 26%, but the sequence identity is not indicative of the similarity in overall fold. The dihydrofolate binding site extends inward forming a deep hydrophobic pocket with the pterin portion of DHF binding deepest in the pocket and the glutamate pointing outwards to the solvent. While the exact residues are not conserved between all species, the network of four hydrogen bonds that interact with the pterin are highly conserved due to their importance in catalysis. But while the interior portion of the substrate binding site is largely unchanged between species, the outer portion of the substrate binding site displays interesting and potentially useful diversity.

Both the *Mtb* and *P. falciparum* DHFR share a commonality missing in the human counterpart; the glycerol binding pocket. In the pathogenic DHFRs just outside the substrate binding site is a small depression loosely surrounded by hydrophilic residues which is not present in human DHFR. These features are also present in the quadruple mutant (QM) *Pf* DHFR, whose mutations do not impact the overall fold of the protein much. In the human DHFR this region is tightly crowded with hydrophobic residues. There are also a key difference in the human DHFR due to Phe31, corresponding to Gln28 in *Mtb* and Met55 in *P. falciparum*, which has reduced rotational freedom due to its bulky phenyl group creating a much smaller space in the substrate binding site compared to the pathogenic proteins. This represents a potential avenue for inhibitor development.

DHFRs from *M. tuberculosis*, *P. falciparum*, and humans show little sequence identity between them. The sequence identity between *Mtb* and human DHFR is just 29%, and between *Mtb* and *Pf* DHFR-TS is 20%, however, they exhibit a surprising similarity in their overall fold (Cody, Luft et al. 1992, Li, Sirawaraporn et al. 2000, Yuvaniyama, Chitnumsub et al. 2003). The general DHFR active site structure is characterized by two main clefts; one cleft fits the cofactor, while the other cleft fits the substrate (dihydrofolate). As in previously solved DHFR structures from *E. coli* and *M. tuberculosis* (Matthews, Alden et al. 1977, Li, Sirawaraporn et al. 2000), our DHFR structures from *M. tuberculosis*, *P. falciparum,* and human have eight central β-strands and four surrounding α-helices. In *Mtb* DHFR, the substrate binding site is surrounded by three β-sheets (Val2-Ala9, Thr39-Gly43, and Thr91-Gly95) and three α-helices

(Pro25-Thr35, Arg44-Trp47, and Ala52-Val54). There are also two loop regions (Thr10-Leu24 and Asp48-Pro51) close to the substrate binding site. (Figure 4-4)

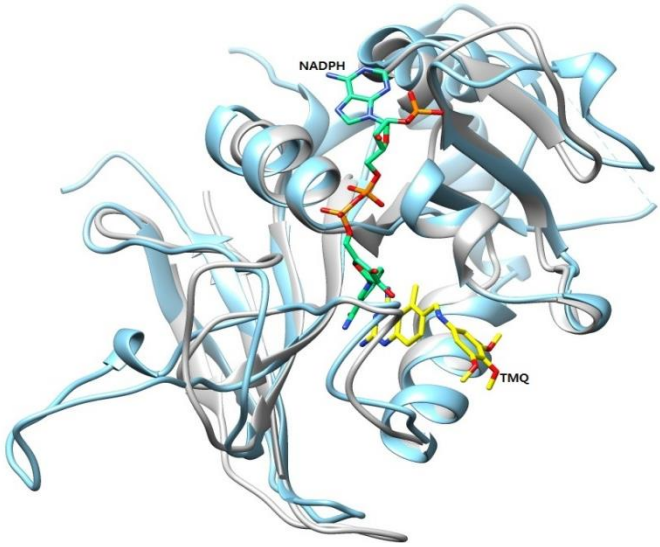

Figure 4-4. Superimposed structure of *Mtb* DHFR:TMQ (gray) and wild-type *Pf* DHFR-TS:TMQ. TMQ (yellow) and NADPH (green) are shown for the active site shape. They share the common structural scaffold, 8 beta-strands and 4 alpha-helices. In *Pf* DHFR-TS structures, depending on the inhibitors bound, showed some additional helices or strands.

Unlike *Mtb* and human DHFR, the *plasmodium* DHFR forms a complex with thymidylate synthase (TS), and *Pf* DHFR-TS forms a dimer linked by the two TS regions. However, the overall folding and the core residues of the DHFR active site are similar to *Mtb* and human DHFR (Yuvaniyama, Chitnumsub et al. 2003). There are three extra α-helices in *Pf* DHFR-TS (Val5-Phe9, Glu67-Leu81, and Val146-Lys155). The

Val5-Phe9 helix is close to the N-terminus and the other two helices are on the surface, all distant from the active site. None of these helices affect the overall fold or binding interactions of the inhibitors.

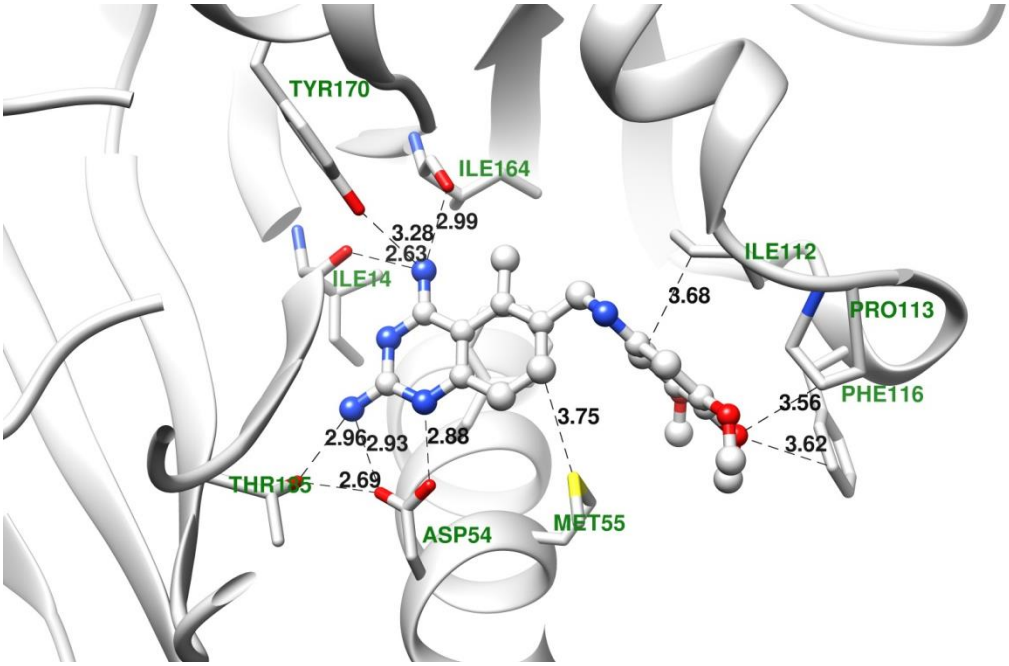

Figure 4-5. The important hydrogen bond interactions in wild type *Pf* DHFR-TS:TMQ structure. The interactions are very similar to *Mtb* DHFR, especially the 2,4-diaminoquinazoline side. On the other hand, interactions on 3,4,5-trimethoxybenzene ring side are not hydrogen bonds, yet they could be non-hydrogen bonding interactions including hydrophobic interactions or van der Waals interactions and potential leverage for the further SAR study

Similar to *Mtb* DHFR:TMQ structure, the 2,4-diaminoquinazoline ring of TMQ has well-conserved hydrogen bond interactions with WT *Pf* DHFR (Figure 4-5). This WT *Pf* DHFR structure bound with TMQ displayed the well-conserved hydrogen

bonding interactions between WT *Pf* DHFR and TMQ similar to *Mtb* DHFR:TMQ structure. Asp54 (corresponding to Asp27 in *Mtb* DHFR) has two hydrogen bonding interactions with 2-amino group and N-1 nitrogen of the quinazoline with the distances of 2.93 Å and 2.88 Å, respectively. Asp54 further forms the hydrogen bonding network with Thr185 and the distance is 2.69 Å. Thr185 has another hydrogen bonding network with 2-amino group of the quinazoline ring of TMQ, and the distance is 2.96 Å.

For 4-amino group of the 2,4-diaminoquinzaoline ring of TMQ has three hydrogen bonding interactions with the main chain carbonyl group of Ile14, with the main chain carbonyl group of Ile164, and with the carbonyl group of Tyr170. The distances are 2.63 Å, 2.99 Å, and 3.28 Å, respectively.

For the trimethoxyaniline ring side, there are no actual hydrogen-bonding interactions. However, there are some noticeable residues that are within the close proximity. The 2-carbon atom of the trimethoxyaniline is close to Ile112 and the distance is 3.68 Å .The oxygen atom of 4-methoxy group is close proximity with Pro113 and Phe116 with the distances of 3.56 Å and 3.62 Å. Although these methoxy groups are not in hydrogen bonding interactions, they represent a potential venue for enhancing the interactions with DHFR.

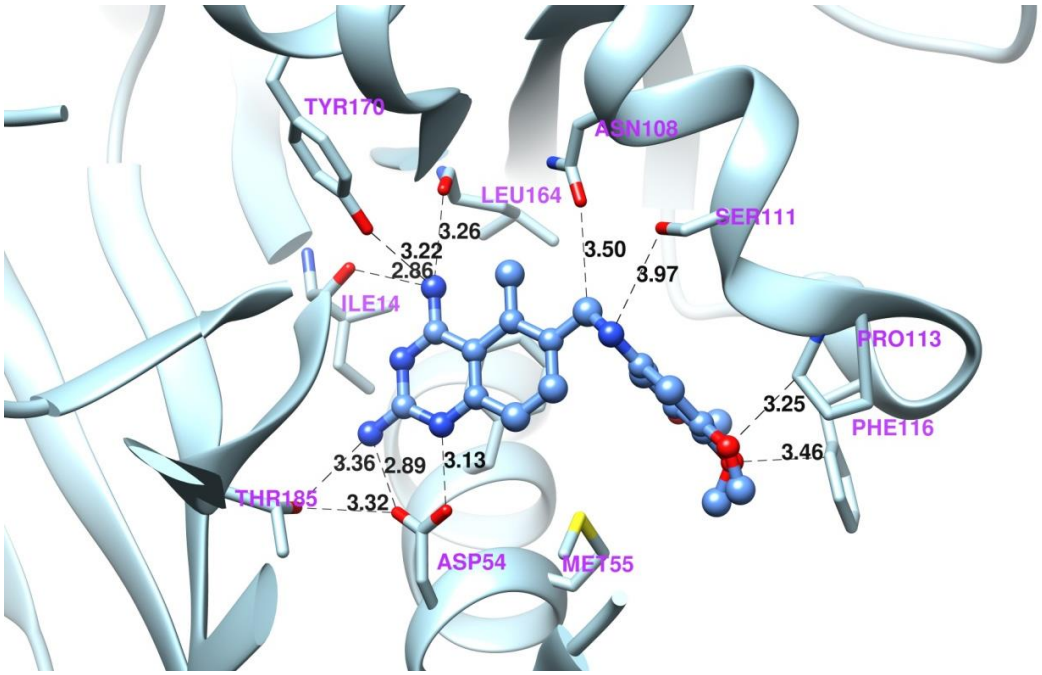

Figure 4-6. The important conserved interaction between TMQ and QM *Pf* DHFR. Met55 was labeled for the further discussion on its role. I164L mutation does not affect much on the interaction with 4-amino group of 2,4-diaminoquinzoline ring, but S108N mutation decrease the distance to TMQ. In TMQ, there is no available interaction with Asn108, but with proper modification, additional interaction with Asn108 could be introduced.

Similar to WT *Pf* DHFR:TMQ structure, the 2,4-diaminoquinazoline ring of TMQ has well-conserved hydrogen bond interactions with QM *Pf* DHFR (Figure 4-6). This QM *Pf* DHFR structure bound with TMQ displayed the well-conserved hydrogen bonding interactions between QM *Pf* DHFR and TMQ similar to *Mtb* DHFR:TMQ or WT *Pf* DHFR:TMQ structure. Asp54 (corresponding to Asp27 in *Mtb* DHFR) has two hydrogen bonding interactions with 2-amino group and N-1 nitrogen of the quinazoline with the distances of 2.89 Å and 3.13 Å, respectively. Asp54 further forms a hydrogen bonding network with Thr185 and the distance is 3.32 Å. Thr185 has another hydrogen

bonding network with 2-amino group of the quinazoline ring of TMQ, and the distance is 3.36 Å. This hydrogen bonding network is much weaker compared to WT *Pf* DHFR or *Mtb* DHFR.

For 4-amino group of the 2,4-diaminoquinzaoline ring of TMQ has three hydrogen bonding interactions with the main chain carbonyl group of Ile14, with the main chain carbonyl group of Leu164, and with the carbonyl group of Tyr170. The distances are 2.85 Å, 3.26 Å, and 3.22 Å, respectively. One thing noticeable here is that I164L mutation caused the distance 0.27 Å extended compared to the wild type.

For the 3,4,5-trimethoxyaniline ring side, there are no actual hydrogen-bonding interactions just as WT *Pf* DHFR. However, there are some noticeable residues that are within the close proximity. The aniline nitrogen has hydrogen bond interaction with the oxygen of Ser111 with the distance of 3.97 Å. The oxygen atom of 3-methoxy group is in close proximity with Pro113 with the distance of 3.25 Å, and the oxygen atom of 4-methoxy group is in close proximity with Phe116 with the distances of 3.46 Å .Although these methoxy groups are not in hydrogen bonding interactions, they represent a potential venue for enhancing the interactions with DHFR. It is intriguing to see that S108N mutation caused Asn108 comes into 3.50 Å away from TMQ. In WT *Pf* DHFR-TS:TMQ structure, Ser108 was more than 4 Å away from TMQ. Even though there is no hydrogen bonding interaction available with Asn108 here, some modification on that position could develop a QM *Pf* DHFR-TS specific inhibitor.

Since there is no apo or cofactor (NADPH) bound structures of *Pf* DHFR-TS available, the RMSD calculation was done using the wild-type *Pf* DHFR-TS structure

bound with the substrate, dihydrofolate (4DPD). The RMSD over 205 Cα carbons with 96.4% sequence identity is 0.29 Å. The sequence difference comes from a missing loop (Ser22-Asn29) in the substrate bound structure. There also is a common missing loop region (Val86-Ser95) in both structures.

As in the previously published *Mtb* DHFR structures (1DG5 or 1DF7), our *Mtb* DHFR substrate binding site is loosely surrounded by hydrophilic residues such as Trp22 or Gln28, while the analogous site in human DHFR is tightly crowded by hydrophobic residues. *Pf* DHFR's substrate binding site is slightly larger than that of *Mtb* DHFR. One of the crucial differences is between Gln28 in *Mtb* DHFR (Met55 in *Pf* DHFR) and Phe31 in human DHFR. The bulky benzyl group of Phe31 and its reduced rotational freedom compared to Gln28 and Met55 prevent it from flipping away to provide more room for the C-8 functional groups of our modified TMQ inhibitors.

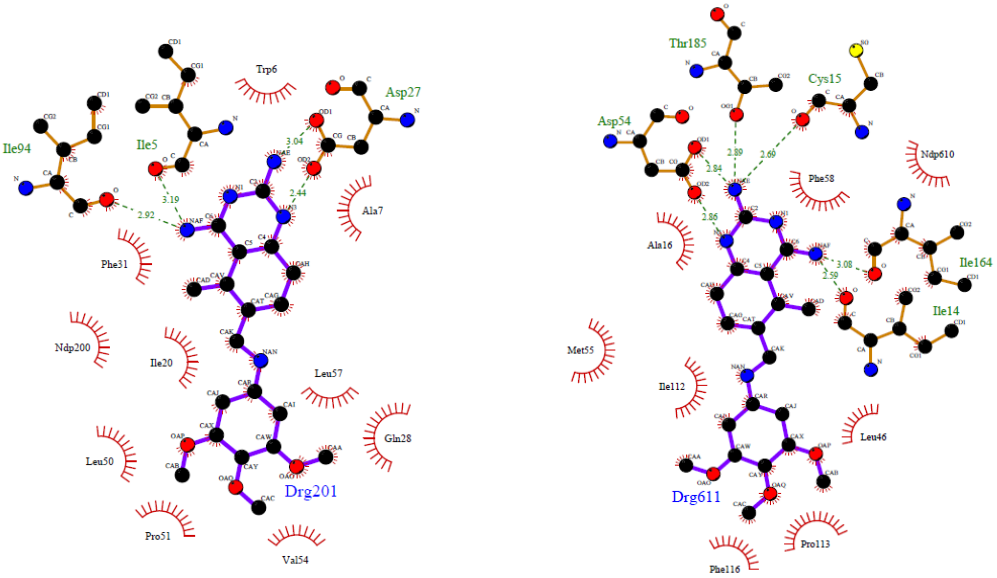

Figure 4-7. Graphical diagram of the interactions of TMQ with *Mtb* DHFR (left), and with wild-type *Pf* DHFR-TS. Both structures showed well conserved interactions with acidic residue (Aps27 in *Mtb* DHFR and Asp54 in *Pf* DHFR-TS), with isoleucines via 4-amino group of the quinazoline ring and *pi* stacking interaction with Phe31 in *Mtb* DHFR and Phe58 in *Pf* DHFR-TS.

The substrate binding sites of the known structures of *Mtb* DHFR and *Pf* DHFR-TS were closely examined (Figure 4-7). For the TMQ bound DHFR structures, the RMSD between *Mtb* DHFR and human DHFR is 1.28 Å over 144 Cα carbons with 33% sequence identity, and between *Pf* DHFR-TS and human DHFR the RMSD is 1.09 Å over 164 Cα carbons with 31% sequence identity.

The *Mtb* DHFR structures show TMQ and its analogs interact with Asp27 through the 2-amino group and N-1 nitrogen of the quinazoline ring, and with the main chain carbonyl groups of Ile94 and Ile5 through the 4-amino group of the quinazoline ring

(Figure 3). In *Mtb* DHFR, Asp27, which corresponds to Glu30 in human DHFR and Asp54 in *Pf* DHFR-TS, is the acid that gives up a hydrogen atom to the substrate (DHF). In the *Mtb* DHFR:TMQ structure, the distances between Asp27 and N-1, and Asp27 and the 2-amino group are 2.62 Å and 2.74 Å. TMQ and the C-8 benzyl-2,4-diaminoquinazoline TMQ analogs form hydrogen bonds with Ile5 and Ile94 in *Mtb* DHFR through the backbone carbonyl groups. In the *Mtb* DHFR:TMQ structure, the distance between Ile5 and the 4-amino group of the quinazoline is 2.86 Å and that of Ile94 and the same 4-amino group is 2.86 Å. These two isoleucines correspond to Ile14 and Ile164 in *Pf* DHFR-TS. Tyr100 in *Mtb* DHFR, which is Tyr170 in *Pf* DHFR-TS, could form another hydrogen bond with the 4-amino group of the quinazoline ring at a distance of 3.40 Å between Tyr100 and the 4-amino group. However, in the *Mtb* DHFR:TMQ structure, Tyr100 is not at a favorable angle to the 4-amino group of the quinazoline ring for a hydrogen bond.

When TMQ is bound to *Mtb* DHFR, it makes only slight conformational changes compared to the *Mtb* DHFR:NADPH structure (1DG8). The RMSD over 159 Cα carbons with 100% sequence identity is 0.69 Å. The biggest deviations are seen between Ser49-Val54 close to the substrate binding site, and Arg143-Arg150, which is a loop region close to the C-terminus. Specifically, Leu50 and Pro51 are closer to the substrate binding site in our TMQ bound structure strengthening their interaction with TMQ.

Trimetrexate (TMQ) exhibited high potency against both *Mtb* and human DHFR with IC_{50}s of 17 nM and 16 nM. In order to increase the potency of TMQ against the pathogenic DHFR in relation to the human DHFR, we made two major types of

modifications to the parent compound (Figure 4). We made changes to the C-8 position of the 2,4-diaminoquinazoline ring and to the aniline ring, and compared the activity and structure of each compound. To facilitate the synthesis of the compounds, 2,4-dimethoxybenzene analogs were introduced instead of 2,3,4-trimethylbenzene as in TMQ. The C-5 methyl group was removed from the 2,4-diaminoquinazoline ring for the same reason. This compound, JCS-1381, lost 10 fold activity against both *Mtb* and the human DHFR.

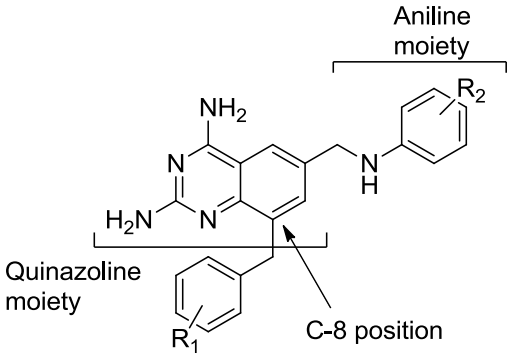

TMQ modifications

TMQ also exhibited strong potency against both wild-type (WT) and quadruple-mutant (QM) *Pf* DHFR-TS with IC_{50}s of 5 nM and 6 nM. The RMSD for the TMQ bound structures of WT and QM *Pf* DHFR-TS was 0.43 Å for 217 residues with a 96.8% sequence identity, with the largest deviation arising from the loop region (residues 21-28) and residues near the missing region (residues 86-95). This missing region came from the model (1J3I and 4DP3), and the density was missing in our data as well.

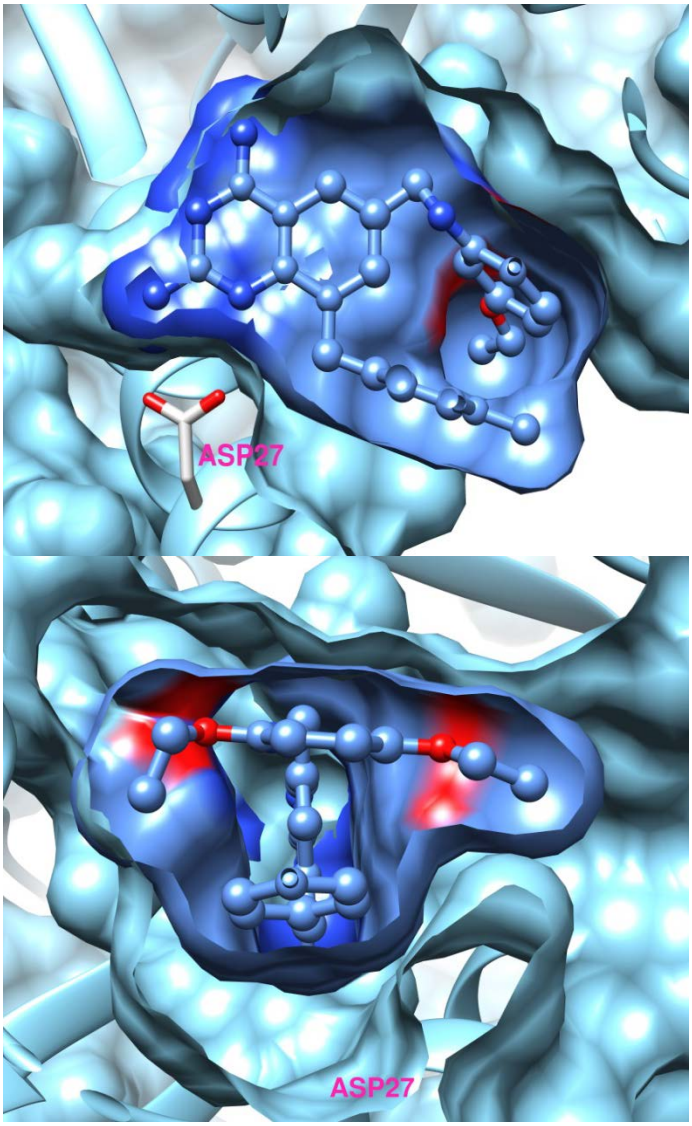

Figure 4-8. JCS-1474 in the active site of *Mtb* DHFR. Views from the front (top) and from the aniline ring side (bottom). JCS-1474 sits snugly in the active site thanks to the flexible Gln28 residue in *Mtb* DHFR.

JCS-1474, one of the C-8 benzyl TMQ analogs, exhibited an exceptional selectivity against Mtb DHFR over human counterpart (90 fold). According to the structure, *Mtb* DHFR:JCS-1474, significant clues could be drawn (Figure 4-8, 4-9).

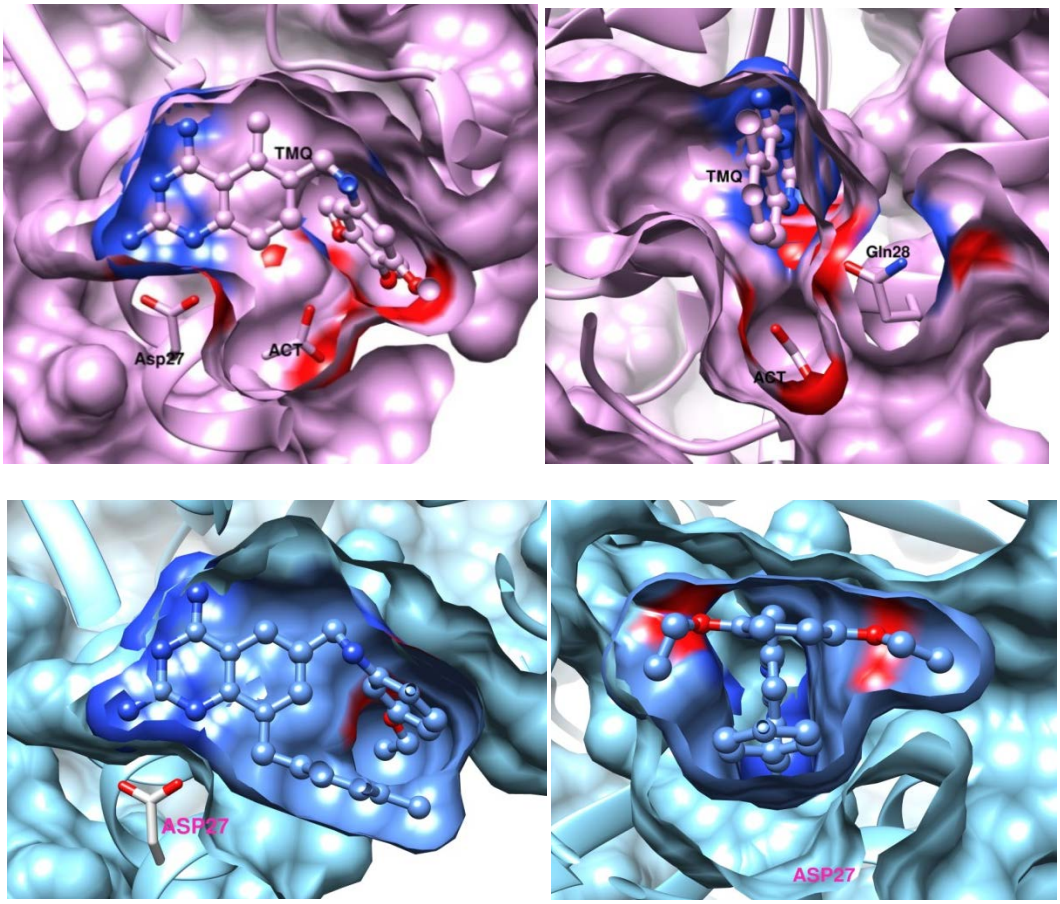

Figure 4-9. TMQ (purple) and JSF-1474 in the active site of *Mtb* DHFR. Views from the front (left) and from the aniline ring side (right). JSF-1474 sit snugly in the active site by creating space that was not available in *Mtb* DHFR:TMQ structure due to Gln28's orientation. The acetate (ACT) molecule that was found in the *Mtb* DHFR:TMQ structure is not found in the *Mtb* DHFR:JSF-1474 structure and C-8 benzyl group occupies that space partially.

2,4-diaminoquinazoline ring occupies the similar space in both *Mtb* DHFR:TMQ and *Mtb* DHFR:JCS-1474 structures. C-8 benzyl group in JCS-1474 occupies the space where an acetate molecule was found in *Mtb* DHFR:TMQ structure. This space is not available in human DHFR due to the bulky Phe31 and its lack of rotational freedom and this caused the drastic potency loss of JCS-1474 in human DHFR with the IC_{50} of 18000 nM. However, in Mtb DHFR, Gln28, with its smaller size and greater rotational freedom, allowed the enough space for C-8 benzyl group and lost just a little bit of potency with the IC_{50} of 200 nM.

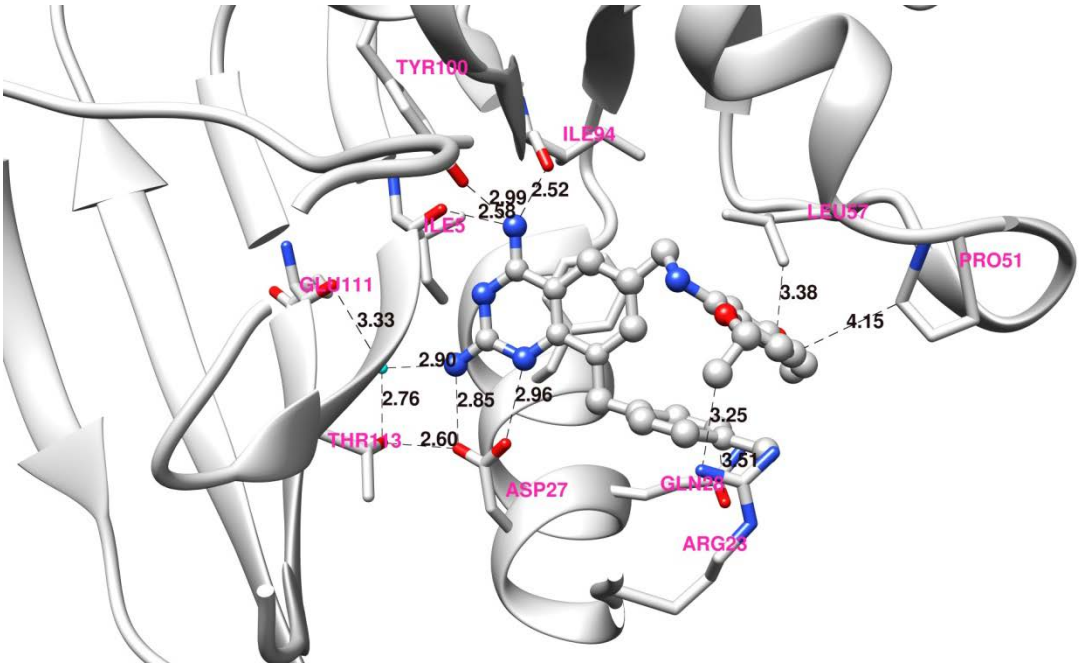

Figure 4-10. The important conserved interactions between JCS-1474 and *Mtb* DHFR. C-8 benzyl group clearly pushed down Gln28 so that the bulky C-8 benzyl group can be accommodated in the pocket. The major hydrogen bond interactions on 2,4-diaminoquinazoline ring side are well conserved. On the other hand, there are a couple of new interactions were found on the 2,5-diethoxyaniline ring side.

When we checked the *Mtb* DHFR:JCS-1474 crystal structure, which were grown from significantly different condition than *Mtb* DHFR:TMQ, has much similarity in the major interactions between the compound and the protein (Figure 4-10). Similar to *Mtb* DHFR:TMQ structure, the 2,4-diaminoquinazoline ring of JCS-1474 has well-conserved hydrogen bond interaction with *Mtb* DHFR. This *Mtb* DHFR structure bound with JCS-1474 displayed the well-conserved hydrogen bonding interactions between *Mtb* DHFR and JCS-1474 similar to TMQ bound *Mtb* DHFR structure. Asp27 has two hydrogen bonding interactions with 2-amino group and N-1 nitrogen with the distances of 2.85 Å and 2.96 Å, respectively. Both distances are about 0.2 Å longer than in *Mtb* DHFR:TMQ structure. Asp27 further forms the hydrogen bonding network with Thr113 and the distance is 2.60 Å. Thr113 has another hydrogen bonding network via a water molecule with 2-amino group of the quinazoline ring of JCS-1474, and the distance between Thr113 and this water molecule is 2.76 Å and between the water molecule and the 2-amino group of TMQ is 2.90 Å. This water molecule has an additional hydrogen bond interaction with the main chain carbonyl of Glu111 and the distance of this interaction is 3.33 Å.

For 4-amino group of the 2,4-diaminoquinzaoline ring of JCS-1474 has three hydrogen bonding interactions with the main chain carbonyl group of Ile5, with the main chain carbonyl group of Ile94, and with the carbonyl group of Tyr100. The distances are 2.59 Å, 2.52 Å, and 2.99 Å, respectively. All of the three distances are shorter than the ones in *Mtb* DHFR:TMQ structure, yet JCS-1474 lost more than 10 fold of potency, and this could indicate that these three hydrogen bond interactions are either not in the

favorable angles or not so significant to the overall interaction between DHFR and JCS-1474.

For the 2,5-dimethoxyaniline ring side, the carbon atom of 2-ethoxy group is in close proximity with Leu57 with the distance of 3.38 Å. The 4-carbon atom of the benzene ring is in close proximity with the carbon atom of Pro51 with the distance of 4.15 Å. The carbon atom of 5-ethoxy group also is in close proximity with Arg23 with the distance of 3.25 Å. Although these ethoxy groups are not technically in hydrogen bonding interactions with DHFR residues, they represent a potential venue for enhancing the interactions with DHFR.

Adding a benzyl group as in JCS-1474 (4-methylbenzyl) improved the selectivity considerably by significantly reducing the potency of this compound against human DHFR (IC_{50} = 18000 nM) versus the *Mtb* protein (IC_{50} = 200 nM) and the wild-type *Pf* DHFR-TS (IC_{50} = 20 nM). JCS-1474 did lose considerable activity against QM *Pf* DHFR-TS (IC_{50} = 70 nM) compared to the wild-type, but still retained sufficient activity to confer selectivity against the human DHFR. The modifications and their effect on IC_{50} are illustrated in Tables 1 and 2. The size of the pocket near the substrate binding site of WT and QM *Pf* DHFR-TS is almost the same and the mutated residues of the mutant (N51I/C59R/ S108N/I164L) do not significantly alter the binding interactions of the C-8 benzyl-2,4-diaminoquinazoline TMQ analogs. For instance, the closest contact comes from between the main chain carbonyl group of I164L of *Pf* DHFR-TS and the 4-amino group of the quinazoline ring. The distance of this contact is 2.8 Å in the WT *Pf* DHFR-TS:JCS-1474 structure, and 2.9 Å in the QM *Pf* DHFR-TS:JCS-1474 structure (Figure

4-12). The reduced potency of the C-8 benzyl group compounds in the quadruple-mutant *Pf* DHFR-TS compared to the wild-type can be explained by the longer distances between interacting residues. In the WT *Pf* DHFR-TS:JCS-1474 structure, the distances between the 4-amino group of the quinazoline ring and the three interacting residues, Ile14, Ile164, and Tyr170 are 2.6 Å, 2.8 Å, and 2.6 Å, respectively. These distances are increased in the QM *Pf* DHFR-TS:JCS-1474 structure to 2.8 Å, 2.9 Å, and 2.9 Å, reducing the strength of the interactions (Table 4-1).

JCS-1474	Asp27 (O) : 2-amino (N)	Asp27 (O) : N-1	Ile5 main (O) : 4-amino (N)	Ile94 main (O) : 4-amino (N)	Tyr100 (O) : 4-amino (N)
Mtb DHFR	2.85	2.96	2.58	2.52	2.99
WT *Pf* DHFR-TS	2.87 (Asp54)	2.99	2.51 (Ile14)	2.79 (Ile164)	2.62 (Tyr170)
QM *Pf* DHFR-TS	2.94	3.22	2.81	2.79 (Leu164)	2.89
DM *Pf* DHFR-TS (JCS-1552)	2.65	2.86	2.49	2.99	2.61
QM *Pf* DHFR-TS (JCS-1552)	2.48	3.21	2.85	2.83	3.07
human DHFR (JCS-1502)	2.80 (Glu30)	2.96	2.67 (Ile7)	2.82 (Val115)	3.01 (Tyr121)

Table 4-1. The conserved hydrogen bond interactions in C-8 benzyl TMQ bound structures from various DHFRs. The major interactions on 2,4-diaminoquinazoline ring with the residues are well conserved, and the distances are consistent with the degree of potency in the corresponding DHFRs. JCS-1474 and JCS-1552 has different substituent on the aniline ring side, and it is not for the cross-comparison.

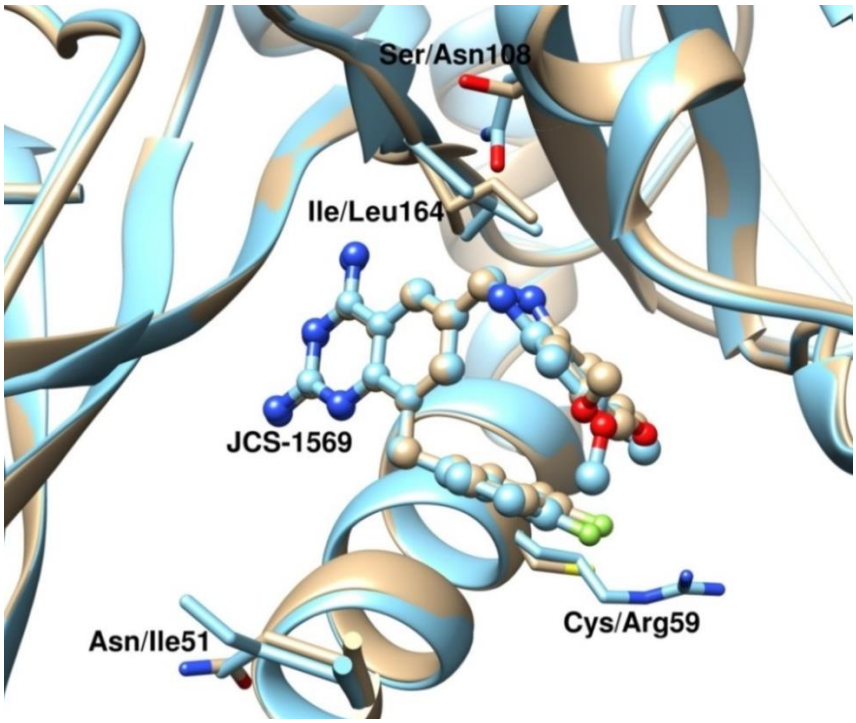

Figure 4-11. Superimposed structure of WT (khaki) and QM *Pf* DHFR:JCS-1569. The four mutations (N51I, C59R, S108N, and I164L) are shown with labels. Other than Ile164 (Leu164), all the other three positions are more than 3.5 Å away from the C-8 benzyl TMQ analogs, and I164L mutation does not have significant impact on the binding of C-8 benzyl TMQ on QM *Pf* DHFR-TS. The reasons for the activity loss on QM *Pf* DHFR-TS remain to be seen.

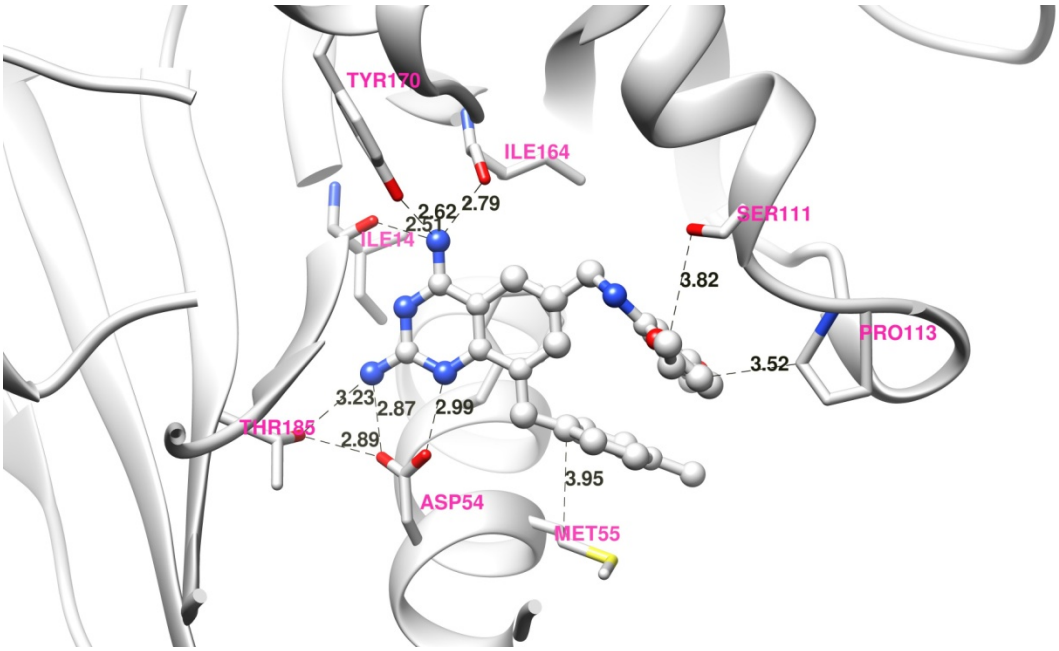

Figure 4-12. The important conserved interactions between WT *Pf* DHFR and JCS-1474. The interactions on 2,4-diaminoquinazoline ring side are well conserved as in WT *Pf* DHFR:TMQ structure. The distances between Asp54 and 2-amino group and 1-nitrogen is significantly longer than WT *Pf* DHFR:TMQ structure. As Gln28 in *Mtb* DHFR, Met55 offered large enough space for C-8 benzyl group due to its rotational freedom and small side chain.

When we checked the WT *Pf* DHFR:JCS-1474 crystal structure, which were grown from significantly different condition than *Mtb* DHFR:TMQ or WT *Pf* DHFR:TMQ structures, has much similarity in the major interactions between the compound and the protein (Figure 4-12). Similar to *Mtb* DHFR:TMQ or WT *Pf* DHFR:TMQ structures, the 2,4-diaminoquinazoline ring of JCS-1474 has well-conserved hydrogen bond interactions with WT *Pf* DHFR. This WT *Pf* DHFR structure bound with JCS-1474 displayed the well-conserved hydrogen bonding interactions between WT *Pf* DHFR and JCS-1474 similar to TMQ bound WT *Pf* DHFR structure.

Asp54, corresponding to Asp27 in *Mtb* DHFR, has two hydrogen bonding interactions with 2-amino group and N-1 nitrogen with the distances of 2.87 Å and 2.99 Å, respectively. Both distances are about 0.1 Å longer than in WT *Pf* DHFR:TMQ structure. Asp54 further forms the hydrogen bonding network with Thr185 and the distance is 2.89 Å. Thr185 has another hydrogen bonding network with 2-amino group of the quinazoline ring of JCS-1474, and the distance between Thr185 and the 2-amino group of JCS-1474 is 3.23 Å.

For 4-amino group of the 2,4-diaminoquinzaoline ring of JCS-1474 has three hydrogen bonding interactions with the main chain carbonyl group of Ile14, with the main chain carbonyl group of Ile164, and with the carbonyl group of Tyr170. The distances between the 4-amino group and those residues are 2.51 Å, 2.79 Å, and 2.62 Å, respectively. All of the three distances are shorter than the ones in WT *Pf* DHFR:TMQ structure, yet JCS-1474 lost more than 4 fold of potency as in *Mtb* DHFR, and this could indicate that these three hydrogen bond interactions are either not in the favorable angles or not so significant to the overall interaction between WT *Pf* DHFR and JCS-1474.

For the 2,5-diethoxyaniline ring side, the carbon atom of 5-ethoxy group is in close proximity with Ser111 with the distance of 3.82 Å. The 4-carbon atom of the benzene ring is in close proximity with the carbon atom of Pro113 with the distance of 3.52 Å. The C-8 benzene ring has pi stacking interaction with Met55 with the distance of 3.95 Å. Although these ethoxy groups are not technically in hydrogen bonding interactions with WT *Pf* DHFR residues, they represent a potential venue for enhancing the interactions with DHFR.

The mutations in the quadruple-mutant do not have a significant impact on inhibitor binding. Ile51 is far away from the active site, and the side chains of Asn108 and Leu164 stretch in the opposite direction from the inhibitor. The main chain oxygen of Leu164 (or Ile164) can have the hydrogen bonding interaction with TMQ or its analogs, but the differences in distance are not crucially altered by the mutation (Figure 4-13). Arg59, similar to Arg23 in *Mtb* DHFR, comes in closer contact with the aniline ring side of the compound but still not close enough to contribute a strong interaction. In the *Pf* DHFR-TS:JCS-1474 structure, the Arg59 in chain B is at a distance of 5.2 Å to JCS-1474.

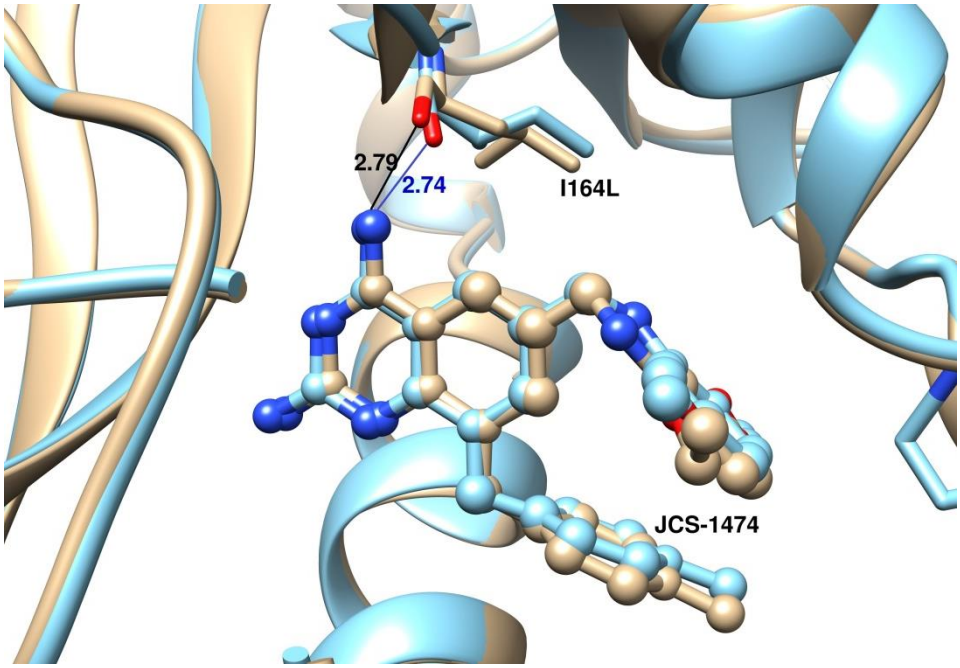

Figure 4-13. Superimposed structure of WT *Pf* DHFR:JCS-1474 (blue) and QM *Pf* DHFR:JCS-1474.

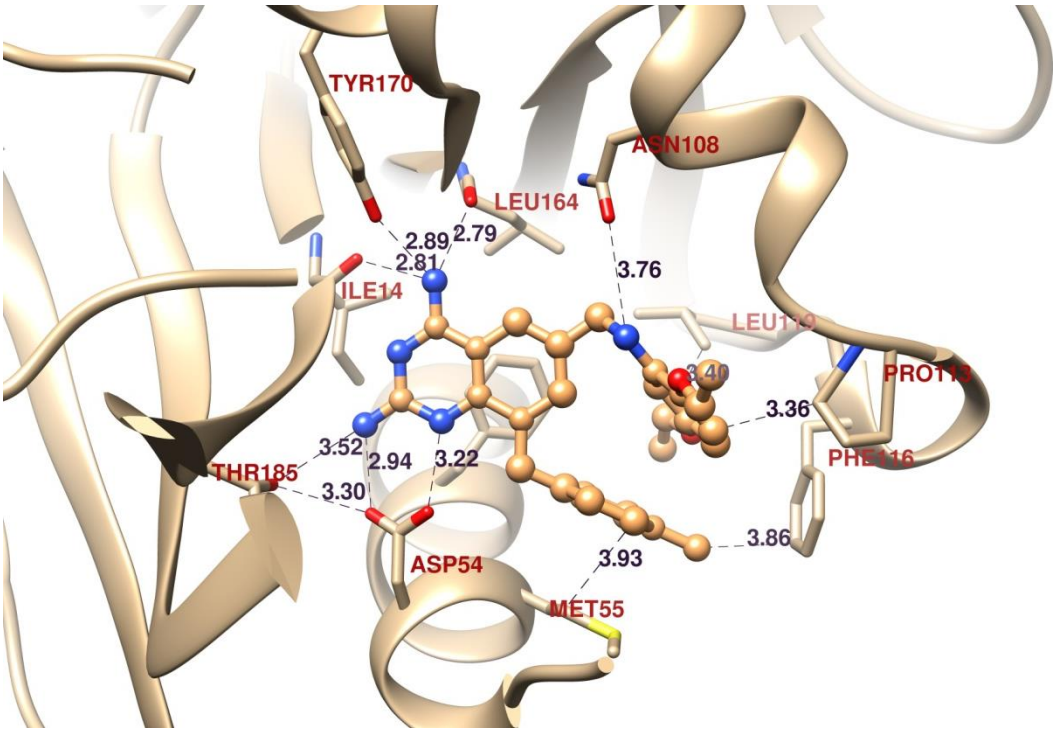

Figure 4-14. The important conserved interactions between QM *Pf* DHFR and JCS-1474. As other TMQ analogs, JCS-1474's 2,4-diaminoquinazoline ring retains all the major hydrogen bonding interactions with QM Pf DHFR. Met55 flipped down as in the WT Pf DHFR:JCS-1474 to be able to accommodate the C-8 benzyl group. Leu164 and Asn108 have better interactions than WT's counterpart.

When the QM *Pf* DHFR:JCS-1474 crystal structure was inspected, which were grown from a different condition than *Mtb* DHFR:TMQ or WT *Pf* DHFR structures, it has much similarity in the major interactions between the compound and the protein (Figure 4-14). Similar to *Mtb* DHFR:TMQ or WT *Pf* DHFR:TMQ structures, the 2,4-diaminoquinazoline ring of JCS-1474 has well-conserved hydrogen bond interactions with QM *Pf* DHFR. This QM *Pf* DHFR structure bound with JCS-1474 displayed the well-conserved hydrogen bonding interactions between QM *Pf* DHFR and JCS-1474

similar to TMQ bound QM *Pf* DHFR structure. Asp54, corresponding to Asp27 in *Mtb* DHFR, has two hydrogen bonding interactions with 2-amino group and N-1 nitrogen with the distances of 2.94 Å and 3.22 Å, respectively. Both distances are about 0.1 Å longer than in QM *Pf* DHFR:TMQ structure. This increase in distances was also observed in WT *Pf* DHFR. Asp54 further forms the hydrogen bonding network with Thr185 and the distance is 3.30 Å. Thr185 has another hydrogen bonding network with 2-amino group of the 2,4-diaminoquinazoline ring of JCS-1474, and the distance between Thr185 and the 2-amino group of JCS-1474 is 3.52 Å. These two interactions and their distances are about 0.3 Å longer than in WT *Pf* DHFR:JCS-1474 structure.

For 4-amino group of the 2,4-diaminoquinzaoline ring of JCS-1474 has three hydrogen bonding interactions with the main chain carbonyl group of Ile14, with the main chain carbonyl group of Ile164, and with the carbonyl group of Tyr170. The distances between the 4-amino group and those residues are 2.81 Å, 2.79 Å, and 2.89 Å, respectively. The distance between the 4-amino group and the main chain carbonyl group of Ile14 is about 0.05 Å shorter than QM *Pf* DHFR:TMQ structure, and the other two distances are about 0.3 Å shorter than the ones in QM *Pf* DHFR:TMQ structure, yet JCS-1474 lost more than 4 fold of potency as in *Mtb* DHFR, and this could indicate that these three hydrogen bond interactions are either not in the favorable angles or not so significant to the overall interaction between QM *Pf* DHFR and JCS-1474. It is interesting to see that S108N mutation caused 0.42 Å increase in the distance from JCS-1474, and I164L mutation caused 0.05 Å increase in the distance from the 4-amino group of the 2,4-diaminoquinazoline ring.

For the 2,5-diethoxyaniline ring side, the carbon atom of 5-ethoxy group is in close proximity with Lue119 with the distance of 3.81 Å .The 3-carbon atom of the 2,5-diethoxyaniline ring is in close proximity with the carbon atom of Pro113 with the distance of 3.36 Å .The C-8 benzene ring has *pi* stacking interaction with Met55 with the distance of 3.93 Å. The carbon atom of the 4-methyl group of the C-8 benzyl group is in close proximity with Phe116 with the distance of 3.86 Å. Although these ethoxy groups are not in the hydrogen bonding interactions with QM *Pf* DHFR residues, they represent a potential venue for enhancing the interactions with DHFR.

The closest contact among the 4 mutations in the quadruple mutant of *Pf* DHFR-TS, comes from I164L mutation. The side chains are a bit far from the substrate binding site. However, the distance from the main chain carbonyl is close enough to have a hydrogen bond interaction with the 4 amino group of 2,4-diaminoquinazoline ring of TMQ and C-8 benzyl TMQ analogs.

The distance between the man chain carbonyl of Ile164 and TMQ in WT *Pf* DHFR-TS is 2.99 Å. The same distance between Leu164 and TMQ became 3.26 Å in QM *Pf* DHFR-TS, and the I164L mutation caused the distance longer, and weaken the interaction of TMQ and the protein as a result. However, this difference in the distances between wild type and quadruple mutant DHFR is much smaller with C-8 benzyl TMQ analogs. For example, as previously seen, with JCS-1474 bound QM *Pf* DHFR the distance between Leu164 and the 4-amino group is 2.79 Å, and it is just 0.05 Å longer than the distance between Ile164 and the 4 amino group in WT *Pf* DHFR-TS (2.74 Å).

In the JCS-1569 bound structures, the distance is even 0.08 Å shorter in QM *Pf* DHFR-TS (2.71 Å) than in WT *Pf* DHFR-TS (2.79 Å).

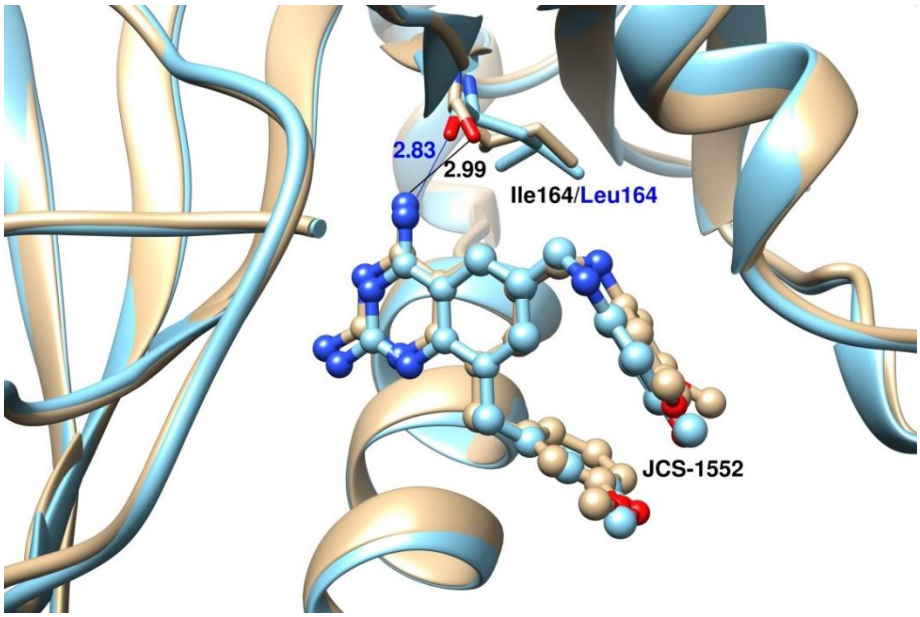

Figure 4-15. Superimposed structure of DM *Pf* DHFR-TS:JCS-1552 (khaki) and QM *Pf* DHFR-TS:JCS-1552. The distance of the hydrogen bonding interaction between the main chain carbonyl of Ile164 and the 4-amino group of JCS-1552 in DM *Pf* DHFR is 2.99 Å, and the same distance of Leu164 and 4-amino group of JCS-1552 in QM *Pf* DHFR is 0.16 Å shorter and 2.83 Å. This is an example of the inversed distance in the quadruple mutant.

In the case of double mutant (DM) *Pf* DHFR-TS:JCS-1552 structure, the inversed distance was observed when compared to QM *Pf* DHFR-TS:JCS-1552 (Figure 4-15). This particular case might be an exception for the general trend of the increase of the distance with the quadruple mutant especially, I164L mutation. However, the decrease in

the distance of Leu164 main chain carbonyl group and the 4-amino group of JCS-1552 in QM *Pf* DHFR-TS is 0.16 Å and this is significantly shorter, for there was about 0.05-0.1 Å increase in the same distance found in other *Pf* DHFR-TS structures bound with TMQ or other C-8 benzyl TMQ analogs.

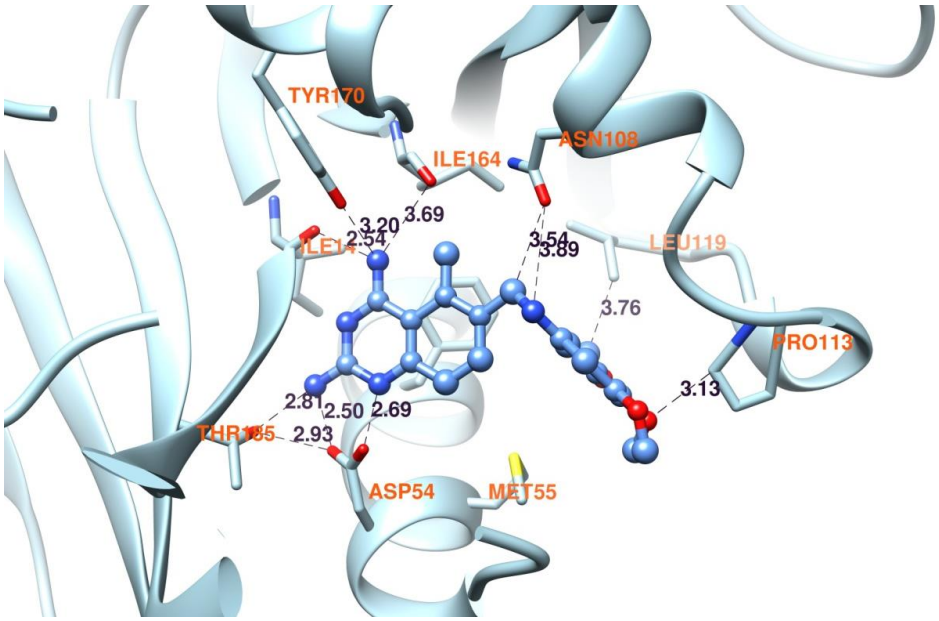

Figure 4-16. The important conserved interactions between DM *Pf* DHFR-TS and TMQ. Double mutant (C59R/S108N) *Pf* DHFR displayed similar interactions with WT or QM *Pf* DHFR:TMQ structures, and the distances are pretty similar to them. Note that interactions with Asn108 are available which are not available in WT *Pf* DHFR.

Similar to WT or QM *Pf* DHFR:TMQ structures, the 2,4-diaminoquinazoline ring of TMQ has well-conserved hydrogen bond interactions with DM *Pf* DHFR (Figure 4-16). This DM *Pf* DHFR structure bound with TMQ displayed the well-conserved hydrogen bonding interactions between DM *Pf* DHFR and TMQ similar to *Mtb*

DHFR:TMQ or WT *Pf* DHFR:TMQ structure. Asp54 (corresponding to Asp27 in *Mtb* DHFR) has two hydrogen bonding interactions with 2-amino group and N-1 nitrogen of the quinazoline with the distances of 2.50 Å and 2.69 Å, respectively. Asp54 further forms a hydrogen bonding network with Thr185 and the distance is 2.93 Å. Thr185 has another hydrogen bonding network with 2-amino group of the 2,4-diaminoquinazoline ring of TMQ, and the distance is 2.81 Å.

For 4-amino group of the 2,4-diaminoquinzaoline ring of TMQ has three hydrogen bonding interactions with the main chain carbonyl group of Ile14, with the main chain carbonyl group of Leu164, and with the carbonyl group of Tyr170. The distances are 2.54 Å, 3.69 Å, and 3.20 Å, respectively. One thing noticeable here is that I164L mutation caused the distance 0.70 Å extended compared to the wild type, this is even 0.47 Å longer than the quadruple mutation and it could be the reason of the mediocre potency of DM *Pf* DHFR despite the shorter distances between TMQ and Asp54.

For the 3,4,5-trimethoxyaniline ring side, there are no actual hydrogen-bonding interactions just as WT *Pf* DHFR. However, there are some noticeable residues that are within the close proximity. The aniline nitrogen has a possible hydrogen bond interaction with the oxygen of Asn108 with the distance of 3.69 Å .This Asn108 oxygen is in close proximity with the aniline carbon with the distance of 3.54 Å. The oxygen atom of 4-methoxy group is in close proximity with Phe116 with the distances of 3.13 Å . Although these methoxy groups are not in hydrogen bonding interactions, they represent a potential venue for enhancing the interactions with DHFR. It is intriguing to see that S108N mutation caused Asn108 comes into 3.54 Å away from TMQ. In WT *Pf* DHFR-

TS:TMQ structure, Ser108 was more than 4 Å away from TMQ. Even though there is no hydrogen bonding interaction available with Asn108 here, some modification on that position could develop DM or QM *Pf* DHFR-TS specific inhibitor.

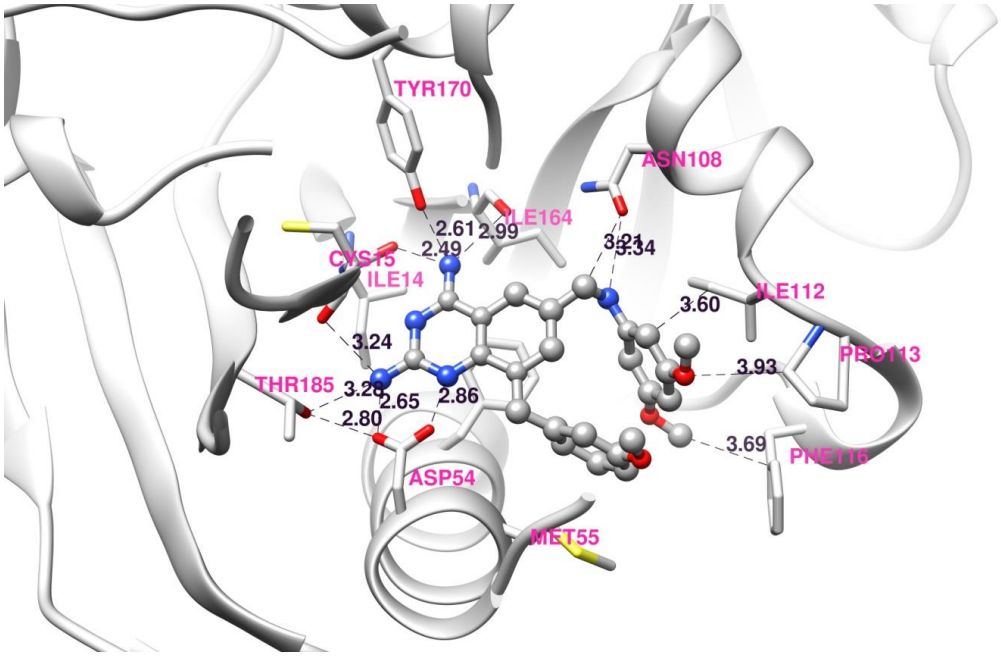

Figure 4-17. The important conserved interactions between DM *Pf* DHFR-TS and JCS-1552. Double mutant (C59R/S108N) *Pf* DHFR displayed similar interactions with WT or QM *Pf* DHFR:TMQ or JCS-1474 structures, and the distances are pretty similar to them. Note that interactions with Asn108 are available which are not available in WT *Pf* DHFR.

When we checked the DM *Pf* DHFR:JCS-1552 crystal structure, which were grown from significantly different condition than *Mtb* DHFR:TMQ or WT *Pf* DHFR structures, has much similarity in the major interactions between the compound and the

DM *Pf* DHFR-TS protein (Figure 4-17). Similar to *Mtb* DHFR:TMQ or WT *Pf* DHFR:TMQ or DM *Pf* DHFR:TMQ structures, the 2,4-diaminoquinazoline ring of JCS-1552 has well-conserved hydrogen bond interactions with DM *Pf* DHFR. This DM *Pf* DHFR structure bound with JCS-1552 displayed the well-conserved hydrogen bonding interactions between DM *Pf* DHFR and JCS-1552 similar to TMQ bound WT or DM *Pf* DHFR structure. Asp54, corresponding to Asp27 in *Mtb* DHFR, has two hydrogen bonding interactions with 2-amino group and N-1 nitrogen with the distances of 2.65 Å and 2.86 Å, respectively. Both distances are about 0.15 Å longer than in DM *Pf* DHFR:TMQ structure. Asp54 further forms the hydrogen bonding network with Thr185 and the distance is 2.80 Å. Thr185 has another hydrogen bonding network with 2-amino group of the quinazoline ring of JCS-1552, and the distance between Thr185 and the 2-amino group of JCS-1552 is 3.28 Å. This 2 amino group further forms another hydrogen bond interaction with the main chain carbonyl group of Cys15 with the distance of 3.24 Å .

For 4-amino group of the 2,4-diaminoquinzaoline ring of JCS-1552 has three hydrogen bonding interactions with the main chain carbonyl group of Ile14, with the main chain carbonyl group of Ile164, and with the carbonyl group of Tyr170. The distances between the 4-amino group and those residues are 2.49 Å, 2.99 Å, and 2.61 Å, respectively. All of the three distances are significantly shorter than the ones in DM *Pf* DHFR:TMQ structure, yet JCS-1552 lost more than 4 fold of potency compared to DM *Pf* DHFR:TMQ as in *Mtb* DHFR or WT *Pf* DHFR or QM *Pf* DHFR, and this could

indicate that these three hydrogen bond interactions are either not in the favorable angles or not so significant to the overall interaction between DM *Pf* DHFR and JCS-1552.

For the 3,5-dimethoxyaniline ring side, there are no actual hydrogen-bonding interactions just as WT *Pf* DHFR. However, there are some noticeable residues that are within the close proximity. The aniline nitrogen has a possible hydrogen bond interaction with the oxygen of Asn108 with the distance of 3.34 Å .This Asn108 oxygen is in close proximity with the aniline carbon with the distance of 3.21 Å. The 2-carbon atom of the aniline ring is in close proximity with Ile112 with the distance of 3.60 Å. The oxygen atom of 3-methoxy group is in close proximity with Pro113 with the distances of 3.93 Å, and the carbon atom of 5-methoxy group is in close proximity with Phe116 with the distance of 3.69 Å. Although these methoxy groups do not have hydrogen bonding interactions with DM *Pf* DHFR-TS, they represent a potential venue for enhancing the interactions with DHFR.

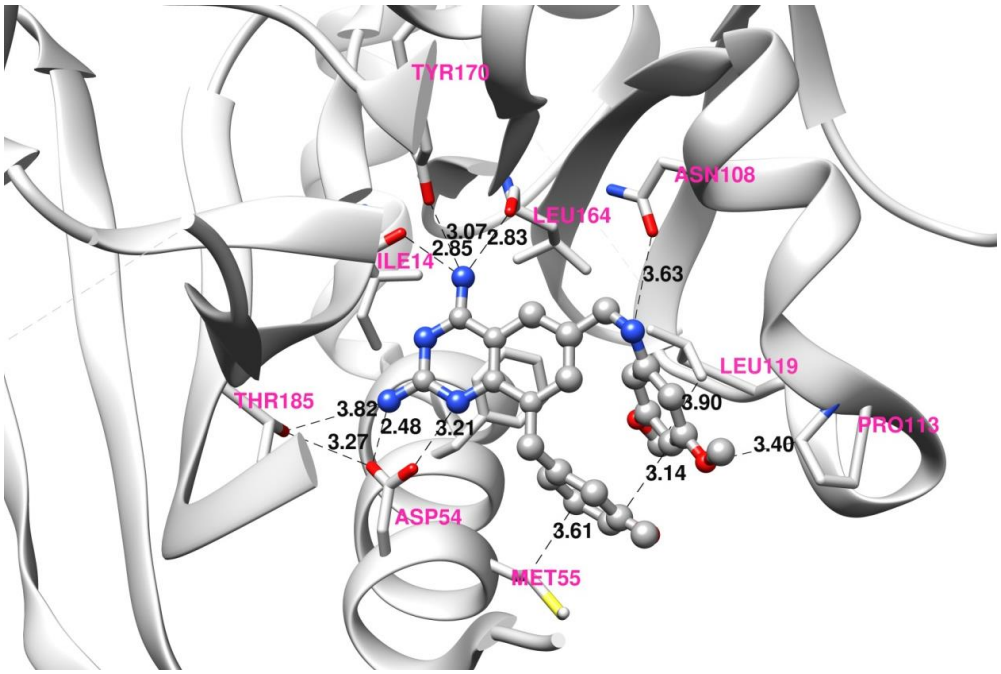

Figure 4-18. The important conserved interactions between QM *Pf* DHFR and JCS-1552. As in other structures bound with C-8 benzyl TMQ analogs, 2,4-diaminoquinazoline ring retains all the major hydrogen bonding interactions. C-8 benzyl group has pi stacking interaction with Met55 and the 3,5-dimethoxyaniline ring, and the 3,5-dimethoxyaniline ring is in close proximity with some of the QM *Pf* DHFR residues.

JCS-1552 bound structures were also elucidated on WT and QM *Pf* DHFR. When we checked the QM *Pf* DHFR:JCS-1552 crystal structure, which were grown from a different condition than *Mtb* DHFR:TMQ or DM *Pf* DHFR structures, has much similarity in the major interactions between the compound and QM *Pf* DHFR (Figure 4-18). Similar to *Mtb* DHFR:TMQ or WT *Pf* DHFR:TMQ or DM *Pf* DHFR:TMQ or DM *Pf* DHFR:JCS-1552 structures, the 2,4-diaminoquinazoline ring of JCS-1552 has well-conserved hydrogen bond interactions with QM *Pf* DHFR as well. This QM *Pf* DHFR structure bound with JCS-1552 displayed the well-conserved hydrogen bonding

interactions between QM *Pf* DHFR and JCS-1552 similar to TMQ bound WT or DM *Pf* DHFR structure. Asp54, corresponding to Asp27 in *Mtb* DHFR, has two hydrogen bonding interactions with 2-amino group and N-1 nitrogen with the distances of 2.48 Å and 3.21 Å, respectively. Asp54 further forms the hydrogen bonding network with Thr185 and the distance is 3.27 Å. Thr185 has another hydrogen bonding network with 2-amino group of the 2,4-diaminoquinazoline ring of JCS-1552, and the distance between Thr185 and the 2-amino group of JCS-1552 is 3.82 Å. This 2-amino group further forms another hydrogen bond interaction with the main chain carbonyl group of Cys15 with the distance of 3.57 Å .

For 4-amino group of the 2,4-diaminoquinzaoline ring of JCS-1552 has three hydrogen bonding interactions with the main chain carbonyl group of Ile14, with the main chain carbonyl group of Ile164, and with the carbonyl group of Tyr170. The distances between the 4-amino group and those residues are 2.85 Å, 2.83 Å, and 3.07 Å, respectively. All of the three distances are significantly shorter than the ones in QM *Pf* DHFR:TMQ structure, yet JCS-1552 lost potency compared to QM *Pf* DHFR:TMQ as in *Mtb* DHFR or WT *Pf* DHFR or DM *Pf* DHFR, and this could indicate that, due to C-8 benzyl group in JCS-1552, these three hydrogen bond interactions are either not in the favorable angles or not so significant to the overall interaction between QM *Pf* DHFR and JCS-1552.

For the 3,5-dimethoxyaniline ring side, there are no actual hydrogen-bonding interactions just as WT or DM *Pf* DHFR. However, there are some noticeable residues that are within the close proximity. The aniline nitrogen has a possible hydrogen bond

interaction with the oxygen of Asn108 with the distance of 3.63Å .This Asn108 oxygen is in close proximity with the aniline carbon with the distance of 3.14 Å. The oxygen atom of 3-methoxy group is in close proximity with Pro113 with the distances of 3.40 Å, and the carbon atom of 5-methoxy group is in close proximity with Leu119 with the distance of 3.90 Å .Although these methoxy groups do not have hydrogen bonding interactions with DM *Pf* DHFR-TS, they represent a potential venue for enhancing the interactions with DHFR.

C-8 benzyl group of JCS-1552 has some additional interactions. 5-carbon atom of the C-8 benzyl group has probable pi stacking interaction with Met55 and the distance between the two is 3.61 Å. This C-8 benzyl group has another pi-pi stacking interaction with the aniline ring, and the distance between the two rings is 3.14 Å.

Since the interaction between Ile164 (or Leu164) and the 4-amino group in 2,4-diaminoquinazoline ring in TMQ and its C-8 benzyl analogs is not the only interaction nor the most important one among the all possible interactions, this distance alone could not be any indication for the strength of the overall interaction. Still, it could explain in part why there was a potency loss in QM *Pf* DHFR-TS compare to the wild type and why the available space in the substrate binding site in the quadruple mutant is slightly larger than that of the wild type counterpart. However, it remains to be seen what the exact reason(s) for the potency loss in the quadruple mutant *Pf* DHFR in general and the difference in the degree of the potency loss among the various analogs.

Number (JCS-)	Substitution R_1	Substitution R_2	*Mtb* IC_{50} nM	Human IC_{50} nM	Selectivity Human/*Mtb*
TMQ	H, C5-CH_3	3,4,5-trimethoxy	17	16	1
1381	no C-8 substitution	3,5-dimethoxy	240	240	1
1502	C-8 bromo	3,4,5-trimethoxy	3900	470	0.1
1425	H	3,5-dimethoxy	58	1300	22
1573	2-F	3,5-dimethoxy	82	1540	19
1568	2-CH_3	3,5-dimethoxy	61	1930	32
1552	3-OCH_3	3,5-dimethoxy	32	1230	38
1585	3-CH_3	3,5-dimethoxy	49	5100	104
1595	3-CF_3	3,5-dimethoxy	230	1080	4.7
1569	4-F	3,5-dimethoxy	51	1700	33
1453	4-CH_3	3,5-dimethoxy	33	850	26
1553	4-OCH_3	3,5-dimethoxy	94	1530	16
1513	4-OCF_3	3,5-dimethoxy	240	2330	9.7
1601	2-methylnaphthalene	3,5-dimethoxy	89	1570	18
1443	H	2,5-diethoxy	170	>>20000	>117
1474	4-CH_3	2,5-diethoxy	200	18000	75
1521	H	3,4,5-trimethoxy	45	6400	142
1594	H, N-2 Bn	3,5-dimethoxy	2090	15400	7.4
1596	H, N-2 isobutyl	3,5-dimethoxy	1640	2940	1.8
1623	3,5-dimethoxy	3,5-dimethoxy	37	840	23

Table 4-2. IC_{50} values of C-8 benzyl TMQ analogs on *Mtb* DHFR and human DHFR. All of the C-8 benzyl analogs displayed more than 1 of selectivity and some of them are even more than 100 of selectivity.

ID (JCS-)	*Pf* WT	*Pf* QM	*Mtb* DHFR	human DHFR	EC_{50} on *Pf* 3D7	MIC_{99} on $mc^2$7000
TMQ	5 nM	6 nM	17 nM	16 nM	n/a	5 μM
1474	20 nM	70 nM	200 nM	18000 nM	650 nM	6.3 μM
1425	3 nM	30 nM	58 nM	1320 nM	425 nM	1.6 μM
1552	5 nM	40 nM	32 nM	1230 nM	125 nM	1.6 μM
1569	7 nM	35 nM	60 nM	1700 nM	600 nM	3.1 μM
1585	13 nM	60 nM	48 nM	5140 nM	n/a	3.1 μM

Table 4-3. The major C-8 benzyl TMQ analogs and their selectivity

ID (JCS-)	K_i *Mtb* DHFR (μM)	K_i WT *Pf* DHFR (μM)	K_i QM *Pf* DHFR (μM)	K_i Human DHFR (μM)
TMQ	0.0018	0.0012	0.0016	0.0011
1474	0.020	0.0049	0.0194	1.18
1425	0.0059	0.0012	0.0091	0.086
1552	0.0032	0.0012	0.0114	0.081
1569	0.0061	0.0013	0.0100	0.11
1585	0.0048	0.0029	0.0168	0.34

Table 4-4. Converted K_i values from IC_{50} for selected C-8 benzyl TMQ analogs. The K_i values has been calculated using BotDB (Cer, Mudunuri et al. 2009). K_m values for dihydrofolate (DHF) were found from the following articles. 1) *Mtb* DHFR (4.5 μM), human DHFR (2.8 μM) (White, Ross et al. 2004), and 2) WT (13 μM) and QM (14 μM) *Pf* DHFR-TS (Sirawaraporn, Sathitkul et al. 1997).

While the activities of the major compounds were derived (Table 4-2, 4-3, 4-4), several compounds were co-crystallized to obtain comparative structures from each of the four DHFR proteins. Between wild-type *Pf* DHFR-TS:TMQ and WT *Pf* DHFR-TS:JCS-1474 the RMSD over 220 Cα carbons with 100% sequence identity was 0.36 Å. The RMSD between *Mtb* DHFR:TMQ and *Mtb* DHFR:JCS-1474 over 159 Cα carbons with 100% sequence identity was 0.48 Å. In *Mtb* DHFR, the greatest deviation was seen in the active site near the aniline moiety of TMQ (Leu50-Arg55).

All 6 α carbons showed more than 1 Å deviation and the Cα of Lys53 showed more than 2 Å deviation. This same region was found to be the most flexible when comparing the binary complex of *Mtb* DHFR:NADPH with the ternary complex of *Mtb* DHFR:TMQ. In *Pf* DHFR-TS, the corresponding region (Ser111-Phe116) exhibited much less deviation and only two Cα carbons (Ser111 and Pro 113) showed more than 1 Å deviation. Considering the sheer size of 2,5-diethoxy group attached to the aniline ring of JCS-1474, it was clear that *Pf* DHFR-TS has a larger substrate binding site than *Mtb* DHFR. The crystallographic data and the structure statistics of *Mtb* DHFR, WT *Pf* DHFR-TS, and QM *Pf* DHFR-TS bound with JCS-1474 structures are shown in the table 4-5.

	Mtb:1474 (4MAW)	WT *Pf*:1474 (4M7Q)	QM P*f*:1474 (4M8F)
Space group	P1	P212121	P212121
Unit cell dimension	36.68, 66.15, 69.63 (Å)	57.49, 156.42, 165.98	56.99, 156.09, 165.60
	93.76, 94.48, 100.61 (°)	90.00, 90.00, 90.00	90.00, 90.00, 90.00
Resolution (Å)	45.47-2.01 (2.09-2.01)	50.00-2.62 (2.67-2.62)	49.66-2.80 (2.85-2.80)
R_{sym}	0.069 (0.203)	0.208 (0.771)	0.142 (0.685)
I/σ	6.7 (2.4)	11.9 (9.6)	6.4 (1.7)
Completeness (%)	93.4 (89.8)	99.8 (99.2)	96.1 (82.3)
Redundancy	2.15 (2.12)	7.1 (6.6)	5.5 (3.1)
# of reflections	39516	43303	38282
R_{work}/R_{free}	23.1/29.4	20.2/25.9	19.7/25.7
# of atoms – Protein	4976	9076	9053
Ligand/Ion	328	204	186
Water	439	291	14
B factor – Protein	28.5	54.6	51.1
Ligand/Ion	28.0	48.1	52.4
Water	32.5	44.7	34.5
RMSD – length	0.005	0.004	0.005
angle	0.749	0.642	0.726

Table 4-5. Crystallographic data and structure statistics for *Mtb* DHFR and WT *Pf* DHFR-TS, and QM *Pf* DHFR-TS bound with JCS-1474

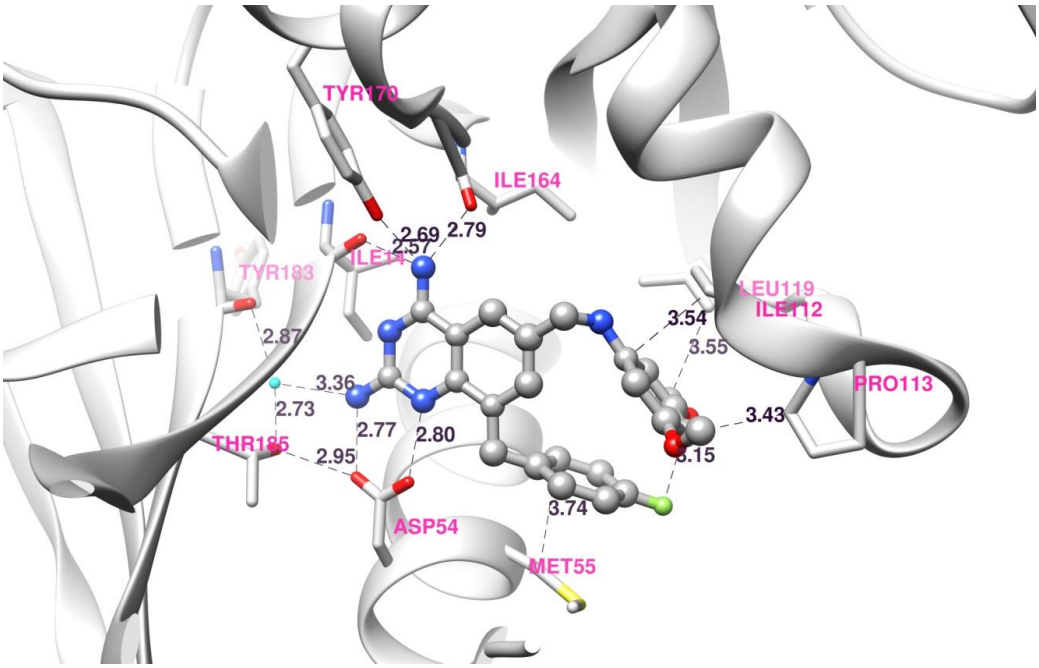

Figure 4-19. The important conserved interactions between JCS-1569 and WT *Pf* DHFR. As in other structures, 2,4-diaminoquinazoline ring has all the major interactions with WT *Pf* DHFR. One of the noticeable differences is that the fluoride atom is about 3 Å away from the oxygen atom of the methoxy group of the aniline ring. Met55 flipped down to accommodate the C-8 benzyl group of JCS-1569.

Another C-8 benzyl TMQ analog we have structures in both WT and QM *Pf* DHFR is JCS-1569. When we checked the WT *Pf* DHFR:JCS-1569 crystal structure, it has much similarity in regard to the major interactions between the compound and the protein (Figure 4-19). Similar to *Mtb* DHFR:TMQ or WT *Pf* DHFR:TMQ structures, the 2,4-diaminoquinazoline ring of JCS-1569 also has well-conserved hydrogen bond interactions with WT *Pf* DHFR. This WT *Pf* DHFR structure bound with JCS-1569 displayed the well-conserved hydrogen bonding interactions between WT *Pf* DHFR and JCS-1569 similar to TMQ bound WT *Pf* DHFR structure. Asp54, corresponding to

Asp27 in *Mtb* DHFR, has two hydrogen bonding interactions with 2-amino group and N-1 nitrogen with the distances of 2.77 Å and 2.80 Å, respectively. Both distances are significantly longer than in WT *Pf* DHFR:TMQ structure. Asp54 further forms the hydrogen bonding network with Thr185 and the distance is 2.95 Å. Thr185 has another hydrogen bonding network with 2-amino group of the quinazoline ring of JCS-1569 via a water molecule, and the distance between Thr185 and this water molecule is 2.73 Å and the distance between this water molecule and the 2-amino group of JCS-1569 is 3.36 Å. This water molecule further forms additional hydrogen bonding interaction with the main chain carbonyl group of Tyr183, and the distance between the two is 2.87 Å.

For 4-amino group of the 2,4-diaminoquinzaoline ring of JCS-1569 has three hydrogen bonding interactions with the main chain carbonyl group of Ile14, with the main chain carbonyl group of Ile164, and with the carbonyl group of Tyr170. The distances between the 4-amino group and those residues are 2.57 Å, 2.79 Å, and 2.69 Å, respectively. All of the three distances are shorter than the ones in WT *Pf* DHFR:TMQ structure, yet JCS-1569 lost more than 4 fold of potency as was seen in *Mtb* DHFR, and this could indicate that these three hydrogen bond interactions are either not in the favorable angles or not so significant to the overall interaction between WT *Pf* DHFR and JCS-1569 and other C-8 benzyl TMQ analogs.

For the 3,5-dimethoxyaniline ring side, the carbon atom of 3-methoxy group is in close proximity with Leu119 with the distance of 3.55 Å .The oxygen atom of this 3-methoxy group has potential hydrogen bonding interaction with the distance of 3.15 Å. The 1-carbon atom of the 3,5-dimethoxyaniline ring is in close proximity with the

carbon atom of Ile112 with the distance of 3.54 Å .The carbon atom of 5-methoxy group is in close proximity with Pro113, and the distance between the two is 3.43 Å. The C-8 benzene ring has *pi* stacking interaction with Met55 with the distance of 3.74 Å. Although these methoxy groups are not technically in hydrogen bonding interactions with WT *Pf* DHFR residues, they represent a potential venue for enhancing the interactions with DHFR. Also, unlike some other structures, there is no available interaction on the nitrogen atom of the aniline ring.

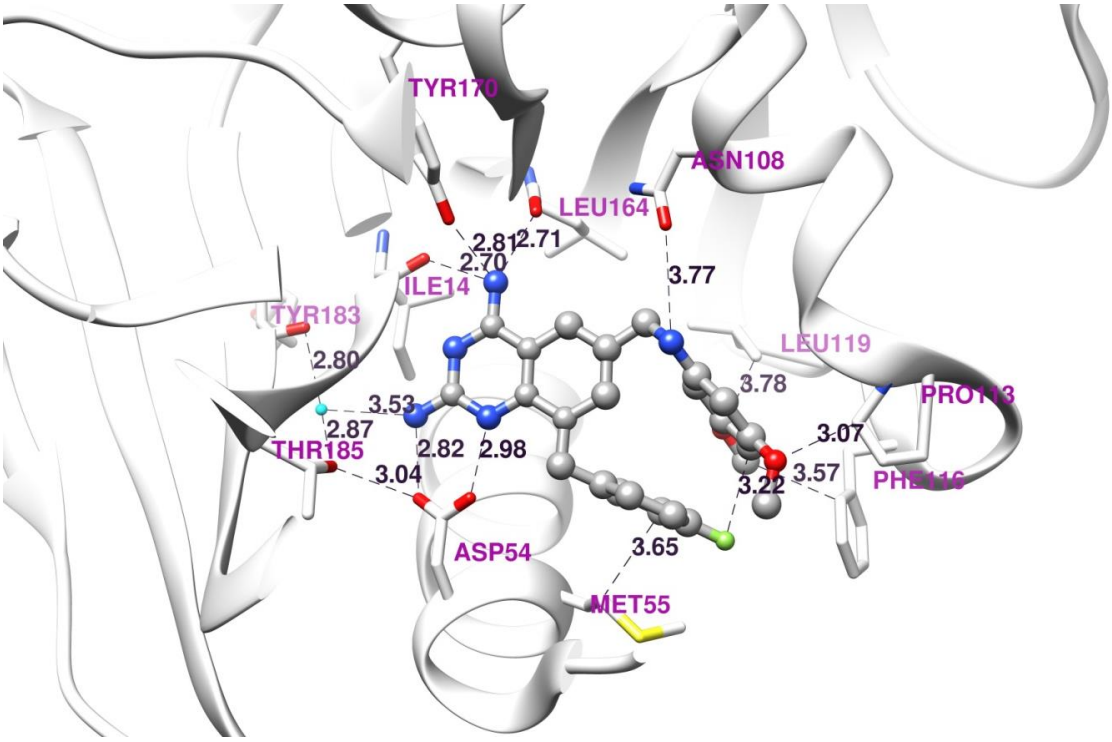

Figure 4-20. The important conserved interactions between JCS-1569 and QM *Pf* DHFR. As in other structures, 2,4-diaminoquinazoline ring has all the major interactions with QM *Pf* DHFR.

As previously stated, JCS-1569 bound structure was elucidated in QM *Pf* DHFR as well. When we checked the QM *Pf* DHFR:JCS-1569 crystal structure, which were grown from a different condition than *Mtb* DHFR or WT *Pf* DHFR structures, this structure has much similarity in the major interactions between the compound and the protein (Figure 4-20). Similar to *Mtb* DHFR:TMQ or WT *Pf* DHFR:TMQ structures, the 2,4-diaminoquinazoline ring of JCS-1569 has well-conserved hydrogen bond interactions with QM *Pf* DHFR as well. This QM *Pf* DHFR structure bound with JCS-1569 displayed the well-conserved hydrogen bonding interactions between QM *Pf* DHFR and JCS-1569 similar to TMQ bound WT or DM *Pf* DHFR structure. Asp54, corresponding to Asp27 in *Mtb* DHFR, has two hydrogen bonding interactions with 2-amino group and N-1 nitrogen with the distances of 2.82 Å and 2.98 Å, respectively. Asp54 further forms the hydrogen bonding network with Thr185 and the distance is 3.04 Å. Thr185 has another hydrogen bonding network with 2-amino group of the 2,4-diaminoquinazoline ring of JCS-1569 via a water molecule, and the distance between Thr185 and this water molecule is 2.87 Å, and the distance between the water molecule and the 2-amino group of JCS-1569 is 3.53 Å. This water molecule further forms another hydrogen bond interaction with the main chain carbonyl group of Tyr183 with the distance of 2.80 Å .

For 4-amino group of the 2,4-diaminoquinzaoline ring of JCS-1569 has three hydrogen bonding interactions with the main chain carbonyl group of Ile14, with the main chain carbonyl group of Ile164, and with the carbonyl group of Tyr170. The distances between the 4-amino group and those residues are 2.70 Å, 2.71 Å, and 2.81 Å,

respectively. All of the three distances are significantly shorter than the ones in QM *Pf* DHFR:TMQ structure and even shorter than QM *Pf* DHFR:JCS-1552 structure, yet JCS-1569 lost potency compared to QM *Pf* DHFR:TMQ as in *Mtb* DHFR or WT *Pf* DHFR, and this could indicate that, due to C-8 benzyl group in JCS-1569, these three hydrogen bond interactions are either not in the favorable angles or not so significant to the overall interaction between QM *Pf* DHFR and JCS-1569.

For the 3,5-dimethoxyaniline ring side, there are no actual hydrogen-bonding interactions just as WT or DM *Pf* DHFR. One possible interaction is the one between the oxygen atom of Asn108 and the nitrogen atom of the 3,5-dimethoxyaniline ring, and the distance between the two is 3.77 Å. However, there are some noticeable residues that are within the close proximity. The aniline nitrogen has a possible hydrogen bond interaction with the oxygen of Asn108 with the distance of 3.77 Å .The oxygen atom of 3-methoxy group is in close proximity with Leu119 with the distances of 3.78 Å, and the carbon atom of the 3-methoxy group is in close proximity with Phe116 with the distance of 3.57 Å .The oxygen atom of 5-methoxy group is in close proximity with Pro113 and the distance between the two is 3.07 Å. Although these methoxy groups do not have hydrogen bonding interactions with QM *Pf* DHFR-TS, they represent a potential venue for enhancing the interactions with DHFR.

C-8 benzyl group of JCS-1569 has some additional interactions. The C-8 benzyl group has probable *pi* stacking interaction with Met55 and the distance between the two is 3.65 Å. This C-8 benzyl group has another *pi-pi* stacking interaction with the aniline ring, and the distance between the two rings is 3.24 Å. The 4-fouride group on the C-8

benzene ring is 3.22 Å away from the 4-position of the aniline ring, and this potential interaction could be taken advantage of in the further development of selective inhibitors.

Two of the most important residues to the potency of the C-8 benzyl-2,4-diaminoquinazoline TMQ analogs are Asp27 and Phe31 in *Mtb* DHFR (Asp54 and Phe58 in *Pf* DHFR-TS). These two residues are conserved in many DHFRs as Asp27 is the acid for the last step of the DHFR enzymatic reaction, donating a hydrogen ion to the substrate to generate tetrahydrofolate (THF). Asp27 makes two hydrogen bonds with the nitrogen and the amino group in the 2,4-diaminoquinazoline ring of the TMQ analogs. Phe31 makes a *pi-pi* stacking interaction with the aromatic ring of the quinazoline. In human DHFR, these residues are Glu30 and Phe34, and they retain the same interactions.

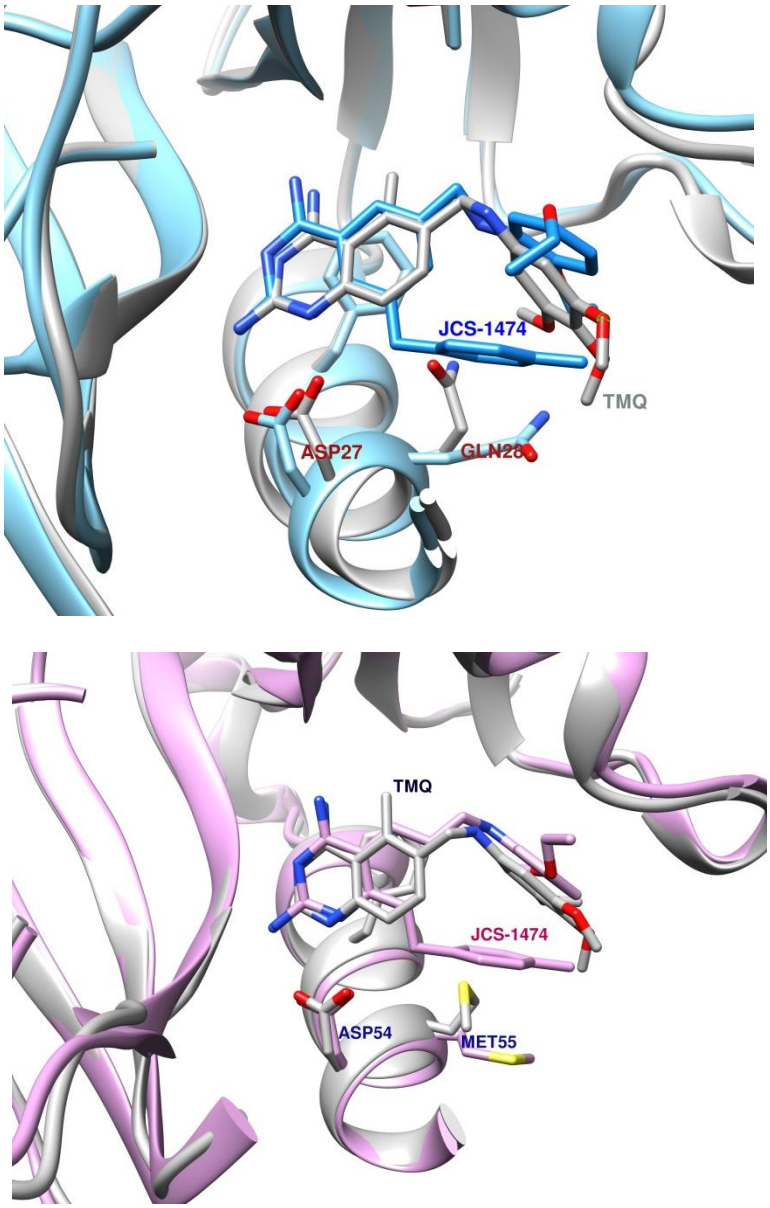

Figure 4-21. Role of the flexibility of Gln28 (*Mtb* DHFR, top) and Met55 (*Pf* DHFR, bottom). The residues are shown in the JCS-1474 bound structures. DHFR:TMQ is in gray in both figures, *Mtb* DHFR:JCS-1474 is in blue, and QM *Pf* DHFR-TS:JCS-1474 is shown in plum. *Mtb* DHFR exhibited more deviation when JCS-1474 is bound compared to QM *Pf* DHFR-TS. Gln28 in *Mtb* DHFR and Met55 in *Pf* DHFR-TS displayed most dramatic changes of orientation, and Asp27 position is clearly different in *Mtb* DHFR unlike *Pf* DHFR-TS.

Our initial modification of the benzyl group resulted in surprisingly little conformational changes to the active site despite the differences in activity. According to the superimposed crystal structures of *Mtb* DHFR:1474 and human DHFR:1502, the selectivity gain is a result of the loss of potency on the human DHFR. The human DHFR Phe31 and the corresponding *Mtb* DHFR Gln28 and *Pf* DHFR-TS Met55 were the only real sites of change (Figure 4-21, 4-22).

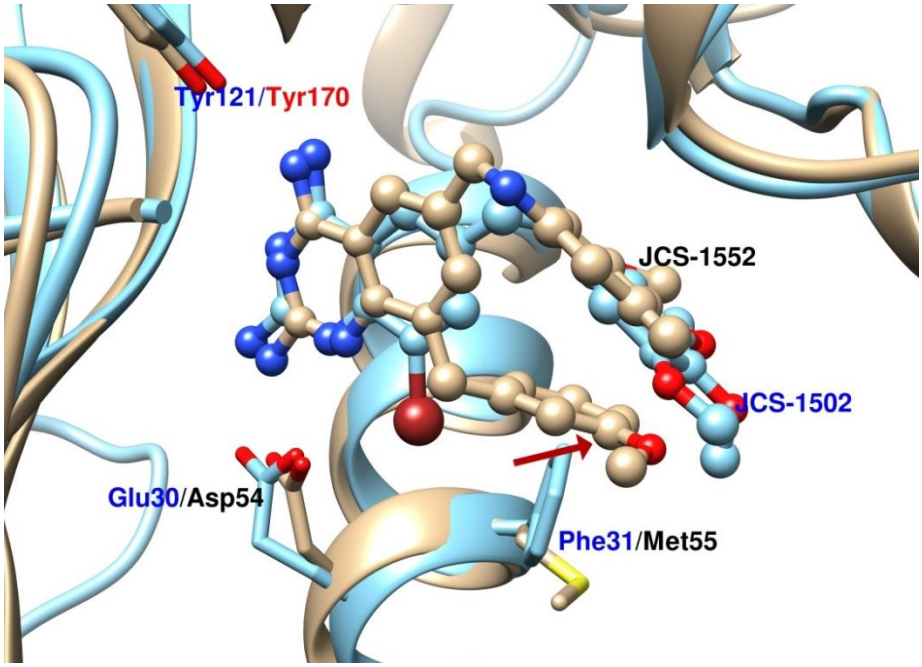

Figure 4-22. Superposed structures of human DHFR:JSF-1502 (blue) and QM *Pf* DHFR:JSF-1552. 3-methoxy group (3 position is at the arrow) of C-8 benzyl in JSF-1552 would have closer contact with human DHFR Phe31 compared to 4-methoxy group. The in-depth study should be done on the positional effect of the substituent on C-8 benzyl group, yet it is at least clear that 3-postion of C-8 benzyl group is closer to the Phe31 or other residue at that position than 4-position of C-8 benzyl group.

This might lead to the lower potency of the 3-methyl (JCS-1585) in human DHFR, compared to the 2-methyl (JCS-1568) or the 4-methyl group (JCS-1453). There should be a lot of more structure-activity relationship experiments on this before drawing any conclusion on the effect of the substitution on C-8 benzyl group, it still can be said 3-position of the C-8 benzyl group could bring the closest contact with Phe31 in human DHFR.

In the human DHFR the C-8 benzyl group is unable to maintain close contact with Phe31 and Leu22 because there is insufficient space for the residues to move and accommodate the C-8 benzyl moiety. In all the C-8 benzyl TMQ structures, Gln28 of *Mtb* DHFR lies lower and aligns almost parallel to the C-8 benzyl group allowing it ample space and effective interaction at the same time. Met55 in *Pf* DHFR-TS plays the same role in the C-8 benzyl-2,4-diaminoquinazoline TMQ bound structures. The side chain of Met55 rotates away from the C-8 benzyl group to allow enough room for the compound to sit in the pocket. The human DHFR Phe31 has a much lower degree of freedom than the *Mtb* DHFR Gln28 because of 1) the small pocket size of human DHFR compared to *Mtb* or *Pf* DHFR-TS, 2) Phe31 has only one virtual axis to rotate on compared to two in *Pf* Met55 and *Mtb* Gln28, and 3) the bulkier phenyl group in Phe31. The size of the C-8 benzyl group prevents Phe31 in the human DHFR from flipping because of the little rotational freedom and smaller space compared with *Mtb* or *Pf* DHFR. The restricted rotational freedom of Phe31 also comes in to play in the human DHFR:JCS-1502 structure. The phenylalanine ring positions between the C-8 bromo group and the aniline ring of TMQ analog. Phe31's rotation is blocked by Arg28, Pro26,

and Gln35. Gln35 is also located in a more rigid and crowded area, leaving no room for Phe31 to rotate away from the C-8 benzyl group. In all the elucidated structure, C-8 benzyl analogs have the similar orientation in the active site (Figure 4-22). The crystallographic data is also available in Table 4-6.

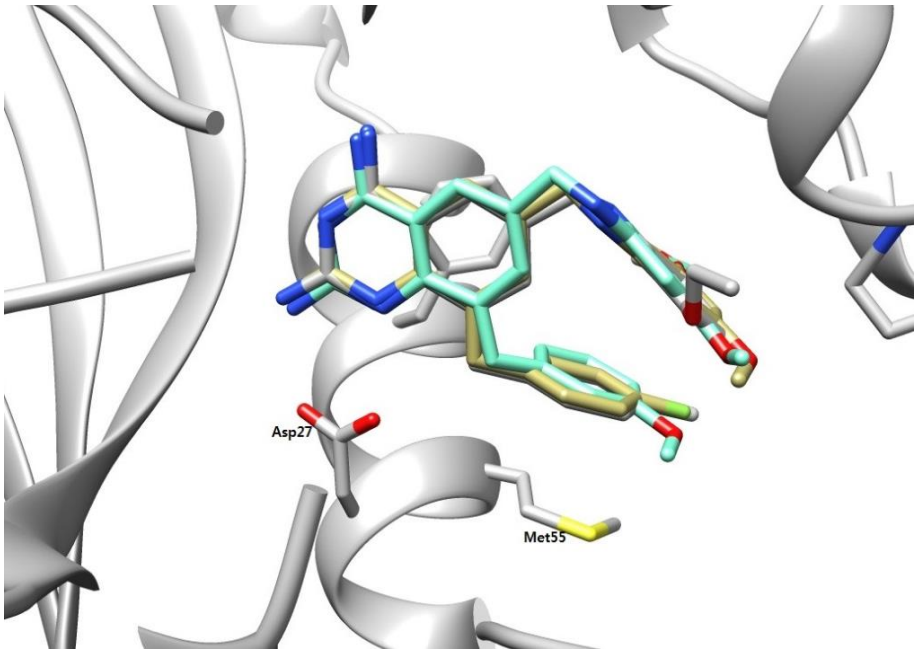

Figure 4-23. Superimposed structure of three C-8 benzyl TMQ analogs. JCS-1474 (Gray), JCS-1569 (Gold), and JCS-1552 (Cyan) have the same conformation in the active site. Asp54 and Met55 are shown together.

	WT *Pf*:1569 (4M6C)	QM *Pf*:1552 (4MA2)	QM *Pf*:1569 (4M8P)
Space group	$P2_12_12_1$	$P2_12_12_1$	$P2_12_12_1$
Unit cell dimension	56.69, 155.78, 165.01 (Å) 90.00, 90.00, 90.00(°)	58.75, 157.05, 166.39 90.00, 90.00, 90.00	56.81, 155.66, 165.11 90.00, 90.00, 90.00
Resolution (Å)	49.53-2.28 (2.32-2.28)	47.96-2.71 (2.76-2.71)	49.50-2.53 (2.57-2.53)
R_{sym}	0.091 (0.509)	0.116 (0.502)	0.140 (0.703)
I/σ	10.3 (3.8)	11.0 (5.4)	9.5 (2.8)
Completeness (%)	99.9 (100.0)	95.4 (87.9)	97.9 (90.7)
Redundancy	7.4 (7.5)	5.3 (4.1)	6.4 (4.3)
# of reflections	67011	58326	50972
R_{work}/R_{free}	19.9/23.1	20.5/26.9	18.8/24.1
# of atoms – Protein	9127	9053	9061
Ligand/Ion	165	191	196
Water	370	169	381
B factor – Protein	56.4	66.2	54.2
Ligand/Ion	47.2	67.4	49.9
Water	49.3	48.4	45.2
RMSD – length	0.005	0.005	0.005
angle	0.694	0.672	0.678

Table 4-6. Crystallographic data and structure statistics for WT *Pf* DHFR-TS and QM *Pf* DHFR-TS bound with C-8 benzyl TMQ analogs, JCS-1552 and JCS-1569.

The crystallographic data and the structure statistical values for WT and QM Pf DHFR-TS bound with two of the C-8 benzyl TMQ analogs, JCS-1552 and JCS-1569 are listed in the table 4-6. Introducing a methyl group to the C-8 benzene ring resulted in increased selectivity. The 2-methyl (JCS-1568) and 4-methyl (JCS-1453) groups modestly raised selectivity by 32 fold and 26 fold. The 3-methyl group (JCS-1585) drastically boosted selectivity by 104 fold in *Mtb* DHFR. According to the crystal structure, the 3-methyl group restricts the rotational freedom of the benzyl group compared to the 2-methyl group, contributing to the increased selectivity. However, the 4-methyl group (IC_{50} = 33 nM) is more potent than the 3-methyl group (IC_{50} = 49 nM). The 4-methoxy group (JCS-1553) decreased the selectivity to 16 fold, whereas the 3-methoxy group (JCS-1552) increased selectivity up to 38 fold. In the superimposed structure of human DHFR:JCS-1502 and QM *Pf* DHFR-TS:JCS-1552, it is clear that steric hindrance from Phe31 of the human DHFR interferes with the C-8 benzyl ring of *Pf* DHFR, and the closest contact is at the 3-position of the C-8 benzene ring (Figure 4-23).

Electronic effect could be seen in the $–CH_3$ and $–CF_3$ comparison. When the hydrogen molecules of the CH_3 group in JCS-1585 were substituted with the fluoride molecules of JCS-1595, the potency against *Mtb* DHFR dropped five fold. To a lesser extent, this was also seen with JCS-1553 and JCS-1513. When the hydrogen of the methoxy group in JCS-1553 was substituted with the fluoride to make the trifluoromethoxy group in JCS-1513, the potency decreased two fold. This could be explained by the electronic effect of the fluoride group. The fluoride, which is an

electron-withdrawing group, lowered the electron density in the C-8 benzyl and the *pi-pi* stacking interaction with Gln28. The intensity of the *pi-pi* stacking interaction with the aniline ring in the same molecule decreased as well. When compared to hydrogen, the greater size of the fluoride could also contribute to the potency loss.

When the DHFR crystal structures bound with TMQ and the C-8 benzyl-2,4-diaminoquinazoline TMQ analogs are superimposed, the effect of the C-8 benzyl moiety on selectivity can be explained. In the *Mtb* DHFR structure with JCS-1474, which has a 4-methylbenzyl group bound to C-8 position of quinazoline ring, the benzyl group occupies the same pocket as water or acetate molecule does in the TMQ bound structure. Gln28 (Met55 in *Pf* DHFR-TS) is pushed down to allow the C-8 benzyl group to sit near the pocket so that Gln28, the C-8 benzyl ring, and the aniline ring of TMQ align with each other so that the interaction with each other is available. Gln28 in *Mtb* DHFR and Met55 in *Pf* DHFR-TS align parallel to the C-8 benzyl group enabling the hydrophobic interaction.

One of the driving forces stabilizing the C-8 benzyl compounds in the pocket of the pathogenic DHFRs is the *pi-pi* stacking interaction between the C-8 benzyl ring and the aniline ring. In the QM *Pf* DHFR-TS:JCS-1474 and *Mtb* DHFR:JCS-1474 structures, the distances between these two rings is 3.6 Å and this distance allows a favorable interaction between the two rings. *Mtb* DHFR Gln28 and *Pf* DHFR-TS Met55 offer additional van der Waals interactions with the C-8 benzyl ring.

It was found that there was about 20^{o} of distortion of the 2,4-diaminoquinazoline ring of the C-8 benzyl TMQ analogs, compared to the same ring in the *Mtb* DHFR:TMQ structure or *Pf* DHFR-TS:TMQ structures (Figure 4-24). This distortion significantly forced the 2,4-diaminoquinazoline ring of the C-8 benzyl TMQ analogs to position in the non-optimal position compared to *Mtb* DHFR:TMQ and caused the compounds to interact with Asp27 and Phe31 (Asp54 and Phe58 in *Pf* DHFR-TS) unfavorably. However, this distortion gave more space to C-8 benzyl TMQ analogs and allowed a better arrangement of the C-8 benzyl moiety in the active site, subsequently allowed a much better interaction with Gln28 of *Mtb* DHFR (Met55 of *Pf* DHFR-TS) and with the aniline ring in the same molecule.

The distortion angle ranged from 19^{o} to 21^{o}, and the distortion is observed in all C-8 benzyl-2,4-diaminoquinazoline analogs. From the crystal structures of QM *Pf* DHFR-TS:TMQ, the distances between Met55 and N1 and the nitrogen of the 2-amino group of the quinazoline ring are 2.84 Å and 2.87 Å, respectively. The same distances in QM *Pf* DHFR-TS:JCS-1474 are 3.04 Å and 2.94 Å. The loss of optimal interaction with DHFR is compensated by the extra interactions of the aniline:C-8 benzyl and the C-8 benzyl:Met55 in *Pf* DHFR-TS (Gln28 in *Mtb* DHFR). In *Pf* DHFR-TS, the Met55 has an additional interaction with Cys50.

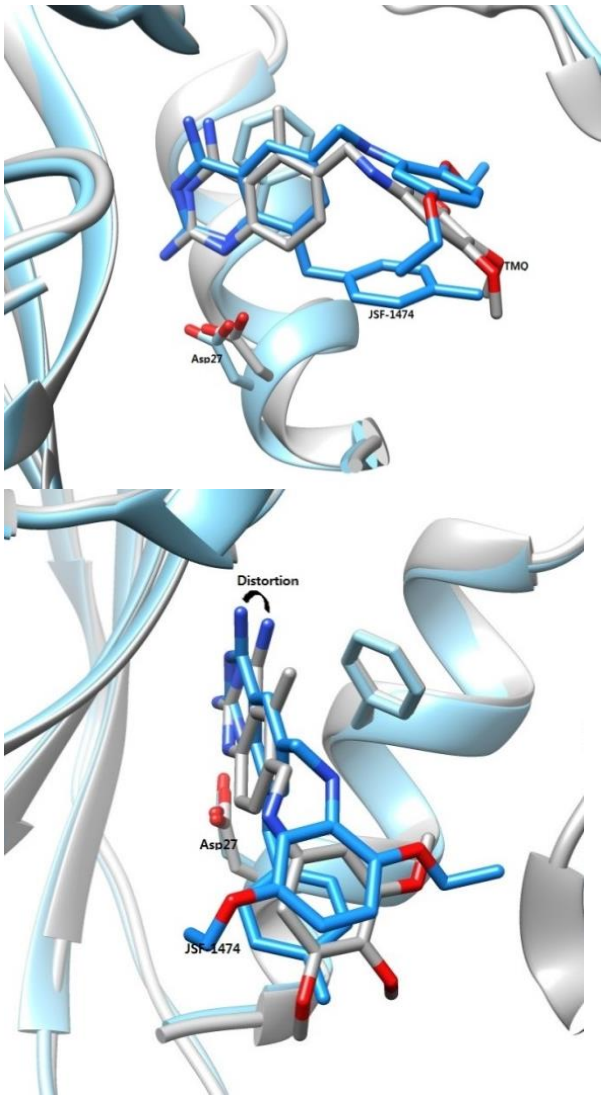

Figure 4-24. Distortion in C-8 benzyl TMQ analogs. 2,4-diaminoquinazoline ring distortion is shown in the superimposed structure of *Mtb* DHFR:TMQ (gray) and *Mtb* DHFR:JCS-1474 (blue). From both front view (left) and top view (right), the quinazoline ring distortion is clearly observable. The distortion angle is about 20 degrees in *Mtb* DHFR, WT *Pf* DHFR-TS, and QM *Pf* DHFR-TS. Still, as seen in the picture *Mtb* DHFR displayed the greatest deviation from TMQ bound structure.

In *Mtb* DHFR, Arg23 is in close contact with the C-8 benzyl moiety and allowed extra interaction. In the *Mtb* DHFR:JCS-1474 structure, the distance between Arg23 and the ethyl group of the aniline moiety is 3.10 Å. In some structures, the density for Arg23 is faint or missing, suggesting that Arg23 is flexible in the protein. Unlike Arg23 in *Mtb* DHFR, the corresponding Lys49 in *Pf* DHFR-TS stretches toward the surface, and instead, Cys50, whose counterpart residue is not present in *Mtb* DHFR, covers Arg23's position. Cys50 has a hydrogen bond with Met55 at a distance of 3.28 Å. In addition to this interaction, Phe116 is in close contact with the aniline moiety of the compound in *Pf* DHFR-TS.

It is necessary to mention the effect of different functionalities on the aniline ring, specifically the 2,5-ethoxy group. Da Cunha et al. pointed out in their 2,5-substituted aniline experiments that 2,5-diethoxy group exhibited much greater selectivity compared to 2,5-dimethoxy counterpart (da Cunha, Ramalho et al. 2008). In our C-8 benzyl TMQ compounds displayed the similar trends.

Both JCS-1443 and JCS-1474, which have 2,5-diethoxybenzyl group instead of 3,5-dimethoxybenzyl, exhibited greater selectivity when compared with their 3,5-methoxy counterparts, JCS-1425 and JCS-1453. JCS-1443 lost about 3 fold potency on *Mtb* DHFR (IC_{50} = 170 nM) compared to its 3,5-dimethoxyaniline counterpart, JCS-1425 (IC_{50} = 60 nM). However, JCS-1443 lost more than 15 fold potency on human DHFR (IC_{50} > 20,000 nM) compared to its 3,5-dimethoxyaniline counterpart, JCS-1425 (IC_{50} = 1300 nM). In the superimposed structure of *Mtb* DHFR:JCS-1425 and *Mtb* DHFR:JCS-1443, bulkier 2,5-diethoxy substituent on the aniline ring pushes the loop

region (Pro51-Gly59) away from the active site. Also C-8 benzene ring position is different in those two structures.

Due to the challenges of synthesis, there are only two compounds available to compare the effect of the 2,5-alkyloxy substitution on the aniline ring, and a conclusive effect remains to be seen. However, when compared with the 3,5-dimethoxyaniline, it is still apparent that the 2,5-ethoxy group has a positive effect on selectivity gain. According to the superimposed structures of human DHFR:JCS-1502 and *Mtb* DHFR:JCS-1474, the bulky 2,5-diethoxy groups of JCS-1474 could be affected more by Ile60 and Asn64 in human DHFR. These residues correspond to Leu50 and Val54 in *Mtb* DHFR, and these smaller residues could allow more space for the bulky 2,5-diethoxy group.

A couple of N-2 of quinazoline ring modification has been tried to evaluate the effect of substitution on the N-2 position. For the TMP analogs, methyl- (JCS-1168) and ethyl- (JCS-1169) exhibited great selectivity. In TMQ analogs, the effect of N-2 modification is smaller than TMP analogs. Also due to the difficulty of synthesis, not too many compounds can be synthesized.

Two TMQ analogs with N-2 substitution were synthesized. JCS-1594 is containing N-2 benzyl group and JCS-1596 has N-2 isobutyl group. The IC_{50} values on *Mtb* DHFR and human DHFR of JCS-1594 are 2090 nM and 15400 nM, respectively, and the IC_{50} values on *Mtb* DHFR and human DHFR of JCS-1596 are 1640 nM and 2940 nM, respectively. The selectivity of JCS-1594 is better than JCS-1596, but JCS-1596's potency on *Mtb* DHFR is slightly better than JCS-1594. Still, the potency in

general was much too low compared other C-8 benzyl TMQ compounds and the detailed effects of N-2 substitution largely remain to be seen.

Several C-8 benzyl-2,4-diaminoquinazoline TMQ analogs were tested on $mc^2$7000, a vaccine strain of *M. tuberculosis*. The minimal inhibitory concentration (MIC_{99}) values ranged from 1.5 μM to 6 μM and show good potency compared to TMQ, whose MIC is 5 μM (Figure 4-25).

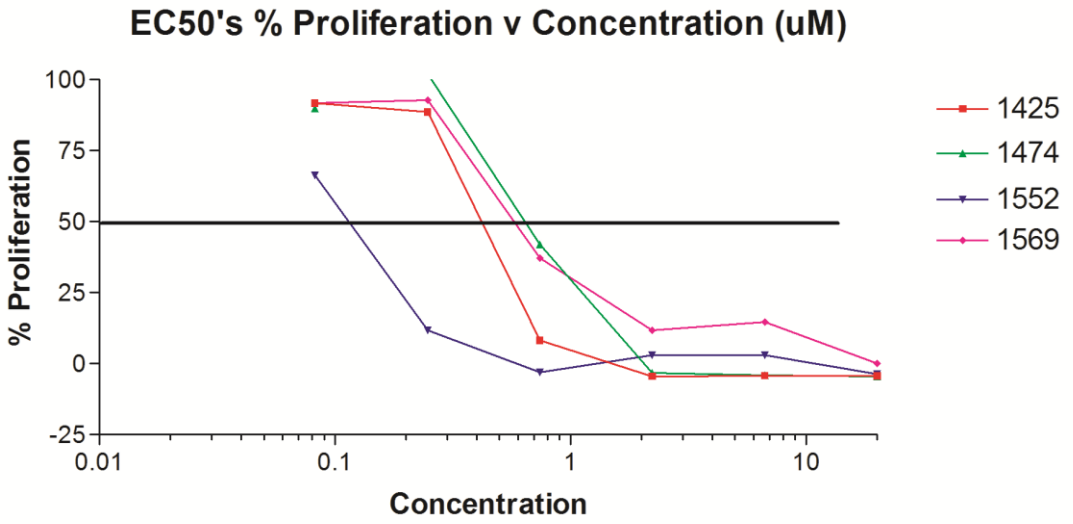

Figure 4-25. EC_{50} of C-8 benzyl TMQ on wild type *P. falciparum* (3D7)

Four of the C-8 benzylquinazoline TMQ analogs, JCS-1425, JCS-1474, JCS-1552, and JCS-1569, were tested on the wild-type (WT) *P. falciparum* 3D7 strain thanks to the collaboration of Dr. Van Voorhis lab. The EC_{50} values ranged from 100 nM to 650 nM, and JCS-1552 exhibited the highest potency on the WT *P. falciparum* strain.

MIC values on $mc^2$7000 and EC_{50} values on the WT *P. falciparum* 3D7 strain agreed with the IC_{50} values from the enzyme assay. For example, JCS-1552, which has the strongest potency in the enzyme assay, exhibited the best MIC and EC_{50} values with 1.6 μM and 125 nM, respectively. This JCS-1552 retained significant degree of the potency even on the low concentration of 1 uM unlike other compounds. On the other hand, JCS-1474, which has the lowest IC50 on the in-vitro enzyme assay, also displayed the lowest EC50 values on this test, yet the difference from the other compounds was not large compared to the enzyme assay.

CHAPTER V

VALIDATION STUDY ON S. AUREUS DHFR

V.1. Validation Study of C-8 Benzyl TMQ's Potential for the Broad Spectrum Selective Antimicrobial on *Staphylococcus aureus* Dihydrofolate Reductase

In this last chapter, we will discuss the effort we put in to broaden the application of our C-8 benzyl TMQ analogs toward the broad-spectrum selective antimicrobial/antibiotic. In fact, quite a few drugs are working on multiple species or diseases, yet it is not easy to find the ones that exclusively work on pathogens. Recent surge of infection rate or persistency that is drastically shown in the case of *M. tuberculosis* presses the urgency even greater.

Staphylococcus aureus is one of the well-known pathogens and it causes infections mainly in the hospital in the past. However, there has been increasing number of reports of community-based infection of this pathogen and the emergence of methicillin-resistant mutant *S. aureus* made it more difficult to treat this infection. Therefore, just like tuberculosis or malaria, there is an urgent need for selective treatment for this pathogen.

Staphylococcus aureus DHFR is similar to *M. tuberculosis* DHFR in many ways including the fact that they both have 159 residues and the active site, specifically substrate binding site, has similar conformation.

The important commonality for selectivity of *M. tuberculosis* DHFR and *P. falciparum* DHFR, a pocket like the glycerol binding pocket in *Mtb* DHFR and a flexible residue next to Aspartate, also partially present in *S. aureus* DHFR as well. This is partial because the flexible residue in *Sa* DHFR is Leu28, which has only one rotational axis yet much smaller than Phe31 in human DHFR.

The overall structure of *Mtb* DHFR and *Sa* DHFR is very similar. In the superimposed structure of *Mtb* DHFR:TMQ and WT *Sa* DHFR:TMQ revealed that the two DHFRs have almost identical β-sheets and α-helices in the structure. The differences come mainly from the loop regions. Even though there was no water molecule or acetate or other molecule was found in *Sa* DHFR structure, there clearly is some space available corresponding to the glycerol binding pocket in *Mtb* DHFR structure. This similarity makes *Sa* DHFR a legitimate comparison for *Mtb* and *Pf* DHFR to evaluate the possibility for C-8 benzyl TMQ analogs' use of broad-spectrum selective antimicrobial.

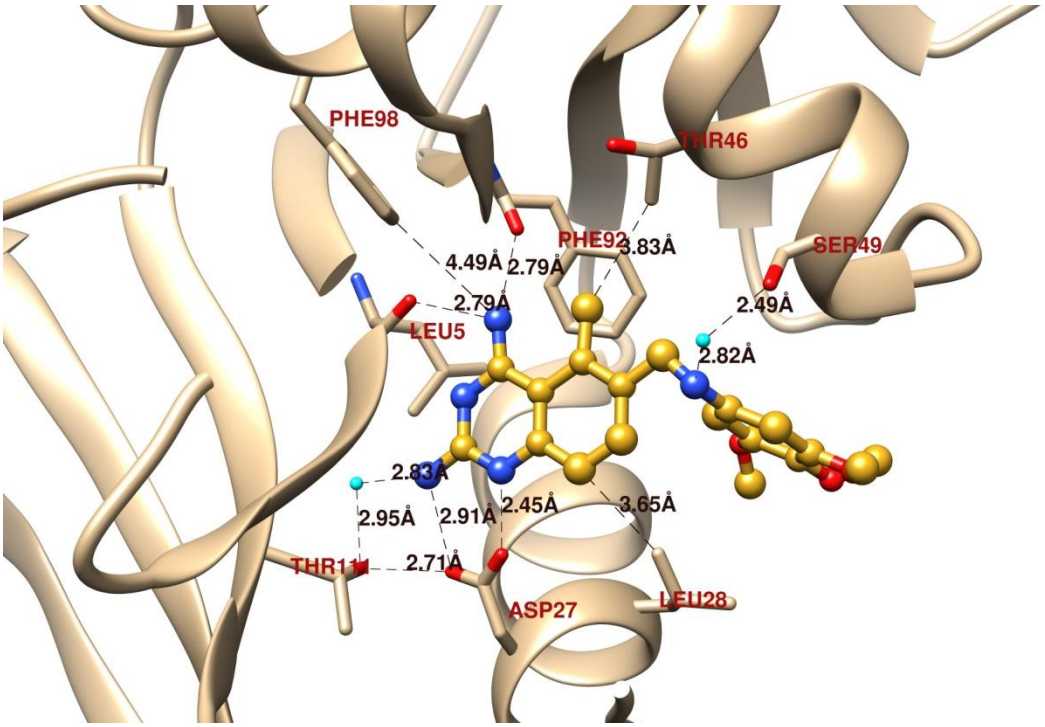

Figure 5-1. The important conserved interactions between TMQ and WT *Sa* DHFR. It is clear that 3,4,5-trimethoxyaniline ring is almost no interaction unlike *Mtb* DHFR or *Pf* DHFR-TS. This solvent access area is much wider than *Mtb* DHFR or *Pf* DHFR-TS, and that is why *Sa* DHFR is more susceptible to the mutation and to the potency loss as a result. The hydrogen bond interactions on 2,4-diaminoquinazoline ring side are well conserved.

Similar to *Mtb* DHFR:TMQ structure, the 2,4-diaminoquinazoline ring of TMQ has well-conserved hydrogen bond interactions with WT *Sa* DHFR (Figure 5-1). This WT *Sa* DHFR structure bound with TMQ displayed the well-conserved hydrogen bonding interactions between WT *Sa* DHFR and TMQ similar to *Mtb* DHFR:TMQ structure. Asp27 (corresponding to Asp27 in *Mtb* DHFR) has two hydrogen bonding interactions with 2-amino group and N-1 nitrogen of the quinazoline with the distances of 2.91 Å and 2.45 Å, respectively. Asp27 further forms the hydrogen bonding network

with Thr111 and the distance is 2.71 Å. Thr111 has another hydrogen bonding network with 2-amino group of the quinazoline ring of TMQ via water molecule and the distance between Thr111 and this water molecule is 2.95 Å and the distance between the water molecule and nitrogen of the 2-amino group is 2.83 Å.

For 4-amino group of the 2,4-diaminoquinzaoline ring of TMQ has two hydrogen bonding interactions with the main chain carbonyl group of Leu5, and with the main chain carbonyl group of Phe92. The distances are 2.79 Å, and 2.79 Å, respectively. Unlike *Mtb* DHFR or *Pf* DHFR-TS, WT *Sa* DHFR has Phe98 and it is far apart from the 4-amino group with the distance of 4.49 Å. 5-methyl group on the 2,4-diaminoquinazoline ring is 3.83 A away from Thr46. Though there is no hydrogen bond interaction is available with Thr46, a proper modification on 5-methyl group, such as carbonyl, could bring additional hydrogen bond interaction with Thr46.

For the 3,4,5-trimethoxyaniline ring side, there are no actual hydrogen-bonding interactions. It remains to be seen how this large and wobbly hole could sustain TMQ so tightly (IC_{50} = 2.5 nM), and one clue could come from Ser49. This Ser49 forms a hydrogen bond network with nitrogen atom of the 3,4,5-trimethoxyaniline ring via water molecule. The distance between Ser49 and the water molecule is 2.49 Å, and the distance between the water molecule and the nitrogen atom of the aniline ring is 2.82 Å. This additional hydrogen bond which is not observed in *Mtb* DHFR of *Pf* DHFR is the reason why TMQ has comparable, if not better, IC_{50} against *Sa* DHFR.

A very important difference was found near the 3,4,5-trimethoxyaniline ring of TMQ is located in the active site (Figure 5-2). The two 3,4,5-trimethoxybenzene ring in

Mtb DHFR and WT *Sa* DHFR displayed significantly different position, and the extra interaction with Arg23 in *Mtb* DHFR is not feasible with the His23 in *Sa* DHFR in the same position. For *Sa* DHFR, the solvent access from the 3,4,5-trimethoxybenzene side is much wider and probably easier to lose activity with a conformational change. Even though Leu28 and Ile50 give hydrophobic interaction, they are more inside compared to Arg23 and Pro51 in *Mtb* DHFR, and it is more probable for *Sa* DHFR to be more sensitive to the conformational changes compared to *Mtb* DHFR or *Pf* DHFR-TS. That is one of the reasons why just a single mutation, F98Y, affect significantly on the potency loss compared to the quadruple mutant of *P. falciparum* DHFR-TS.

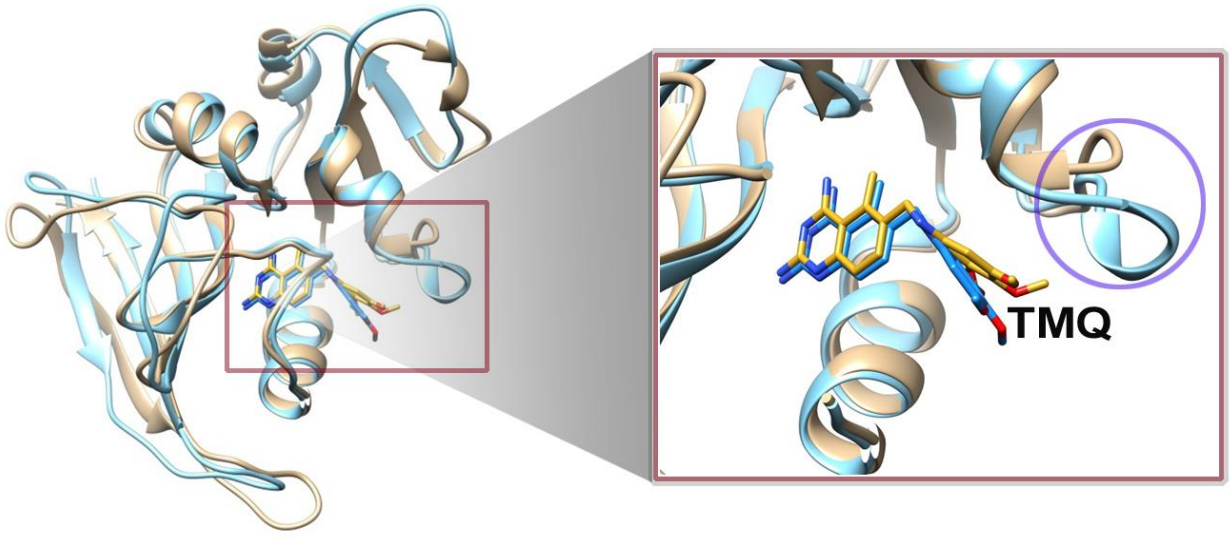

Figure 5-2. Overview of the superimposed structure of *Mtb* DHFR:TMQ (blue) and WT *Sa* DHFR:TMQ. The zoomed view on the helix containing loop region (Ile50-Arg58 in *Sa* DHFR) that is close the trimethoxybenzene side of TMQ. This region showed the only significant difference close to the active site from *Mtb* DHFR.

In *Pf* DHFR-TS, there was no noticeable IC_{50} decrease for TMQ in the QM *Pf* DHFR-TS (6 nM) compared to wild type (5 nM). Even for the C-8 benzyl TMQ analogs, 10 fold loss of potency in JCS-1425 was the greatest among all the analogs.

However, in *Sa* DHFR, there was a drastic potency (IC_{50}) loss on TMQ itself from 2.5 nM in WT *Sa* DHFR to 55 nM in F98Y SM *Sa* DHFR, and this is more than 20 fold loss of potency. For C-8 benzyl TMQ analogs, the potency loss in F98Y SM *Sa* DHFR was greater than QM *Pf* DHFR-TS.

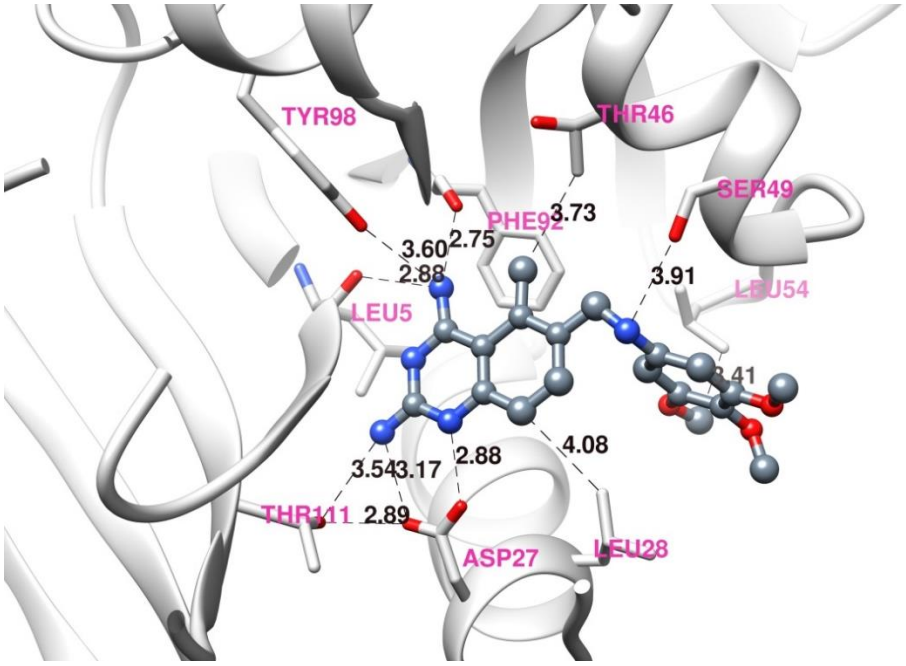

Figure 5-3. The important conserved interactions between F98Y *Sa* DHFR and TMQ. As in the wild type, 3,4,5-trimethoxyaniline ring has no significant interaction with the protein and stay loose. Compared to wild type, Tyr98 offers additional hydrogen bond, yet two water molecules that were formed hydrogen bond network in the wild type are missing in the mutant. Those two weakened interactions along with the unveiled reasons caused potency loss in F98Y *Sa* DHFR.

In the F98Y *Sa* DHFR, we could see the similar interactions between TMQ and the protein (Figure 5-3). Similar to WT *Sa* DHFR:TMQ structure, the 2,4-diaminoquinazoline ring of TMQ has well-conserved hydrogen bond interactions with F98Y *Sa* DHFR. This F98Y *Sa* DHFR structure bound with TMQ displayed the well-conserved hydrogen bonding interactions between F98Y *Sa* DHFR and TMQ similar to WT *Sa* DHFR:TMQ structure. Asp27 (corresponding to Asp27 in *Mtb* DHFR) has two hydrogen bonding interactions with 2-amino group and N-1 nitrogen of the quinazoline with the distances of 3.17 Å and 2.88 Å, respectively. Asp27 further forms the hydrogen bonding network with Thr111 and the distance is 2.89 Å. Thr111 has another hydrogen bonding network with 2-amino group of the quinazoline ring of TMQ and the distance between Thr111 and the nitrogen of the 2-amino group is 3.54 Å .

For 4-amino group of the 2,4-diaminoquinzaoline ring of TMQ has three hydrogen bonding interactions with the main chain carbonyl group of Leu5, and with the main chain carbonyl group of Phe92, and with Tyr98. The distances between the protein and the main chain carbonyls of Leu5 and Phe92 are 2.88 Å, and 2.75 Å, respectively. Unlike WT *Sa* DHFR, F98Y *Sa* DHFR has Tyr98 and it is a little bit far apart from the 4-amino group with the distance of 3.60 Å, but it is still much closer than the Phe98 in WT *Sa* DHFR whose distance from the 4-amino group is 4.49 Å. 5-methyl group on the 2,4-diaminoquinazoline ring is 3.73 A away from Thr46. Though there is no hydrogen bond interaction is available with Thr46 similar to WT *Sa* DHFR, a proper modification on 5-methyl group, such as carbonyl, could bring additional hydrogen bond interaction with Thr46.

For the trimethoxyaniline ring side, there are no significant hydrogen-bonding interactions. The only probable hydrogen bond interaction came from Ser49. This Ser49 forms a hydrogen bond with nitrogen atom of the 3,4,5-trimethoxyaniline ring with the distance of 3.91 Å. This interaction is much weaker compared to the hydrogen bond network via water molecule found in the WT Sa DHFR:TMQ structure. This weakened interaction might be the reason for TMQ's drastic potency loss in F98Y *Sa* DHFR (IC_{50} = 55 nM).

Phe98 in *Sa* DHFR and Tyr100 in *Mtb* DHFR make an interesting comparison because the mutation arose in Phe98 to Tyrosine, and that mutation makes the position exactly the same as *Mtb* DHFR. Still, the drastic potency loss occurred. While the exact reason(s) for the drastic activity loss of TMQ and C-8 benzyl TMQ analogs in F98Y SM Sa DHFR remain to be seen, yet the probable reasons could be deduced from F98Y *Sa* DHFR:TMQ structure and WT *Sa* DHFR:JCS-1474 structure.

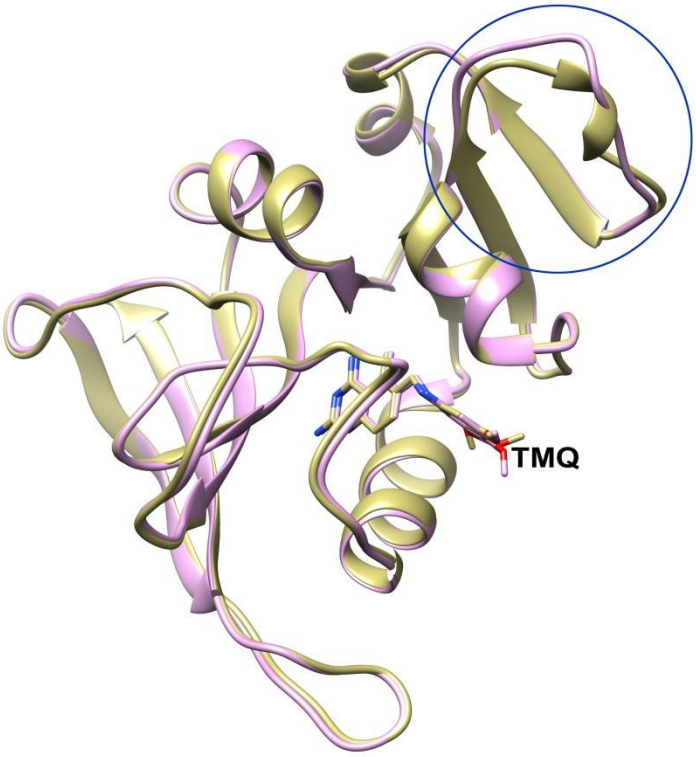

Figure 5-4. Superimposed structure of WT *Sa* DHFR:TMQ (Khaki) and F98Y SM *Sa* DHFR:TMQ. The two structures showed high similarity in the overall folding and the greatest deviation came from a loop region, Thr63-Gly72. The solvent accessible area of the substrate binding site where TMQ is bound is significantly larger than Mtb DHFR of Pf DHFR-TS.

In the superimposed structure of WT *Sa* DHFR:TMQ and F98Y SM *Sa* DHFR:TMQ (Figure 5-4), it is not easy to figure out the reason for the drastic loss of TMQ's activity on F98Y *Sa* DHFR. Other than a loop region of Thr63-Gly72, where the greatest deviation was observed, the two structures are almost identical. Furthermore the Thr63-Gly72 loop region is more than 10 Å away from TMQ in the active site. It was completely out of our expectation in the sense that there was about 20 fold loss of activity in terms of IC_{50} of C-8 benzyl TMQ analogs due to this seemingly small change

in F98Y *Sa* DHFR. Though more in depth study should be done for the reason for this significant loss of activity on F98Y *Sa* DHFR, yet they are still active compared to human DHFR counterparts (Table 5-1).

	IC_{50} WT *Sa* DHFR (nM)	IC_{50} F98Y *Sa* DHFR (nM)	IC_{50} human DHFR (nM)
TMQ	2.5	55	16
JCS-1425	18	350	18000
JCS-1474	95	760	1320
JCS-1552	10	200	1230
JCS-1569	17	340	1700
JCS-1585	35	450	5140

Table 5-1. IC_{50} values of the major C-8 benzyl TMQ analogs and TMQ on WT and F98Y *Sa* DHFR and human DHFR. Note that the IC50 values on F98Y *Sa* DHFR are much higher than the values against WT *Sa* DHFR.

As stated in the beginning part of this chapter, *Sa* DHFR has the same acid residue (Asp27) and the residue next to Asp27 is Leu28. This could be very interesting comparison because leucine has much smaller side chain compared to phenyalanine, which is in human DHFR, but still has just one rotational axis, which is less than *Mtb* DHFR or *Pf* DHFR-TS.

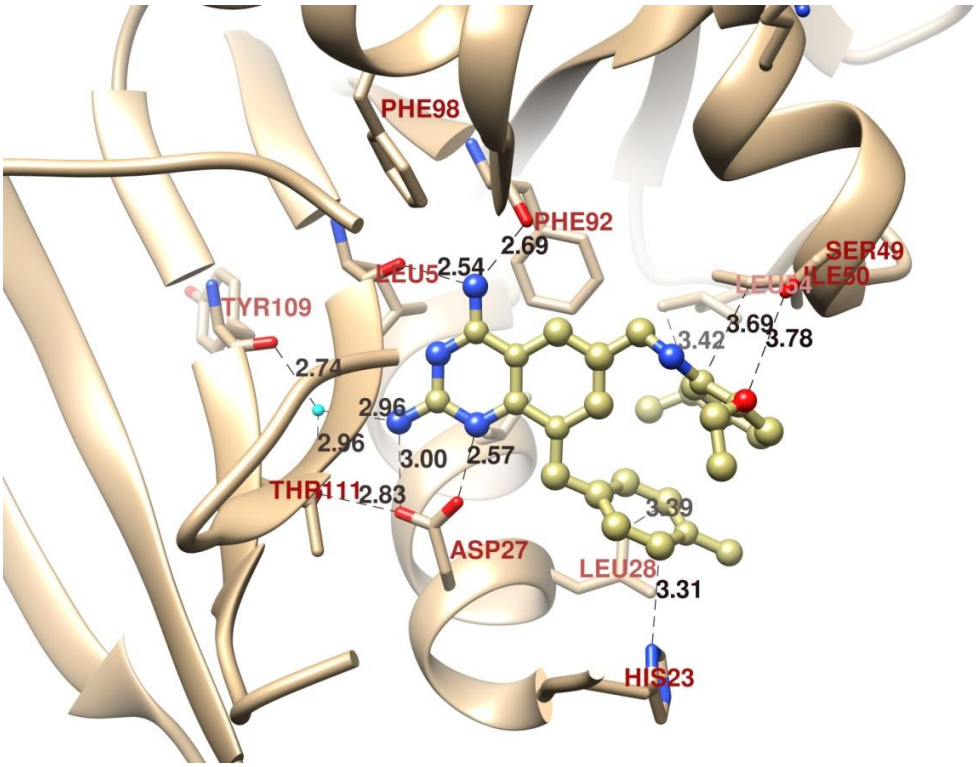

Figure 5-5. Important conserved interactions between WT *Sa* DHFR and JCS-1474. As in WT *Sa* DHFR:TMQ structure, Phe98 has no available hydrogen bond interaction. For 2,4-diaminoquinazoline ring side, all the conserved interactions were found including the interactions with Asp27 and the hydrogen bond network with Thr111 and the main chain carbonyls of Leu5 and Phe92.

In the WT *Sa* DHFR:JCS-1474 structure, we could see the similar interactions between TMQ and the protein (Figure 5-5). Similar to WT *Sa* DHFR:TMQ structure, the 2,4-diaminoquinazoline ring of JCS-1474 has well-conserved hydrogen bond interactions with WT *Sa* DHFR. This WT *Sa* DHFR structure bound with JCS-1474 displayed the well-conserved hydrogen bonding interactions between WT *Sa* DHFR and JCS-1474 similar to WT *Sa* DHFR:TMQ structure. Asp27 (corresponding to Asp27 in

Mtb DHFR) has two hydrogen bonding interactions with 2-amino group and N-1 nitrogen of the quinazoline with the distances of 3.00 Å and 2.57 Å, respectively. Asp27 further forms the hydrogen bonding network with Thr111 and the distance is 2.83 Å. Thr111 has another hydrogen bonding network via a water molecule with 2-amino group of the quinazoline ring of JCS-1474 and the distance between Thr111 and the water molecule is 2.96 Å ,and the distance between the water molecule and the nitrogen of the 2-amino group is 2.96 Å .This water molecule further forms hydrogen bond interaction with the main chain carbonyl group of Tyr109 with the distance of 2.74 Å.

For 4-amino group of the 2,4-diaminoquinzaoline ring of JCS-1474 has two hydrogen bonding interactions with the main chain carbonyl group of Leu5, and with the main chain carbonyl group of Phe92. The distances are 2.54 Å, and 2.69 Å, respectively. Unlike F98Y *Sa* DHFR and similar to WT *Sa* DHFR:TMQ structure, WT *Sa* DHFR has Phe98 and it is a little bit far apart from the 4-amino group with the distance of 4.27 Å.

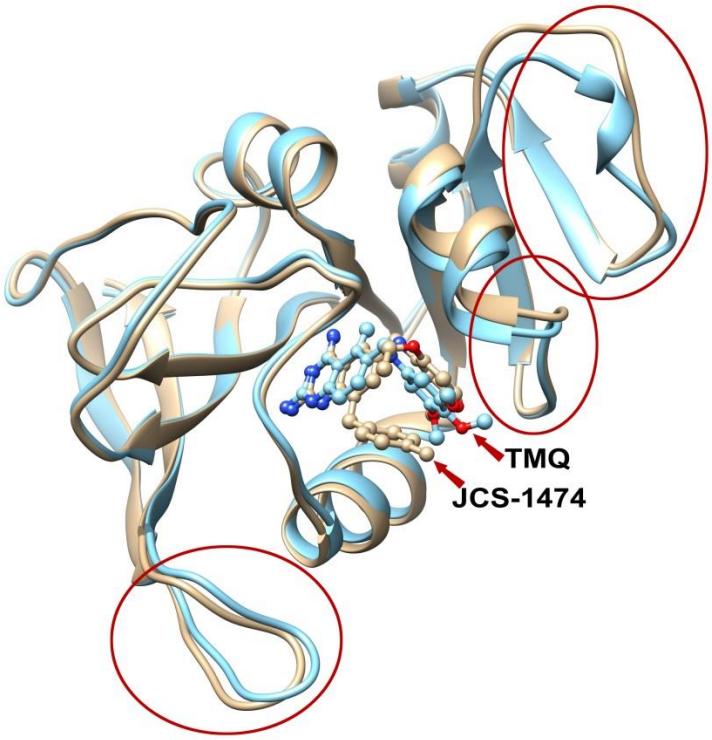

Figure 5-6. Overview of superimposed structure of WT *Sa* DHFR:TMQ (blue) and WT *Sa* DHFR:JCS-1474. The red circled areas are the loop regions that showed large deviations. Gly139-Pro148 (left), Gly51-Arg58 (middle), and Thr63-Gly72 (right) displayed more than 1 A deviation. C-8 benzyl group and 2,5-diethoxybenzyl group of JCS-1474 caused large deviation.

For the 2,5-diethoxyaniline ring side, there are no significant hydrogen-bonding interactions (Figure 5-6). The only probable hydrogen bond interaction came from Ser49. This Ser49 might form a hydrogen bond with oxygen atom of the 2-ethoxy group with the distance of 3.78 Å. This interaction is much weaker compared to the hydrogen bond network via water molecule found in the WT *Sa* DHFR:TMQ structure. 1-carbon atom of the 2,5-diethoxyaniline ring is in close proximity with Ile50 with the distance of 3.69 Å, and the carbon atom of the 5-ethoxy group is in close proximity with Leu54 with the

distance of 3.42 Å, but both interactions are not hydrogen bond interaction. Still these residues could be used as another revenue for further development of more potent inhibitors.

C-8 benzyl TMQ analogs showed great potency against WT *Sa* DHFR ranging from JCS-1552's 10 nM to JCS-1474's 95 nM. 3,5-dimethoxybenzyl containing compounds have great potency on WT *Sa* DHFR. 2,5-diethoxybenzyl containing JCS-1474 displayed low potency of 95 nM, yet it is much better than F98Y SM *Sa* DHFR.

Just like in *Mtb* DHFR and *Pf* DHFR-TS, the flexible residue (Leu28) exhibited drastically different position in WT *Sa* DHFR:JCS-1474 structure (Figure 5-7). Thanks to the flexibility and small size of Leu28, WT *Sa* DHFR could accommodate C-8 benzyl TMQ analog without causing too much loss of activity. The helix near 3,5-dimethoxybenzene or 2,5-diethoxybenzene ring (Arg44-Ile50) also pushed back from the active site (about 1.4 Å) in WT *Sa* DHFR:JCS-1474 structure.

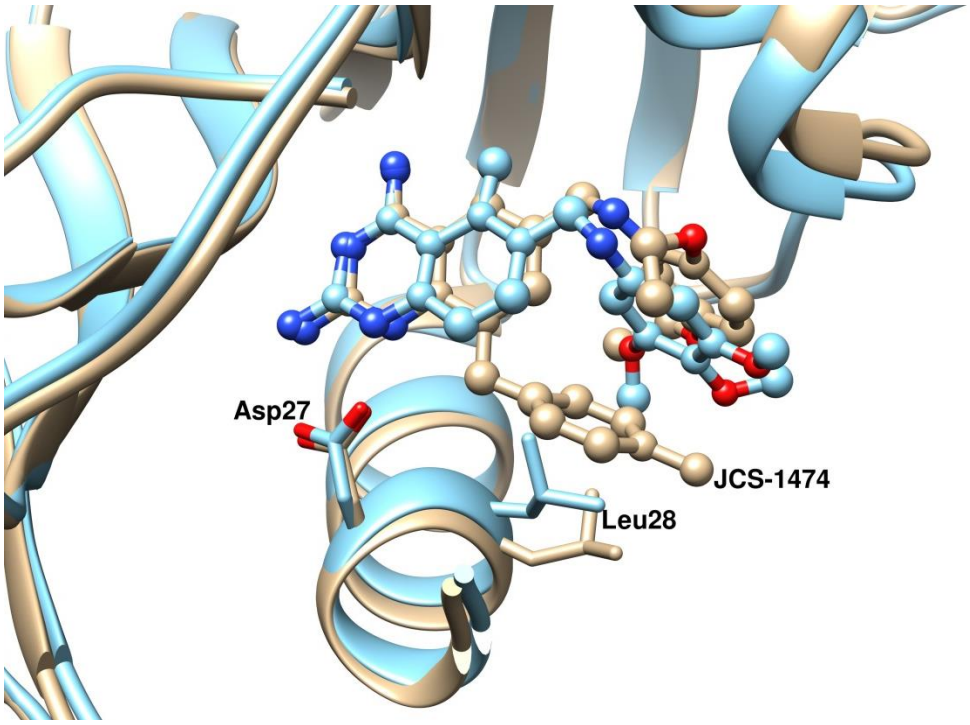

Figure 5-7. Superimposed structure of WT *Sa* DHFR:TMQ (blue) and WT *Sa* DHFR:JCS-1474. The flexible residue next to the acid residue is Leu28 and it flipped down to allow more space to C-8 benzyl group. It proved that just one rotational axis is enough for any DHFR to interact well with C-8 benzyl TMQ if the side chain is not bulky like phenylalanine.

Compared to WT *Sa* DHFR:TMQ, JCS-1474's position in WT *Sa* DHFR was almost the same. Though a similar distortion with *Mtb* DHFR and *Pf* DHFR-TS was found, the degree was smaller with about 10-degree distortion. As anticipated, Leu28 changed its orientation by flipping down in WT *Sa* DHFR:JCS-1474 structure and allowed the increased space to C-8 benzyl group of JCS-1474. Even though there is just one rotation axis that Leu28 could flipping on, the smaller side chain enabled Leu28 to change its orientation without causing any significant contact with other residues. All the crystallographic data is available in Table 5-2.

	WT *Sa*:TMQ (4MO6)	F98Y *Sa*:TMQ (4MP1)	WT *Sa*:JCS-1474
Space group	$P6_1$	$P6_1$	$P6_1$
Unit cell dimension	86.76, 86.76, 96.42 (Å)	87.12, 87.12, 96.41	86.22, 86.22, 101.24
	90.00, 90.00, 120.00 (°)	90.00, 90.00, 120.00	90.00, 90.00, 120.00
Resolution (Å)	50.00-2.15 (2.19-2.15)	50.00-2.65 (2.70-2.65)	50.00-2.84 (2.89-2.84)
R_{sym}	0.15 (0.41)	0.14 (0.80)	0.10 (0.71)
I/σ	11.4 (7.1)	9.3 (4.1)	22.5 (4.1)
Completeness (%)	98.8 (84.2)	99.8 (99.7)	99.7 (99.4)
Redundancy	11.3 (9.0)	11.5 (11.5)	12.6 (12.5)
# of reflections	22151	12126	10093
R_{work}/R_{free}	18.2/23.1	21.5/25.9	18.2/22.7
B factor	31.84	67.87	54.43
RMSD length	0.005	0.009	0.009
RMSD angle	0.747	0.982	0.951

Table 5-2. Crystallographic data and structure statistics for WT and F98Y *Sa* DHFR bound with TMQ and JCS-1474

As stated in the introduction of this chapter, *Sa* DHFR made really interesting comparison with *Mtb* DHFR and *Pf* DHFR in regard to the space induced by C-8 benzyl group in binding with C-8 benzyl TMQ analogs, and the key residue that is next to the

acid residue. In *Sa* DHFR's case, it is Leu28 and Leu28 was able to allow enough space to the C-8 benzyl TMQ analogs including JCS-1474 in WT *Sa* DHFR.

It is interesting to point out that F98Y *Sa* DHFR drastically reduced the activity of C-8 benzyl TMQ analogs and there has not been any crystal structure available for F98Y *Sa* DHFR bound with C-8 benzyl TMQ analogs. We were able to obtain some crystals from F98Y *Sa* DHFR:JCS-1474 and some other C-8 benzyl TMQ analogs, but there was no density for the compounds or very weak and partial density was observed. This indicates that the interaction between C-8 benzyl TMQ analogs and F98Y *Sa* DHFR is very weak, and it could be really intriguing future research point in that the mutation actually brings back the normal tyrosine on the position the same as *Mtb* DHFR or *Pf* DHFR. If this 98 position is really crucial for the interaction, F98Y *Sa* DHFR ought to have better potency with TMQ or C-8 benzyl TMQ analogs. Yet, the enzyme assay results say exactly opposite thing, and the detailed reason should be investigated further.

However, one highly probable possibility could be drawn from the structures we have, and that is the 3,4,5-trimethoxyaninline ring side of TMQ interaction with the protein. This ring is 2,5-diethoxyaniline ring in JCS-1474 and in *Sa* DHFR (both WT and F98Y), the binding is much less and much weaker compared to *Mtb* DHFR or *Pf* DHFR. Therefore, the F98Y mutation could cause TMQ or C-8 benzyl TMQ to be pushed away from the optimal position in the active site. In fact, the F98Y *Sa* DHFR:TMQ structure revealed that there is only one interaction, which is with Ser49, is available for the 3,4,5-trimethoxyaniline ring. This effect could be more drastic in bulkier 2,5-diethoxyaniline ring containing JCS-1474. Even though more in-depth

research should be done to clarify the exact effect and reason for this drastic loss of activity in F98Y mutation *Sa* DHFR in binding with TMQ and its analogs, the structures we have now and the enzyme assay data would tell us much information as well in regard to the interactions between *Sa* DHFR and TMQ analogs.

We tried to acquire the co-crystal structure of several C-8 benzyl TMQ analogs in F98Y *Sa* DHFR, and it was possible to get diffraction quality crystals. However, when we processed and refined the structure, there was no or very little density found in the substrate binding site. It was the same when we tried soaking the inhibitors before collecting the data. What this could indicate are 1) there was no binding (or any significant binding) between F98Y *Sa* DHFR and the C-8 benzyl TMQ analogs in the first place, and that is why we do not see any density in the active site, or 2) Somehow, the C-8 benzyl TMQ analogs became wobbly in the active site due to the extra carbonyl group in F98Y mutation on 98-position, and this flexible position of the compounds along with the wider solvent access point in Sa DHFR compared to Mtb DHFR caused the little or partial density of the compounds in the processed and refined crystal structures.

Further in-depth study should be performed to be able to figure out the effect of F98Y mutation on the mode of action of C-8 benzyl TMQ analogs on Sa DHFR, and that study along with the results we presented here would give us a great opportunity to develop the broad spectrum selective inhibitors.

CHAPTER VI

DISCUSSION AND CONCLUSION

VI.1. Discussion

The similarity of the overall fold between the pathogenic DHFR and human DHFR makes it difficult to design an inhibitor that does not interact with the human protein although some differences exist between the DHFRs from different species. An important difference is that the neighboring pocket of the substrate binding site in *Mtb* DHFR and *Pf* DHFR-TS is larger than the corresponding site in human DHFR. In addition, the large side chain of Phe31 in human DHFR and its low degree of rotational freedom in comparison with Gln28 of *Mtb* DHFR and Met55 of *Pf* DHFR-TS makes the available space in this pocket even smaller. We speculated that an improved selectivity could be achieved if a sufficiently large functional group were added to an inhibitor.

Two major modifications were made to trimetrexate (TMQ) using a structure-based design approach. One modification was on the C-8 position of the 2,4-diaminoquinazoline ring side, and the other modification was on the 3,4,5-trimethoxyaniline ring side. Modifications to the aniline side without a modification on C-8 position of the 2,4-diaminoquinazoline ring exhibited no gain in selectivity. Initially we thought the pocket near the substrate binding site could be reached from either the 2,4-diaminoquinazoline or the aniline ring. However, only compounds with functional

groups on the C-8 of the 2,4-diaminoquinazoline were able to sit in the pocket. Without the C-8 benzyl group attached to the 2,4-diaminoquinazoline ring, no selectivity gain was observed.

We expected to improve selectivity by placing only hydrophilic groups in the pocket because the pocket is surrounded by hydrophilic residues in *Mtb* DHFR. However, the hydrophobic groups, including the benzyl group, were enough to exhibit increased selectivity for *Mtb* DHFR and *Pf* DHFR-TS, and we discovered that the flexibility of the residues (Gln28) in the pocket of *Mtb* DHFR and the length of the bridging carbons were more important for rendering selectivity than the hydrophilicity of the moiety. Structure-based modeling for functionalities on C-8 of the 2,4-diaminoquinazoline ring did not look promising initially because Gln28 of *Mtb* DHFR looked as if it would block functional groups from entering the pocket, but we found that a single carbon bridging from the C-8 position of the quinazoline ring was enough to allow a functional group to fit in the pocket including substituted benzene rings. The flexibility of the side chain of Gln28 of *Mtb* DHFR (Met55 of *Pf* DHFR-TS) played a crucial role in allowing a functional group to enter the pocket.

There has been a successful and ongoing attempt to develop a potent and selective inhibitor against *P. falciparum* DHFR (Yuthavong, Tarnchompoo et al. 2012). A 2,4-diaminopyrimidin derivative, P218, is the one and it is structurally similar to the potent DHFR inhibitor, WR99210 (Fig 2). In the paper published in 2012, the authors found out that a potent DHFR inhibitor, WR99210, which has 1,3,5-triazine ring instead of 2,4-diaminopyriminie, showed poor absorption and bioavailability compared to its 2,4-

diaminopyrimidine counterparts including P218 due to the extensive protonation occurred on 1,3,5-triazine ring in the acidic condition such as in some of the human intestines and that is why WR99210 is not being used for human disease now. However, 2,4-diaminopyrimidine containing compounds including P218 was reported to have much better bioavailability. Beside the bioavailability issue, P218 was reported to improve the selectivity as well. Similar to MTX, WR99210 is potent on human DHFR as well and this lack of selectivity is a significant huddle to be used as antimicrobials. P218 has proved this selectivity issue, and the K_i-ratio between wild type *Pf* DHFR-TS/human DHFR is about 200. For some reason, they did not report the IC_{50} value of P218 against human DHFR, still the K_i difference between *Pf* DHFR and human DHFR is large enough for P218 to be used as selective and potent *Pf* DHFR inhibitor.

As for 2,4-diaminoquinazoline ring, there has not been any report in regard to selective and potent DHFR inhibitor. There should be follow-up study on the bioavailability on our C-8 benzyl TMQ analogs, but as in the case of 2,4-diaminopyrimidine case, 2,4-diaminoquinazoline ring and its protonation would not be a serious issue for bioavailability or permeability when it comes to antimicrobials. There are a couple of reasons why there has not been any selective 2,4-diaminoquinazoline ring based DHFR inhibitors at least so far. First, the 2,4-diaminoquinazoline ring and its sheer size reduce the flexibility of the inhibitor and this flexibility was crucial for P218 to have selectivity over human DHFR. Second, there was not much site in 2,4-diaminoquinazoline containing compounds for modification to improve the selectivity, because most of the important and conserved interactions are on the 2,4-

diaminoquinazoline ring not on the other side of the molecule except for the glutamic acid moiety in MTX.

Our C-8 benzyl TMQ analogs exhibited the potential to be a potent inhibitor not only to the wild type *Pf* DHFR-TS but also to the quadruple mutant *Pf* DHFR-TS. The C-8 benzyl-2,4-diaminoquinazoline TMQ analogs exhibited great potency on both WT and QM *Pf* DHFR-TS with 3 to 10 fold greater potency against WT *Pf* DHFR-TS. This less than 10 fold potency loss was also observed in P218 case as well, and it is not a significant decrease considering the huge potency loss against human DHFR. The size of the pocket near the substrate binding site of WT and QM *Pf* DHFR-TS is almost the same and the mutated residues of QM (N51I/C59R/ S108N/I164L) do not directly affect the binding of the C-8 benzyl-2,4-diaminoquinazoline TMQ analogs. The potency loss in QM *Pf* DHFR-TS comes from effective slight loss in the intensity of the interactions between the compounds and proteins, compared to the wild-type.

The effect of modifications to the 2-amino group of the 2,4-diaminoquinazoline ring also remains to be seen. Unlike the TMP series where methyl and ethyl groups were successfully introduced on the pyrimidine ring (JCS-1168 and 1169, unpublished data), putting an alkyl group on the quinazoline ring has been more challenging. Isobutyl (JCS-1596) and benzyl (JCS-1594) groups have been attached to the N-2 position of 2,4-diaminoquinazoline and they showed reduced potency and selectivity. This is not surprising considering the relatively small space available near N-2 of the 2,4-diaminoquinazoline in both *Mtb* and human DHFR. Based on the crystal structures, N-2 substitution could give potency gain rather than selectivity gain. The only difference

between *Mtb* and human DHFR at that site is His30 in *Mtb* DHFR, which is Tyr33 in the human DHFR. There are potential interactions with the main chain carboxyl group of Val8 and Glu111, and the side chain oxygen of Thr136.

Mtb DHFR and both WT and QM *Pf* DHFR-TS share significant common structural features in the active site, specifically, the pocket near the substrate binding site. Based on our study on *Mtb* DHFR and *Pf* DHFR-TS, the C-8 benzyl-2,4-diaminoquinazoline TMQ analogs can be used as selective and broad spectrum inhibitors for any pathogenic DHFR that has an acid (Asp27 in *Mtb* DHFR) and a residue with flexible side chain next to the residue working as an acid (Gln28 in *Mtb* DHFR). The acid residue (Asp or Glu) interacts with the 2,4-diaminoquinazoline ring and the neighboring residue should be flexible enough to allow space for the C-8 benzyl group by rotating away from the pocket.

The confirmation study on *S. aureus* DHFR gave us a bigger insight on C-8 benzyl TMQ analogs and their application in the future. As stated in the results section, *Sa* DHFR was chosen because it has both similarity and difference with *Mtb* DHFR at the same time. *Sa* DHFR has the same number of residues with *Mtb* DHFR, the acid residue is Asp27 same as *Mtb* DHFR. The overall fold and the active site conformation are very similar as well. There also was a similar space with the glycerol binding pocket in *Sa* DHFR.

However, there is a noticeable difference in *Sa* DHFR compared to *Mtb* DHFR. It is Val28 next to the acid residue, Asp27. This valine is a very helpful control for our SAR study in two reasons. First is that it has just one rotational axis as in human

DHFR's Phe31, and it could be much restricted rotational freedom compared to Gln28 in *Mtb* DHFR or Met55 in *Pf* DHFR-TS. But valine's side chain is much smaller than human DHFR's Phe31, and it could allow more space in the active site for the C-8 benzyl group to position well in the substrate binding site and the pocket available.

As expected the wild type *Sa* DHFR exhibited the similar potency and selectivity on C-8 benzyl TMQ analogs. However, when F98Y mutation was in place, this small change made a huge difference in potency. All the major C-8 benzyl TMQ analogs along with TMQ itself lost almost 20 fold of potency against F98Y *Sa* DHFR. Considering that quadruple mutant of *Pf* DHFR-TS did not affect much on the potency and that there is tyrosine from the beginning in *Mtb* and *Pf* DHFR, this potency loss is somewhat puzzling. The clue from the structure could be the wider solvent access area of *Sa* DHFR compared to *Mtb* and *Pf* DHFR, and when there is a push from F98Y mutation, there is nothing to hold the compounds on that side.

VI.2. Conclusion

Trimetrexate analogs modified with the C-8 benzyl functionalities exhibited exceptional selectivity against *Mtb* and *Pf* DHFR-TS over human DHFR. The selectivity gain largely arose from the significantly reduced potency of these compounds against the human DHFR while retaining their potency against the pathogenic DHFRs. The crystal structures showed that a flexible residue (Gln28 of *Mtb* or Met55 of *Pf*) neighboring an acid residue (Asp or Glu) was crucial to accommodate our C-8 benzyl-2,4-diaminoquinazoline TMQ analogs. The human DHFR Phe31, which has just one axis to rotate on and a considerably bulkier side chain, was unable to allow enough room for our C-8 benzyl-2,4-diaminoquinazoline TMQ analogs.

This work has two important implications. First is that our C-8 benzyl-2,4-diaminoquinazoline TMQ analogs have the potential for development into selective tuberculosis and malaria drugs. The other is that these compounds could provide a significant foundation for developing broad spectrum, selective antimicrobials because our C-8 benzyl-2,4-diaminoquinazoline TMQ analogs were successfully applied to the two different pathogenic DHFRs based on the similarities of their active site structures. The C-8 benzyl-2,4-diaminoquinazoline TMQ analogs could potentially be selective as a DHFR inhibitor against any pathogen that has a similar active site size and has a flexible residue next to the acid residue. Further work could explore the potential of this group of compounds against a broader selection of pathogenic organisms.

The confirmation study on WT and F98Y Sa DHFR displayed that C-8 benzyl TMQ analogs have enough potential to be used as broad-spectrum selective antimicrobials. However, the detailed reason for the loss of potency on F98Y Sa DHFR remains to be seen, and will be important next step for this research.

VI.3. Materials and Methods

Cloning of M. tuberculosis DHFR into plasmid pET28a(+).

cDNA of *M. tuberculosis*, H37Rv, was amplified by PCR to generate blunt-ended DNA with NdeI and HindIII restriction sites at the ends. Then the PCR product was purified using the gel purification kit from Qiagen. The purified DNA product and pET28a(+) vector were double digested with NdeI and HindIII restriction enzymes. The ligation of double digested PCR product and pET28a(+) followed, and the ligation product was then transformed into One Shot Top10 cells by the recommended method supplied by the manufacturer (Invitrogen). The sequence of the plasmid DNA isolated from these cells was confirmed by the Gene Technology Lab at Texas A&M University.

Cloning of human DHFR and P. falciparum DHFR-TS into plasmid pET28b(+).

cDNA of human DHFR purchased from American Type Culture Collection (ATCC, Manassas, VA) was amplified by PCR to generate blunt-ended DNA with NdeI and XhoI restriction sites at the ends. Then the PCR product was purified using the gel purification kit from Qiagen. The purified DNA product and pET28b(+) vector were double digested with NdeI and XhoI restriction enzymes. The ligation of double digested PCR product and pET28b(+) followed, and the ligation product was then transformed into One Shot Top10 cells by the recommended method supplied by the manufacturer (Invitrogen). The sequence of the plasmid DNA isolated from these cells was confirmed by the Gene Technology Lab at Texas A&M University. Genomic DNA of *P.*

falciparum was used as a template for *Pf* DHFR-TS cloning, and it was cloned in a similar way using NheI and HindIII restriction sites at each end. The PCR product was then purified, double digested with NheI and HindIII, and ligated into pET28b(+) . One Shot Top10 competent cell was used for the plasmid extraction.

Cloning of S. aureus DHFR into plasmid pET28b(+).

cDNA of *S. aureus* was amplified by PCR to generate blunt-ended DNA with NdeI and HindIII restriction sites at the ends. Then the PCR product was purified using the gel purification kit from Qiagen. The purified DNA product and pET28b(+) vector were double digested with NdeI and HindIII restriction enzymes. The ligation of double digested PCR product and pET28b(+) followed, and the ligation product was then transformed into One Shot Top10 cells by the recommended method supplied by the manufacturer (Invitrogen). The sequence of the plasmid DNA isolated from these cells was confirmed by the Gene Technology Lab at Texas A&M University.

Site-directed mutagenesis of P. falciparum DHFR-TS.

Stepwise mutagenesis was performed for quadruple mutant *Pf* DHFR-TS using QuikChange II Site-directed mutagenesis kit (Agilent Technologies). Double mutant (C59R and S108N) *Pf* DHFR-TS was generated first, and the further mutations gave quadruple mutant (N51I, C59R, S108N, and I164L) *Pf* DHFR-TS. The sequence of the mutated plasmid DNA was confirmed by the Gene Technology Lab in Texas A&M University.

Site-directed mutagenesis of S. aureus DHFR.

Single-step mutagenesis was performed for F98Y single mutant *S. aureus* DHFR using QuikChange II Site-directed mutagenesis kit (Agilent Technologies). The sequence of the mutated plasmid DNA was confirmed by the Gene Technology Lab in Texas A&M University.

Expression and purification of M. tuberculosis DHFR and human DHFR.

Competent *E. coli* BL21 (DE3) cells (Novagen) were transformed with the recombinant plasmids containing the *Mtb* DHFR gene and human DHFR gene and were grown at 37 ^{o}C to A_{600nm} of 0.7 in LB medium containing 50 ug ml^{-1} of kanamycin. The cells were cooled to 20 ^{o}C, equilibrated for an hour, and induced by the addition of 0.8 mM IPTG for the protein expression. The purification procedures of both DHFRs were similar. The induced cell was allowed to proceed overnight at 20^{o}C. The cells were spun down at 4000 rpm and the pellet was resuspended in the resuspension buffer (20 mM triethanolamine (TEA), 30 mM imidazole, 50 mM KCl, 5% glycerol, pH = 7.8) containing protease inhibitor cocktail (Novagen), 20 mg egg white lysozyme (Sigma), 5 mg DNase I. The resuspended cells were disrupted by cell lysis machine and were spun down at 17,000 rpm for 45 min to remove the cell debris. The supernatant filtered through 0.22 um was applied to 15 ml column of High Performance HisTrap column (GE Healthcare) pre-equilibrated with the loading buffer (20 mM TEA, 30 mM imidazole, 300 mM KCl, 5% glycerol, pH = 7.8). The cell-loaded column was washed

with extensive amount of the loading buffer and then eluted with a linear gradient (350 ml) from 0% to 100% of elution buffer (20 mM TEA, 500 mM imidazole, 300 mM KCl, 5% glycerol, pH = 7.8). The pure-DHFR containing fractions were pooled and concentrated down to 4 ml and treated with 30 ul of thrombin (Novagen) at 16^{o}C for 2 days. The cleaved protein was passed through 5 ml HisTrap HP column (GE Healthcare) pre-equilibrated with the loading buffer. The unbound protein was collected, dialyzed against 4 L of dialysis buffer (25 mM potassium phosphate, 50 mM KCl, 0.1 mM EDTA, 5% glycerol, pH 7.2) for 6 hrs and concentrated down to 15 mg ml^{-1}for crystallization trial.

Expression and purification of WT and QM P. falciparum DHFR-TS.

Competent E. coli Rosetta 2 pLysS (DE3) cell (Novagen) was transformed with the recombinant plasmids containing the wild type (WT) or quadruple mutant (QM) *Pf* DHFR-TS gene and was grown at 37 ^{o}C to A_{600nm} of 0.7 in LB medium containing 50 ug ml^{-1} of kanamycin and 34 ug ml^{-1} of chloramphenicol. The cell was induced with 0.75 mM IPTG at 16 ^{o}C for 20 hrs. The same buffers were used and the remaining steps were similar to *Mtb* and human DHFR purification. Superdex-200 gel filtration column (GE Healthcare) was used for the further purification after Ni-column purification. Pure fractions were collected and dialyzed against 20 mM potassium phosphate buffer (pH=7.2) containing 2 mM dithiothreitol (DTT), 0.1 mM ethylenediaminetetraacetic acid (EDTA), 5% glycerol, and 50 mM potassium chloride for 20 hours at 4^{o}C. The protein solution was concentrated down to 15 mg ml^{-1} for the crystallization trial.

Expression and purification of S. aureus DHFR.

Competent *E. coli* BL21 (DE3) cells (Novagen) were transformed with the recombinant plasmids containing the *S. aureus* DHFR gene and were grown at 37 ^{o}C up to A_{600nm} of 0.7 in LB medium containing 50 ug ml^{-1} of kanamycin. The cells were cooled to 18 ^{o}C, equilibrated for an hour, and induced by the addition of 0.8 mM IPTG for the protein expression. The purification procedure was similar to *Mtb* DHFR. The induced cell was allowed to proceed overnight at 18^{o}C. The cells were spun down at 4000 rpm and the pellet was resuspended in the resuspension buffer (20 mM triethanolamine (TEA), 30 mM imidazole, 50 mM KCl, 5% glycerol, pH = 7.8) containing protease inhibitor cocktail (Novagen), 20 mg egg white lysozyme (Sigma), 5 mg DNase I. The resuspended cells were disrupted by cell lysis machine and were spun down at 17,000 rpm for 50 min to remove the cell debris. The supernatant filtered through 0.22 um filter was applied to 15 ml to 20 ml column of High Performance HisTrap column (GE Healthcare) pre-equilibrated with the loading buffer (20 mM TEA, 30 mM imidazole, 300 mM KCl, 5% glycerol, pH = 7.8). The cell-loaded column was washed with extensive amount of the loading buffer and then eluted with a linear gradient (350 ml) from 0% to 100% of elution buffer (20 mM TEA, 500 mM imidazole, 300 mM KCl, 5% glycerol, pH = 7.8). The pure-DHFR containing fractions were pooled and concentrated down to 4 ml and treated with 30 ul of thrombin (Novagen) at room temperature for 3 hours. The cleaved protein was passed through 5 ml HisTrap HP column (GE Healthcare) pre-equilibrated with the loading buffer. Further purification via S200 or S75 size exclusion column did not make protein any purer. The unbound

protein was collected, dialyzed against 4 L of dialysis buffer (25 mM potassium phosphate, 50 mM KCl, 0.1 mM EDTA, 5% glycerol, pH 7.2) for 6 hrs and concentrated down to 15 mg ml^{-1} for crystallization trial.

Designing and validation of TMQ analogs including C-8 benzyl TMQ.

TMQ bound crystal structure of *Mtb* DHFR was used for the designing the compounds that could take advantage of the glycerol binding pocket of *Mtb* DHFR and similar pocket in *Pf* DHFR-TS. We used the density of TMQ and the acetate molecule found in the glycerol binding pocket. First, TMQ and the acetate were removed from PDB file, and then the designed molecules were fit in the density one by one using COOT. The PDB files of the designed molecules were generated on PRODRG website. All the models that caused a close contact with the protein less than 2 Å were excluded from consideration.

In vitro assay for M. tuberculosis, P. falciparum, S. aureus and human DHFR.

The enzyme assays for *M. tuberculosis, P. falciparum, and S. aureus* DHFR were performed in 100 mM HEPES, 50 mM KCl, pH 7.0, and for human DHFR were in 100 mM potassium phosphate buffer, 100 mM KCl, pH 7.5 at 25 ^{o}C. 20 nM of *M. tuberculosis* DHFR (5 nM of *P. falciparum* or *S. aureus* DHFR), 40 uM of NADPH, and the inhibitor of various concentrations were added to a 1 ml cuvette, and the reaction was initiated by the addition of 40 uM of dihydrofolate. The absorbance decrease at 340 nm

representing the oxidation of NAPDH was monitored for 2 minutes with a spectrophotometer, Cary 50.

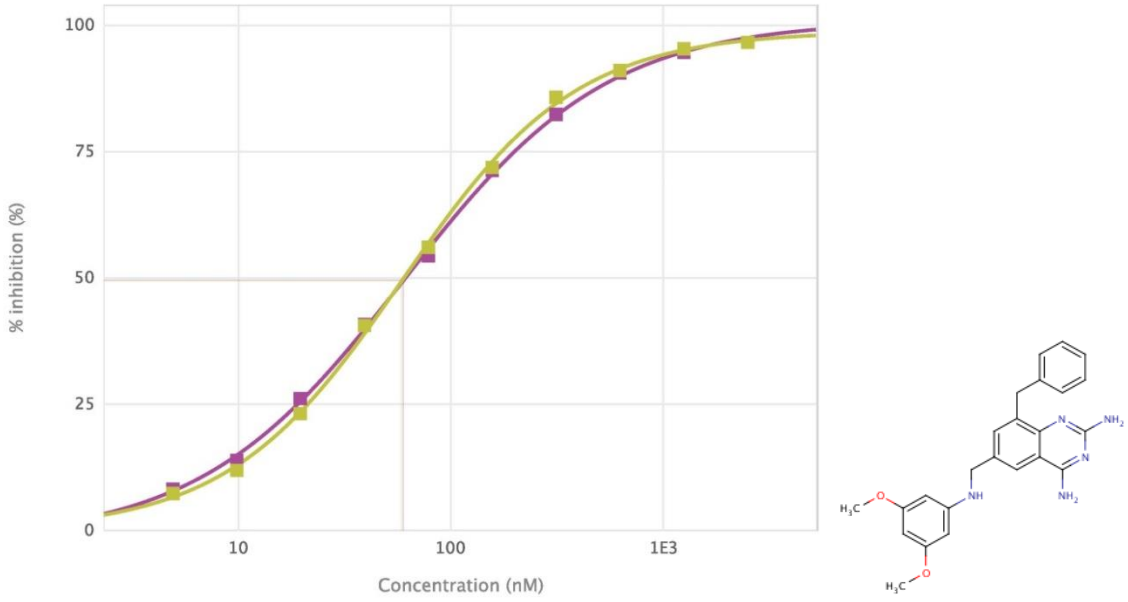

Fig E-1. Example of IC_{50} determination by the CDD program. IC_{50} curve, along with the chemical structure, of JCS-1425 on *Mtb* DHFR is shown.

IC_{50} determination.

5-20 nM of DHFRs were incubated with 40 uM of cofactor NADPH and 7 or 8 different concentrations of the inhibitors (where applicable) for 1 minute. The reaction was initiated by the addition of 40 uM dihydrofolate. The reaction progress was measured for 2 minutes, and the linear region was used to determine the initial velocity parameters. Percent inhibition values from different concentration points were acquired

and fit into the IC_{50} curve by the curve fitting program supported by the Collaborative Drug Discovery website.

Whole cell assay for MIC determination on mc^{2}7000 strain.

The vaccine strain of tuberculosis, mc^{2}7000, was given by Dr. Jacobs. 7H9 medium containing pantothenate, OADC, tyloxapole and malachite green was used to grow mc^{2}7000. When the starter culture reaches $A_{600\ nm}$ of 0.5-0.7, it was added into the testing media comprising dextrose, NaCl, tyloxapole, pantothenate and malachite green along with the inhibitors usually in 96 well plates and left to grow at 37^{o}C for 5 days. After 5 days, all of the wells were stained with alamar blue, and the next day, the cell viability was checked according to the color of the well with blue representing successful inhibition.

P. falciparum strains and culture.

The *P. falciparum* strains used in this study were 3D7 (Netherlands, sensitive), obtained from the MR4 Unit of the American Type Culture Collection (ATCC, Manassas, VA). *P. falciparum* culture was maintained in RPMI-1640 (Sigma, St. Louis, MI) with L-Glutamine, 25 mM HEPES, 33mM $NaHCO_3$, hypoxanthine, and 0.25% Ablumax (Gibco 11020-039). Type A+ erythrocytes were obtained from lab donors and washed three times with RPMI without Albumax and re-suspended in 50% RPMI and stored at 4 ^{o}C. Parasites were grown in 10-ml of a 2% Hematocrit (hct)/RPMI (v/v) mix in 50-ml flasks under a 5% CO_2, 5% O_2, and balance N_2 atmosphere. Media and gas

were replenished daily and culture growth followed by microscopy. When parasites reached 3-5%, cultures were adjusted to 0.5% parasites in fresh RPMI and erythrocytes.

P. falciparum EC_{50} determination.

Test compounds were diluted 6 times in RPMI 1640 media in serial 3 dilutions starting at 20 μM. 10μl of each dilution was distributed in duplicate wells of a 96-well plate. 190 μl of *P. falciparum* culture at 0.5% infected RBC (iRBC) and 0.5% hct was added to each well. Control wells with 0.5% iRBC in RPMI media, 0.5% uninfected RBCs in RPMI media, and 0.5% iRBC in RPMI media with 6.25 nM, 12.5 nM, and 25 nM chloroquine were included. Plates were flushed with 5% CO_2, 5% O_2, and balance N_2 then incubated at 37°C for 48h. At 48h RMPI media containing 0.3 Ci of ^{3}H-hypoxanthine monohydrochloride was added to cultures and incubated for an additional 24h. Cells were harvested onto a filter mat using an Inotech Biosystems Cell Harvester System. The filter mat was quenched with scintillation fluid and counted in a Perkin Elmer 2450 MicroBeta2. EC_{50} values were determined by linear regression analysis of the plots of growth inhibition vs. concentration of compound.

Crystallization of M. tuberculosis, P. falciparum and human DHFRs.

Crystallization screening of both DHFRs was performed using the sitting-drop and hanging-drop methods with Crystal Screen I and II, Index (Hampton Research), Wizard I and II (Emerald Biosystems), and previously successful conditions in our lab. Initial

crystallization screening was carried out with apo DHFR, DHFR with a trimethoprim analog bound (binary complex), and DHFR with NADPH and inhibitor bound (ternary complex). 50 ul of *Mtb* DHFR (12 mg/ml) was mixed with 9 ul of 10 mM NADPH and 10 mM inhibitors and incubated in ice for 20 min. The initial condition contains 10% glycerol, 40% ammonium sulfate and 100 mM sodium acetate pH 4.6 at 4 ^{o}C, and gave diffraction quality crystals in 2 weeks. 50 ul of human DHFR (15 mg/ml) was mixed with 8 ul of 10 mM trimethoprim analogs and 8 ul of 10 mM NADPH, and was incubated on ice for 20 min.

Data collection, Structure determination and Refinement.

Crystals from a droplet were directly transferred to the cryo-protectant of 8% glycerol for a minute, and then transferred to 15% glycerol. The crystals were mounted on nylon loops and flash frozen in a liquid nitrogen stream at 120K before data collection. Most of the data were collected on the R-axis (Rigaku) and some of them were collected in APS in Chicago, IL, and were reduced using Crystal Clear software, and intensities were scaled with SCALEPACK in the CCP4 suite. Integrated and scaled data indicated that human DHFR belongs to $P2_12_12_1$ space group. The binary complex of *Mtb* DHFR with trimethoprim analogs and the ternary complex of human DHFR with NADPH and inhibitors were crystallized in the same space group. The ternary complex of *Mtb* DHFR with C-8 benzylquinazoline TMQ was crystallized in P1 space group. The structures of the binary complex of *Mtb* DHFR with trimethoprim analogs were solved by molecular replacement method using previously solved structure (PDB ID: 1DG5) as

a search model. The structure was refined against the data using PHENIX whereas interactive model building was done by using COOT (Emsley and Cowtan 2004).

REFERENCES

American Thoracic Society. (1986). "Supplement on future research in tuberculosis. Prospects and priorities for elimination. Endorsement of the American Thoracic Society Board of Directors in March 1986." Am Rev Respir Dis **134**(2): 401-423.

Amyes, S. G. (1982). "Bactericidal activity of trimethoprim alone and in combination with sulfamethoxazole on susceptible and resistant Escherichia coli K-12." Antimicrob Agents Chemother **21**(2): 288-293.

Bjorkman, A. and A. Bhattarai (2005). "Public health impact of drug resistant Plasmodium falciparum malaria." Acta Trop **94**(3): 163-169.

Bloom, B. R. and C. J. Murray (1992). "Tuberculosis: commentary on a reemergent killer." Science **257**(5073): 1055-1064.

Boucher, H. W., et al. (2009). "Bad bugs, no drugs: no ESKAPE! An update from the Infectious Diseases Society of America." Clin Infect Dis **48**(1): 1-12.

Cer, R. Z., et al. (2009). "IC50-to-Ki: a web-based tool for converting IC50 to Ki values for inhibitors of enzyme activity and ligand binding." Nucleic Acids Res **37**(Web Server issue): W441-445.

Cody, V. (1985). "Design of anticancer drugs: computer graphic analysis of dihydrofolate reductase inhibitors." Prog Clin Biol Res **172B**: 275-284.

Cody, V., et al. (1992). "Crystal structure determination at 2.3 A of recombinant human dihydrofolate reductase ternary complex with NADPH and methotrexate-gamma-tetrazole." Anticancer Drug Des **7**(6): 483-491.

da Cunha, E. F., et al. (2008). "Binding mode analysis of 2,4-diamino-5-methyl-5-deaza-6-substituted pteridines with Mycobacterium tuberculosis and human dihydrofolate reductases." J Biomol Struct Dyn **25**(4): 377-385.

Das, S., et al. (2013). "Malaria treatment failure with novel mutation in the Plasmodium falciparum dihydrofolate reductase (pfdhfr) gene in Kolkata, West Bengal, India." Int J Antimicrob Agents.

Ditiu, L. (2011). "A new era for global tuberculosis control." Lancet **378**(9799): 1293.

Douglas, K. T. (1987). "The thymidylate synthesis cycle and anticancer drugs." Med Res Rev **7**(4): 441-475.

Forgacs, P., et al. (2009). "Tuberculosis and trimethoprim-sulfamethoxazole." Antimicrob Agents Chemother **53**(11): 4789-4793.

Garcia, A. A., et al. (2003). "Phase II clinical trial of 5-fluorouracil, trimetrexate, and leucovorin (NFL) in patients with advanced pancreatic cancer." Int J Gastrointest Cancer **34**(2-3): 79-86.

Ge, Y., et al. (2007). "Prognostic role of the reduced folate carrier, the major membrane transporter for methotrexate, in childhood acute lymphoblastic leukemia: a report from the Children's Oncology Group." Clin Cancer Res **13**(2 Pt 1): 451-457.

Hitchings, G. H. and S. L. Smith (1980). "Dihydrofolate reductases as targets for inhibitors." Adv Enzyme Regul **18**: 349-371.

Hoffman, V. A. and W. J. Welsh (1995). "Conformational analysis of the lipophilic antifolate trimetrexate." Cancer Biochem Biophys **14**(4): 281-295.

Krieger, I. V., et al. (2012). "Structure-guided discovery of phenyl-diketo acids as potent inhibitors of M. tuberculosis malate synthase." Chem Biol **19**(12): 1556-1567.

Li, R., et al. (2000). "Three-dimensional structure of M. tuberculosis dihydrofolate reductase reveals opportunities for the design of novel tuberculosis drugs." J Mol Biol **295**(2): 307-323.

Matin, K., et al. (2005). "A phase I/II study of trimetrexate and capecitabine in patients with advanced refractory colorectal cancer." Am J Clin Oncol **28**(5): 439-444.

Matthews, D. A., et al. (1977). "Dihydrofolate reductase: x-ray structure of the binary complex with methotrexate." Science **197**(4302): 452-455.

Mbugi, E. V., et al. (2006). "Drug resistance to sulphadoxine-pyrimethamine in Plasmodium falciparum malaria in Mlimba, Tanzania." Malar J **5**: 94.

Meng, X. Y., et al. (2011). "Molecular docking: a powerful approach for structure-based drug discovery." Curr Comput Aided Drug Des **7**(2): 146-157.

Mitchison, D. A. (2012). "Prevention of drug resistance by combined drug treatment of tuberculosis." Handb Exp Pharmacol(211): 87-98.

Ong, W., et al. (2010). "Mycobacterium tuberculosis and sulfamethoxazole susceptibility." Antimicrob Agents Chemother **54**(6): 2748; author reply 2748-2749.

Pina, J. M., et al. (2012). "Cost-effectiveness of rifampin for 4 months and isoniazid for 9 months in the treatment of tuberculosis infection." Eur J Clin Microbiol Infect Dis.

Punt, C. J., et al. (2002). "Trimetrexate as biochemical modulator of 5-fluorouracil/leucovorin in advanced colorectal cancer: final results of a randomised European study." Ann Oncol **13**(1): 81-86.

Ramanathan, R. K., et al. (1999). "Phase II trial of trimetrexate for patients with advanced gastric carcinoma: an Eastern Cooperative Oncology Group study (E1287)." Cancer **86**(4): 572-576.

Senkovich, O., et al. (2005). "Lipophilic antifolate trimetrexate is a potent inhibitor of Trypanosoma cruzi: prospect for chemotherapy of Chagas' disease." Antimicrob Agents Chemother **49**(8): 3234-3238.

Short, C. E., et al. (2009). "Trimetrexate and folinic acid: a valuable salvage option for Pneumocystis jirovecii pneumonia." AIDS **23**(10): 1287-1290.

Sirawaraporn, W., et al. (1997). "Antifolate-resistant mutants of Plasmodium falciparum dihydrofolate reductase." Proc Natl Acad Sci U S A **94**(4): 1124-1129.

Suling, W. J., et al. (1998). "Susceptibilities of Mycobacterium tuberculosis and Mycobacterium avium complex to lipophilic deazapteridine derivatives, inhibitors of dihydrofolate reductase." J Antimicrob Chemother **42**(6): 811-815.

Terlouw, D. J., et al. (2003). "Sulfadoxine-pyrimethamine in treatment of malaria in Western Kenya: increasing resistance and underdosing." Antimicrob Agents Chemother **47**(9): 2929-2932.

Velayati, A. A., et al. (2009). "Emergence of new forms of totally drug-resistant tuberculosis bacilli: super extensively drug-resistant tuberculosis or totally drug-resistant strains in iran." Chest **136**(2): 420-425.

Wang, Y., et al. (2004). "Characterization of a folate transporter in HeLa cells with a low pH optimum and high affinity for pemetrexed distinct from the reduced folate carrier." Clin Cancer Res **10**(18 Pt 1): 6256-6264.

Wernsdorfer, W. H. and D. Payne (1991). "The dynamics of drug resistance in Plasmodium falciparum." Pharmacol Ther **50**(1): 95-121.

White, E. L., et al. (2004). "Cloning, expression, and characterization of Mycobacterium tuberculosis dihydrofolate reductase." FEMS Microbiol Lett **232**(1): 101-105.

White, N. J. (2010). "Artemisinin resistance--the clock is ticking." Lancet **376**(9758): 2051-2052.

World Health Organization. (2011). Consideration of mass drug administration for the containment of artemisinin-resistant malaria in the Greater Mekong subregion: report of a consensus meeting, 27-28 September 2010, Geneva, Switzerland. Geneva, World Health Organization.

World Health Organization. Director-General's Office. Communications Office. (2006). WHO announces pharmaceutical companies agree to stop marketing single-drug artemisinin malaria pills. Geneva, World Health Organization.

World Health Organization. Regional Office for Europe., et al. (2012). Extensive review of TB prevention, care and control services Tuberculosis programme in Armenia, 21 April - 4 May 2011. Copenhagen, WHO Regional Office for Europe.

Yuthavong, Y., et al. (2012). "Malarial dihydrofolate reductase as a paradigm for drug development against a resistance-compromised target." Proc Natl Acad Sci U S A **109**(42): 16823-16828.

Yuvaniyama, J., et al. (2003). "Insights into antifolate resistance from malarial DHFR-TS structures." Nat Struct Biol **10**(5): 357-365.

Zink, M., et al. (2004). "Structural variations of piritrexim, a lipophilic inhibitor of human dihydrofolate reductase: synthesis, antitumor activity and molecular modeling investigations." Eur J Med Chem **39**(12): 1079-1088.